CHEMISTRY – PERFORMANCE CORRELATIONS IN ALTERNATIVE AVIATION FUELS TOWARDS A SUSTAINABLE FUTURE

by

Petr Vozka

A Dissertation

Submitted to the Faculty of Purdue University

In Partial Fulfillment of the Requirements for the degree of

Doctor of Philosophy

Department of Engineering Technology

West Lafayette, Indiana

August 2019

THE PURDUE UNIVERSITY GRADUATE SCHOOL
STATEMENT OF COMMITTEE APPROVAL

Dr. Gozdem Kilaz, Chair

School of Engineering Technology

Dr. Hilkka Kenttämaa

Department of Chemistry

Dr. Nathan S. Mosier

Agricultural & Biological Engineering

Dr. James L. Mohler

Computer Graphic Technology

Dr. Michael E. Peretich

Naval Air Warfare Center Aircraft Division, U.S. Navy

Approved by:

Dr. Kathryne A. Newton

Associate Dean for Graduate Program

To my mother.

Tuto dizertační práci bych chtěl věnovat své
matce, která mě vždy podporovala ve
studiu a bez které bych takhle daleko nikdy nedošel.

ACKNOWLEDGMENTS

I would like to deeply thank my advisor, Dr. Gozdem Kilaz, for always supporting me during my doctoral study. She helped me understand the academic life, connected me with many collaborators, and enabled me to study what I love. I would like to express my thanks to all my committee members - Dr. Hilkka Kenttämaa, Dr. Nathan S. Mosier, Dr. James L. Mohler, and Dr. Michael E. Peretich. Additionally, I would like to thank to my co-authors – Dr. Pavel Šimáček, Dr. Huaping Mo, Dr. Bruce Cooper, Dr. Dianne J. Luning Prak, and Dr. Rodney Trice and all my collaborators (NEPTUNE and LORRE team). I also thank my family for their unconditional support and love. I am very thankful for my funding sources, provided by the US Navy, Office of Naval Research (N000141613109) and by the US Department of Transportation, Federal Aviation Administration (FAA) Cooperative Agreement (12-C-GA-PU).

TABLE OF CONTENTS

LIST OF TABLES 8
LIST OF FIGURES 10
LIST OF ABBREVIATIONS 11
ABSTRACT 11
CHAPTER 1. INTRODUCTION 13
1.1 Scope 14
1.2 Significance 15
1.3 Assumptions 15
1.4 Limitations 16
1.5 Delimitations 16
1.6 Summary 16
CHAPTER 2. REVIEW OF LITERATURE 17
2.1 Aviation Kerosene 17
2.2 Alternative Aviation Gas Turbine Fuels 19
2.3 Fuel Approval Process 20
2.4 Fuel Chemical Composition 23
2.4.1 Comprehensive Two-Dimensional Gas Chromatography 24
2.5 Fuel Properties 25
2.6 Composition-Property Correlations 26
2.7 Summary 32
CHAPTER 3. MIDDLE DISTILATES HYDROGEN CONTENT VIA GC×CG-FID 33
3.1 Introduction 33
3.2 Experimental 35
3.2.1 Materials 35
3.2.2 NMR Experiment Description 36
3.2.3 GC×GC-FID Experiment Description 37
3.2.3.1 Analysis 37
3.2.3.2 Classification 38
3.2.3.3 Quantitative Analysis 40

3.2.4 Weighted Average Method 40
3.3 Results and Discussion 43
3.3.1 GC×GC Quantitative Analysis 43
3.3.2 GC×GC Linearity 49
3.3.3 Hydrogen Content (GC×GC vs. NMR) 49
3.3.4 Hydrogen Content (GC×GC and D3343 vs. NMR) 51
3.4 Conclusion 52
CHAPTER 4. JET FUEL DENSITY VIA GC×GC-FID 53
4.1 Introduction 53
4.2 Experimental 55
4.2.1 Materials 55
4.2.2 Density Measurements 56
4.2.3 Analysis of the chemical composition of the fuel samples 56
4.2.3.1 GC×GC-TOF/MS analysis 56
4.2.3.2 GC×GC-FID analysis 57
4.2.3.3 Chemical composition-density correlation algorithms 58
4.3 Results and discussion 60
4.3.1 GC×GC qualitative analysis 60
4.3.2 GC×GC quantitative analysis 61
4.3.3 WA Method 66
4.3.4 PLS and SVM method 71
4.4 Conclusion 75
CHAPTER 5. IMPACT OF HEFA FEEDSTOCK ON FUEL COMPOSITION AND PROPERTIES IN BLENDS WITH JET A 76
5.1 Introduction 76
5.2 Experimental Section 80
5.2.1 Materials 80
5.2.2 GC×GC analyses 81
5.2.3 Physical Properties 83
5.3 Results and Discussion 84
5.3.1 Composition of Neat Blending Components 84

5.3.2 Composition of Fuel Blends 88
5.3.3 Physical Property Analyses 90
5.3.4 Distillation Profile 90
5.3.5 Density 93
5.3.6 Viscosity 95
5.3.7 Freezing Point 96
5.3.8 Flash Point 98
5.3.9 Net Heat of Combustion 100
5.4 Summary and Conclusion 102
CHAPTER 6. CONCLUSION 104
6.1 Limitations 105
6.1.1 Middle distillates hydrogen content via GC×GC-FID 105
6.1.2 Jet fuel density via GC×GC-FID 106
6.1.3 Impact of HEFA feedstock on fuel comp. and properties in blends with Jet A 106
6.2 Future Work 106
6.3 Summary 107
APPENDIX A. DENSITY PAPER 108
APPENDIX B. HEFA PAPER 114
LIST OF REFERENCES 126
PUBLICATIONS 133

LIST OF TABLES

Table 2.1 Selected Requirements for Aviation Kerosene Properties (ASTM D1655, 2017) 18

Table 2.2 Selected Parameters of Approved Blending Components (ASTM D7566, 2016) 19

Table 2.3 Chemical Composition of Jet A and Fuel Blending Components 24

Table 2.4 Previous and Current Values for Specification 30

Table 3.1 List of All Tested Samples 35

Table 3.2 Experiment conditions of GC×GC-FID analysis 37

Table 3.3 Hydrocarbon Classes Determined for Carbon Number in the Range C7 to C26 39

Table 3.4 Molecular Weight for Hydrocarbons C7 to C17 (g/mol) 41

Table 3.5 Molecular Weight for Hydrocarbons C18 to C27 (g/mol) 41

Table 3.6 Hydrogen Content (wt. %) for Hydrocarbons C7 to C17 (wt. %) 42

Table 3.7 Hydrogen Content (wt. %) for Hydrocarbons C18 to C27 (wt. %) 42

Table 3.8 Fuel Chemical Composition (wt. %) of Low Sulfur F-76, Jet A (Exxon Mobil), Fischer–Tropsch IPK (Sasol), and Green Diesel (Neste Oil, #1) Obtained from GC×GC-FID 45

Table 4.1 List of Tested Samples 55

Table 4.2 The Chemical Compositions (wt. %) of SIP Kerosene (Amyris Bio.), HEFA from Camelina (UOP), Jet A-1 (Unipetrol, a.s.), and F-24 (Luke AFB, AZ) Obtained by Using GC×GC-FID. 62

Table 4.3 Selected compounds and their density values at 15 °C; 68

Table 4.4 Correlation Coefficients for PLS and SVM Using Seven Predictors 73

Table 4.5 Comparison of Mean Absolute Percentage Errors (MAPE) and Correlation Coefficients (R^2) 73

Table 5.1 Mixture Compositions and Designations 81

Table 5.2 Chromatographic Conditions for GC×GC-FID Using DB-17MS and DB-1 MS Columns 82

Table 5.3 Hydrocarbon Type Composition (wt.%) of Jet A and CAME, TALL, and MFAT 86

Table 5.4 Hydrocarbon Type Composition (wt.%) of CAME with Jet A Mixtures 89

Table 5.5 Hydrocarbon Type Composition (wt.%) of TALL with Jet A Mixtures 89

Table 5.6 Hydrocarbon Type Composition (wt.%) of MFAT with Jet A Mixtures 90

Table 5.7 Density at 15 °C (g/cm3) for Jet A, CAME, TALL, MFAT, and Their Mixtures 94

Table 5.8 Freezing Point of Jet A, CAME, TALL, MFAT, and Their Mixtures (°C)..... 98

Table 5.9 Net Heat of Combustion (MJ/kg) of Neat HEFA Samples and Their Mixtures with Jet A Determined Using ASTM D4809 and Calculated from Eq. (5.4) and ASTM D3338..... 101

LIST OF FIGURES

Figure 2.1 Overview of ASTM D4054 approval process (adapted from ASTM D4054, 2016) .. 21

Figure 2.2 Test Program (adapted from ASTM D4054, 2016) 22

Figure 2.3 Aviation fuel composition region that meets the main Tier 1 properties (adapted from Cookson, Lloyd, and Smith, 1987). 28

Figure 2.4 Updated Model (Cookson, Lloyd, & Smith, 1987) of Required Aviation Fuel Composition to Meet the Abovementioned Properties 31

Figure 3.1 GC×GC Classification Developed in ChromaTOF Software for Reversed Phase Separation 39

Figure 3.2 F–76 Military Diesel Chromatogram with Classification Obtained from GC×GC-FID 44

Figure 3.3 Plot of GC×GC-FID versus NMR hydrogen content with weight average (WA) method 50

Figure 3.4 A Representative Comparison of Bias of GC×GC and D3343 Methods and Hydrogen Content Obtained by NMR 51

Figure 4.1 F-24 (Luke AFB, AZ) GC×GC-FID Chromatogram Showing Classification Regions Used 62

Figure 4.2 Measured Density Versus Density Obtained Using GC×GC-FID Data and the WA Method 71

Figure 4.3 Measured Density Versus Density Derived from GC×GC-FID Data and the PLS Method 74

Figure 4.4 Measured Density Versus Density Derived from GC×GC-FID Data and the SVM Method 74

Figure 5.1 GC×GC-FID Chromatogram Illustrating the Jet Fuel Classification for Analyzed Samples with the Following Classes: 83

Figure 5.2 Comparison of GC×GC Chromatograms of HEFA Samples 85

Figure 5.3 Distillation Profile of Jet A, CAME, TALL, and MFAT 91

Figure 5.4 Distillation Profile of Jet A, CAME, and Their Mixtures 92

Figure 5.5 Distillation Profile of Jet A, TALL, and Their Mixtures 92

Figure 5.6 Distillation Profile of Jet A, MFAT, and Their Mixtures 93

Figure 5.7 Comparison of Kinematic Viscosity at -20 °C for All Prepared Samples 96

Figure 5.8 Flash Point (°C) Results Obtained from D56, Calculated from D2887, and Eq. (5.3) 100

LIST OF ABBREVIATIONS

AFRL	Air Force Research Laboratory
ASTM	American Society for Testing and Materials
ATJ	Alcohol to Jet
CHCJ	Catalytic Hydrothermal Conversion Jet fuel
DCD	Dual Coordinate Method
FID	Flame Ionization Detector
FLORE	Fuel Laboratory of Renewable Energy
FT-SPK	Fisher-Tropsch Synthesized Paraffinic Kerosene
GC×GC	comprehensive two-dimensional gas chromatography
HEFA	Hydroprocessed Esters and Fatty Acids
HPLC	High-Pressure Liquid Chromatography
HRJ	Hydrotreated Renewable Jet
MAPE	Mean Average Percent Error
MS	Mass Spectrometry
NMR	Nuclear Magnetic Resonance
OEM	Original Equipment Manufacturer
PLS	Partial Least-squares
SGD	Stochastic Gradient Descent
SIM DIST	Simulated Distillation
SIP	Synthesized Iso-Paraffinic Kerosine
SPK/A	Synthesized Paraffinic Kerosine with Aromatics
SVM	Support Vector Machines
TOF	Time of Flight

ABSTRACT

Author: Vozka, Petr. PhD
Institution: Purdue University
Degree Received: August 2019
Title: Chemistry – Performance Correlations in Alternative Aviation Fuels Towards a Sustainable Future
Committee Chair: Gozdem Kilaz

Determination of the chemical composition of liquid transportation fuels emerged as a novel and important field of study after the introduction of advanced analytical instruments, which are capable of very detailed chemical analyses of complex mixtures. Aviation fuels make up a crucial portion of liquid transportation fuels. There are several significant challenges in the field of aviation fuels, including the development of optimal analytical methods for the determination of the chemical compositions of the fuels, fuel properties measurements, and correlations between fuel properties and chemical composition. This dissertation explores possible correlations between fuel chemical composition and its properties and proposes novel approaches. First, a detailed description of a method for the determination of the detailed chemical composition of all middle distillate fuels (diesel and aviation fuels) is presented. Second, the density was correlated to fuel composition. Additionally, the approach of measuring the density, the hydrogen content, and the carbon content via a GC×GC-FID was introduced. Lastly, it was discovered that minute differences in chemical composition can influence fuel properties. This finding is described in the last chapter, where three HEFA samples were investigated.

CHAPTER 1. INTRODUCTION

Especially in the past 20 years, demands towards an increasing biofuel production have encouraged research in alternative aviation fuels. The effort of increasing biofuel production is led by the US government, academia, and corporations to lower CO_2 emissions and enable domestic energy independence. One challenge in the deployment of alternative aviation fuels is the cumbersome "fuel approval process", which costs millions of dollars and can take many years (DOE/EE-1515 7652, 2017). A candidate aviation fuel needs meet the requirements outlined in the ASTM standard D4054. This standard provides the guideline for the main four Tiers of experiments that any test fuel has to go through before being approved (ASTM D4054, 2016). The quantity of fuel required as well as the costs associated with the required testing increases exponentially as the fuel moves from the chemical and physical property Tier 1 tests to the large scale Tier 4 engine tests. The fuel manufacturer faces the risk of not receiving the ASTM approval after significant financial and time investment, which currently acts as a considerable hindrance to broadening the alternative aviation fuel options in our commercial and military aircraft.

This research is targeting to mitigate this challenge by establishing correlations between the fuel chemical composition and properties (density, viscosity, flash point, etc.). The goal is to build bridges between fuel chemical composition and the ASTM D4054 Tier 1 and 2 tests, which consecutively will enable candidate fuel performance screening without the need for severely expensive Tier 3 and 4 tests. Such an accomplishment could bring the advantage of significantly increasing the portfolio of available alternative aviation fuels. To attain this, currently utilized aviation fuels will be analyzed, their properties will be measured, and the impact of fuel chemical composition on fuel properties will be evaluated. This project has a vast global impact on sustainability as alternative aviation fuels have the great promise to lower emissions while enabling domestic energy security. Similarly, enhanced utilization of multiple bio-based renewable resources will serve towards one of the potential future energy crisis remedies.

1.1 Scope

The most important chemical and physical properties for aviation fuels and alternative aviation fuels are density, viscosity, net heat of combustion, flash point, and freezing point. The main goal of this work is to correlate these properties to the fuel chemical composition and develop predictive models between fuel chemical composition and properties. Fuel composition is analyzed via two-dimensional gas chromatography with a time-of-flight mass spectrometer and a flame ionization detector. These state-of-the-art analytical instruments enable precise and accurate chemical compositional analyses. As fuel chemical composition is being established, parallel efforts are underway towards measuring its chemical and physical properties via ASTM approved methods at Purdue's new *Fuel Laboratory of Renewable Energy* (FLORE). ASTM Aviation Turbine Fuel - (Jet A) Proficiency Testing Program, which allows the comparison of our results to those of other laboratories on a global scale, will be used as the benchmark. The scope of this work will include the conventional jet engine fuels (Jet A and A-1) and military jet fuels (JP-5, F-24), as well as the ASTM approved, blending components for aviation fuels: Fisher-Tropsch, Hydroprocessed Esters and Fatty Acids, Synthetized Iso-Paraffins, and Alcohol-to-Jet.

Development of chemical composition-property correlations has been attempted by previous researchers. However, current advancements in technology provide us with a much higher chance of success. For instance, an older chemistry-property predictive model (Cookson, Lloyd, & Smith, 1987) is referring to aviation fuel as "complex" due to the fact that they contain three main hydrocarbon groups. Recent findings show that are at least 11 functional hydrocarbon groups in Jet A. Not to mention, previous models could not even include the composition of biofuels in their studies as all these work belong to an era prior to biofuel introduction.

The required first step of developing such correlations is the development of an analytical method that can accurately determine the detailed chemical composition of fuels. Detailed chemical composition in this study refers to a reliable data on the exact distribution of each hydrocarbon class (*n*-paraffins, isoparaffins, monocycloparaffins, etc.) for each carbon number (C6 to C20).

In order to correlate fuel properties with its composition, it is necessary to update previous models with today's operational requirements and limitations. The researcher targets to overcome this challenge by expanding the previous work via implementing new and more

detailed compositional data of aviation fuels and fuel blending components. The primary goal will be to discover the impact of each hydrocarbon class on fuel properties.

1.2 Significance

A thorough understanding of the composition and its relationship with properties would mean significant advantages for enhanced utilization of alternative aviation fuels. Once the fuel certification process becomes considerably shorter and more affordable, fuel manufacturers will be encouraged to diversify the alternative aviation fuels production. De-risking the alternative aviation fuel industry for the investors may, in turn, allow our nation to produce fuels with lower emissions and approach closer to the much needed domestic energy independence. Another substantial impact would be the elimination of multiple fuel property testing instruments with a substitution of one analytical instrument (GC×GC-FID), which would bring significant operating and capital cost savings. Last but not least, this research has a very broad global scope as bio-based renewable resources for aviation fuels may be utilized not only by the US but throughout the world.

1.3 Assumptions

The following assumptions were made during performing this research:

1. The fuel property testing capabilities (density meter, viscometer, flash point tester, bomb calorimeter, freezing point apparatus, and distillation) were operating reliably within calibration throughout all aviation fuel sample analyses.
2. The GC×GC-FID fuel chemical composition analysis instrument was precise yielding data with a standard deviation of 0.1 wt. % for each hydrocarbon class.
3. The NIST database utilized for the molecules analyzed via GC×GC-TOF/MS is accurate and up-to-date.
4. The data analysis system (Chemometrics; multivariate analysis; neural network) was chosen wisely after a thorough literature survey.

1.4 Limitations

The limitations of this study are:

1. The number of compounds identified in each fuel sample was limited by the analytical techniques available at the time of experiments.
2. This research was limited by the current compositional awareness of the baseline fuel, Jet A, in the alternative aviation fuel analyses.

1.5 Delimitations

The delimitations of this study are:

1. This study focused only on the currently approved aviation fuels and fuel blending components. Potential fuel formulations to be developed in the future could not be considered.
2. This research only involved gas turbine aviation fuels. Aviation gasoline, the fuel utilized in piston engine aircraft, was not studied.
3. This study was limited to the civil and military aviation fuels deployed only in US aircraft; only two samples of international jet fuels (Jet A-1) were used.

1.6 Summary

This chapter has summarized the main importance of this study together with the scope, significance, research question, assumptions, limitations, and delimitations. In the following chapter, a summary of relevant literature covering alternative and conventional aviation fuel composition measurements, fuel property measurements, and ASTM standards are presented.

CHAPTER 2. REVIEW OF LITERATURE

The purpose of this study is to correlate aviation fuel chemical composition to fuel chemical and physical properties. A representative set of fuel properties was chosen based on the most basic characteristics required for fuel performance. This set includes density, viscosity, flash point, freezing point, net heat of combustion, and distillation range. The literature review will provide a better understanding of these parameters while displaying the current knowledge gaps. This chapter contains the following sections: alternative aviation gas turbine fuels, fuel approval process, fuel chemical composition, fuel properties, and correlations between the composition and properties.

2.1 Aviation Kerosene

Jet A-1 and Jet A are currently the most widely used civilian gas turbine aviation kerosene. Jet A-1 is globally utilized while Jet A is mainly used for intracontinental US flights. The only difference between Jet A and Jet A-1 properties is the freezing point. Freezing points of Jet A and Jet A-1 are -40 °C and -47 °C, respectively. For aircraft utilized in significantly cold climates, another type of "wide cut" fuel is available: Jet B (civilian version of JP-4). Jet B is produced only at low quantities as its very low flash point; thus high flammability brings along safety issues during storage. Ranges of allowable limits for Jet A and Jet A-1 properties are listed in Table 2.1. Kerosene must be visually clear, without mechanical impurities, and without undissolved water at ambient temperature. The main requirements for aviation kerosene are rapid and perfect combustion, low deposit formation, thermal stability, and short flame length. Calorific value is supported by a large hydrogen to carbon (H/C) ratio in the fuel, which is typical for paraffins and cycloparaffins, while this ratio is much lower in aromatic compounds. This is one the reasons to why the amount of aromatic compounds in aviation kerosene is limited. Another reason stems from the fact that aromatics have a much higher tendency for soot generation during combustion. The quantity of soot generated during combustion is directly proportional to the H/C ratio in the fuel. Soot is undesirable as it has an adverse erosive effect on the gas turbine engine, especially at higher speeds. Similar to the aromatics content, the concentration of *n*-paraffins in aviation fuel is also limited as higher concentrations of *n*-

paraffins increase the freezing point. Distillation range of aviation fuels stay mostly between 180 and 290 °C. Water content is limited to a maximum of 0.003 wt. % to control the amount of ice formation at higher altitudes. Viscosity is another property that is monitored to ensure the optimal operation of the injection nozzles and the entire fuel system at low temperatures (Blažek, & Rábl, 2006).

Similar to gasoline or diesel, aviation fuel properties may be adjusted by the use of additives. Storage stability is enhanced by the addition of antioxidants (oxidation inhibitors), corrosiveness is diminished with corrosion inhibitors, and antifreeze agents prevent trace amounts of water solidifying at higher altitudes.

Table 2.1 Selected Requirements for Aviation Kerosene Properties (ASTM D1655, 2017)

PROPERTY	Jet A/Jet A-1
Acidity (mg KOH/g), max	0.10
Flash point (°C), min	38
Density at 15 °C (kg/m^3)	775-840
Freezing point (°C), max	-40/-47
VOLATILITY	
10 % recovered (°C), max	205
50 % recovered (°C), max	report
90 % recovered (°C), max	report
Final boiling point (°C), max	300
Distillation residue (%), max	1.5
Distillation loss (%), max	1.5
COMPOSITION	
Aromatics (vol.%), max	25
Sulfur, mercaptan (wt.%), max	0.003
Sulfur, total (wt.%), max	0.30

2.2 Alternative Aviation Gas Turbine Fuels

ASTM D4054, *Standard Practice for Qualification and Approval of New Aviation Turbine Fuels and Fuel Additives* is the guideline currently utilized for the evaluation and approval of jet fuel blend components from non-petroleum sources. The cumbersome fuel approval process of alternative aviation fuels and blend components is described in various sources (ASTM D4054, 2016; Hemighaus, & Rumizen, 2016; Wilson III, Edwards, Corporan, & Freerks, 2013). Once the fuel or blending component is approved, it is incorporated into ASTM D7566, *Standard Specification for Aviation Turbine Fuel Containing Synthesized Hydrocarbons* (ASTM D7566, 2016). ASTM D7566, first introduced in 2009, allows for the use of synthetically manufactured blending components in jet fuel (ASTM D4054, 2016; Hemighaus, & Rumizen, 2016). As of this writing, five Annexes have been added to the ASTM D7566. Each Annex describes the production technology and the feedstock of the approved fuel blending component (currently, no alternative aviation jet fuel blending components have been approved for use in the US without mixing with Jet A). Annex A1, *Fisher-Tropsch Hydroprocessed Synthesized Paraffinic Kerosin* (FT-SPK), was a part of the standard in 2009. Annex A2 *Synthesized Paraffinic Kerosine from Hydroprocessed Esters and Fatty Acids* (HEFA) was added in 2011. Annex A3 *Synthesized Iso-Paraffins from Hydroprocessed Fermented Sugars* (SIP) was added in 2014. Annex A4 *Synthesized Kerosine with Aromatics Derived by Alkylation of Light Aromatics from Non-Petroleum Sources* (SPK/A) was added in 2015, and Annex A5 *Alcohol-to-Jet Synthetic Paraffinic Kerosene* (ATJ) was added in 2016 (ASTM D4054, 2016; Hemighaus, & Rumizen, 2016). Every Annex contains a table that lists the criteria that the blending component must meet. A summary of selected parameters is shown in Table 2.2 along with the maximum allowable concentration of each neat synthetic blend component.

Table 2.2 Selected Parameters of Approved Blending Components (ASTM D7566, 2016)

Blending Component	FT-SPK	HEFA	SIP	SPK/A	ATJ
Permitted blending (vol.%), max	50	50	10	50	30
Annex	A1	A2	A3	A4	A5
PROPERTY					
Acidity (mg KOH/g), max	0.015	0.015	0.015	0.015	0.015
Flash point (°C), min	38	38	100	38	38
Density at 15 °C (kg/m^3)	730-770	730-770	765-780	755-800	730-770
Freezing point (°C), max	-40	-40	-60	-40	-40

Table 2.2 continued

VOLATILITY					
10 % recovered (°C), max	205	205	250	205	205
50 % recovered (°C), max	report	report	report	report	report
90 % recovered (°C), max	report	report	report	report	report
Final boiling point (°C), max	300	300	255	300	300
T90-T10 (°C), min	22	22	5	22	21
Distillation residue (%), max	1.5	1.5	1.5	1.5	1.5
Distillation loss (%), max	1.5	1.5	1.5	1.5	1.5
Hydrocarbon Composition					
Cycloparaffins (wt.%), max	15	15	-[a]	15	15
Aromatics (wt.%), max	0.5	0.5	0.5	20	0.5
Carbon and Hydrogen (wt.%), min	99.5	99.5	99.5	99.5	99.5

[a]Saturated Hydrocarbons, min 98 wt.%; Farnesane, min 97 wt.%

2.3 Fuel Approval Process

Approval of all US candidate fuels and fuel additives must follow the protocol defined in the ASTM D4054, *Standard Practice for Qualification and Approval of New Aviation Turbine Fuels and Fuel Additives* (ASTM D4054, 2016). This standard was developed by a broad group of fuel manufacturers, international fuel certification experts (ASTM International and United Kingdom Ministry of Defence), Original Equipment Manufacturers (OEMs such as General Electric, Rolls Royce, and Pratt & Whitney), airframe manufacturers (Boeing and Airbus) as well as the end users (commercial airlines and military branches such as US Navy and US Air Force), and policymakers.

The fuel approval process (Figure 2.1) has three main sections: (1) Test Program, (2) OEM Internal Review, and (3) Specification Change Determination. One important note to make here is that even though the Test Program displays the option of bypassing further stages of testing, in practice there has been no candidate fuel that was not evaluated at each tier sequentially between Tier 1 (Specification Properties) through Tier 4 (Engine Test) (ASTM D4054, 2016).

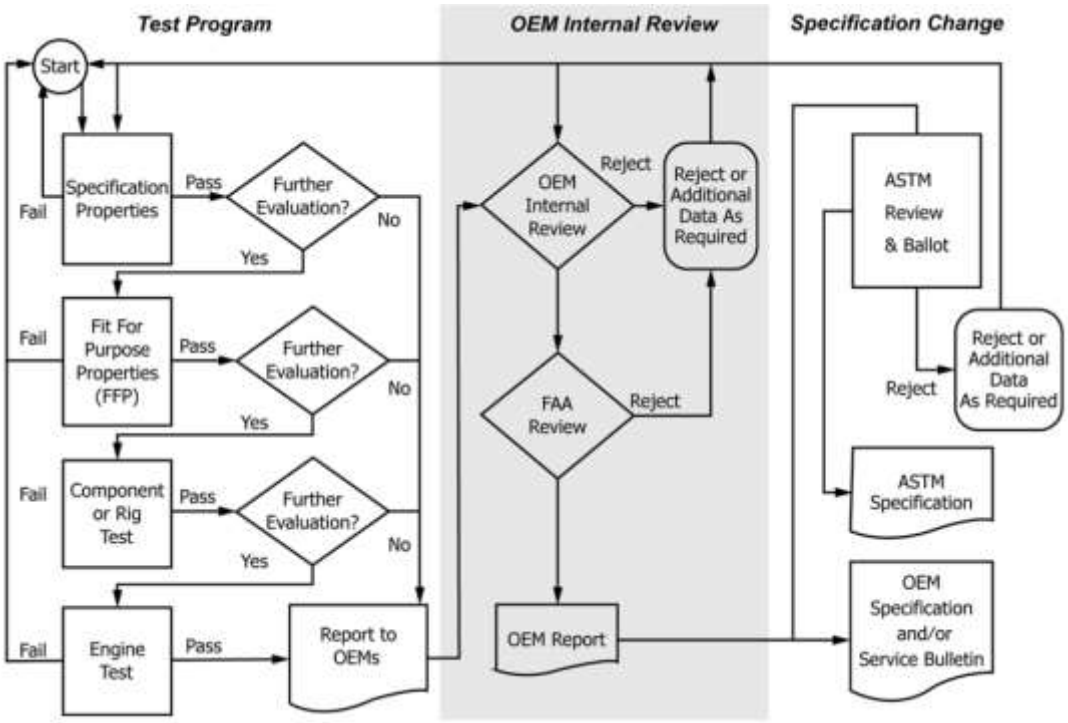

Figure 2.1 Overview of ASTM D4054 approval process (Reproduced, with permission from ASTM D4054, 2016, copyright ASTM International, 100 Barr Harbor Drive, West Conshohocken, PA 19428.)

The ASTM 4054 test Program part is the most essential scope of this research. This section consists of four Tiers (Tiers 1–4). The test program flowchart, displayed in greater detail in Figure 2.2, is followed to assure that the fuel candidate has no adverse effects on the engine safety, performance, and durability. Tier 1 covers the fuel specification properties that are the ones included in the "Table 1" of the standards regulating the conventional aviation gas turbine fuels: ASTM D1655 (US civilian), Def Stan 91-91(UK), Mil-DTL-83133 (US military), and Mil-DTL-5624 (US military). These properties are discussed in further detail in the Fuel Properties chapter of this document. Tests within Tier 2 were designed to assure the safety in operational environments; thus the fuel chemistry, physical performance, electrical and compatibility properties. Throughout the certification process, as the testing continues with Tiers 3 and 4, the volumes of sample fuel necessary increases exponentially because Tiers 3 and 4 are steered towards simulating the actual fuel delivery in the airframe and utilization in the combustion chamber. Tier 3 tests help evaluate if the fuel is fit for interacting with components within the fuel delivery system and the combustor rig. During the Tier 4 tests, the largest scale

runs, data are collected while the candidate fuel is deployed and utilized in real aircraft jet engines (ASTM D4054, 2016; Yildirim & Abanteriba, 2012). Experiments within Tiers 1 and 2 are relatively more manageable in terms of the associated costs and the volumes of test fuel required. Tiers 3 and 4 are tremendously costly, time-consuming, and labor intensive as these tests are basically real-life demonstrations as opposed to the controlled and scaled down laboratory settings.

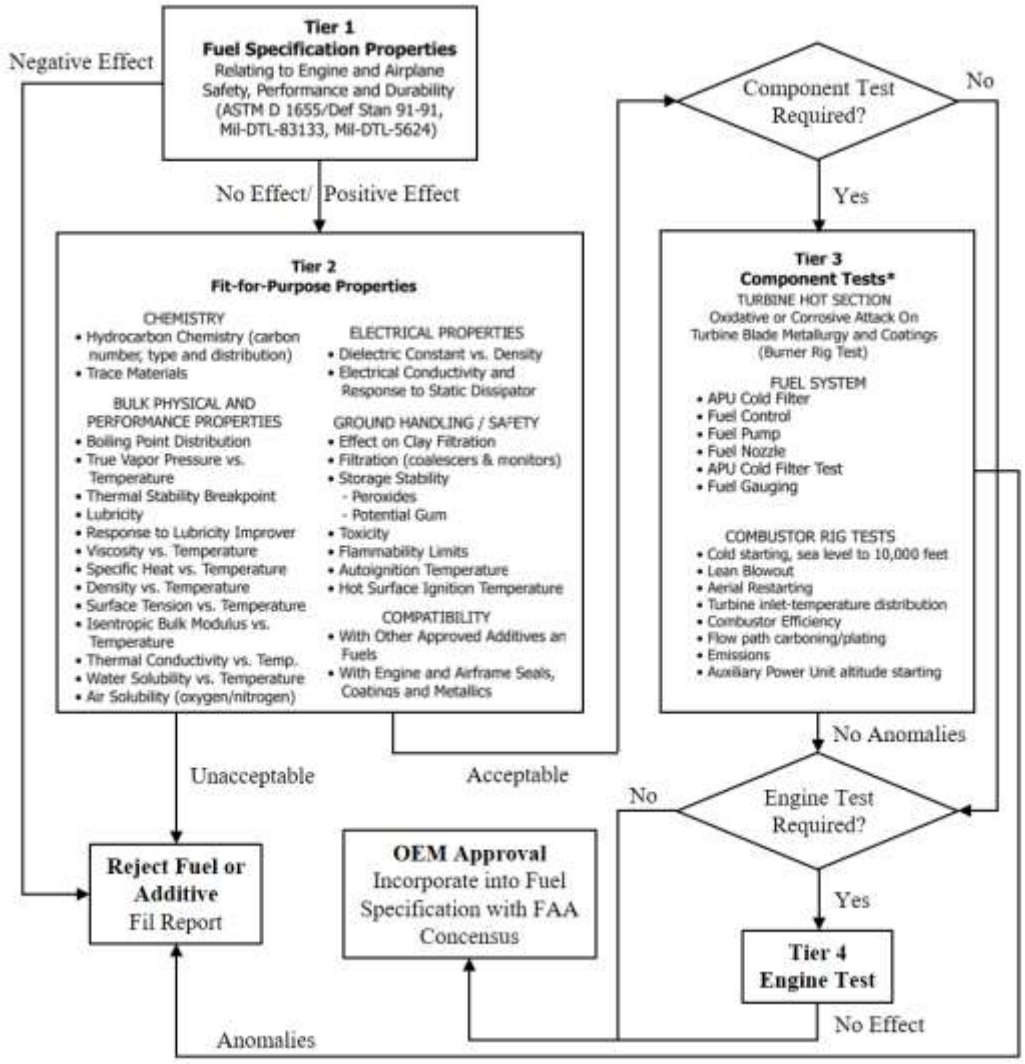

Figure 2.2 Test Program (Reproduced, with permission from ASTM D4054, 2016, copyright ASTM International, 100 Barr Harbor Drive, West Conshohocken, PA 19428.)

Rumizen (2016) pointed out some limitations of the ASTM D4054, such as each Annex being limited to a specific conversation pathway and/or a specific feedstock. Another restriction is that currently, GC×GC is not standardized as a chemical composition analysis instrument for

aviation fuels. During his presentation, Rumizen (2016) also introduced the audience to the most recently adopted approach of the Federal Aviation Administration (FAA) for the ASTM D4054 protocol: there will be a report submitted to the ASTM committee post Tiers 1 and 2 as opposed to waiting for the results from Tiers 3 and 4. This newly acquired practice is very encouraging to our work as it is the indication that Tier 1 and 2 can be accurately correlated to Tier 3 and 4. Typically, the fuel certification process takes 3 to 5 years, costing approximately $10 to 15 million (Csonka, 2016, Colket, Heyne, Rumizen, Gupta, Edwards, Roquemore, Andac, Boehm, Lovett, Williams, Condevaux, Turner, Rizk, Tishkoff, Li, Moder, Friend, & Sankaran, 2017). Thus there is a clear and imminent need to decrease the certification costs and duration to increase the incentive for alternative fuel production. A multi-agency-led initiative in the US, the National Jet Fuels Combustion Program aims to streamline these costs while diversifying the alternative fuels and resources; a highly desirable consequence of an efficient ASTM fuel certification process (Colket et al. 2017).

2.4 Fuel Chemical Composition

Group-type analysis helps determine the content of structurally similar compounds, e.g. content of saturated compounds, monoaromatics, diaromatics, etc. The structural analysis of petroleum products has been improved significantly in the past years. Historically, aromatics content was measured using ^{13}C and ^{1}H nuclear magnetic resonance (NMR) spectroscopy method, which was the most advanced technology available at the time. High-pressure liquid chromatography (HPLC) was utilized to distinguish aromatics from saturates. As of this writing, novel approaches for measuring the detailed chemical composition have been developed, such as one utilizing the state-of-the-art instrument: comprehensive two-dimensional gas chromatography coupled with high-resolution time-of-flight mass spectrometry and flame ionization detector. Two-dimensional gas chromatography provides a very precise compositional analysis - both qualitatively and quantitatively.

Mostly, Jet A/A-1 is composed of all main hydrocarbon classes and their subgroups – paraffins (*n*-paraffins, isoparaffin), cycloparaffins (mono-, di-, and tri-), aromatics (mono-, di-, and tri-) with a carbon number between C7 and C18. Sulfur, oxygen, and nitrogen compounds may also be present at trace concentrations. The content of each class may vary between different batches. A representative Jet A chemical composition is shown in Table 2.3.

Table 2.3 Chemical Composition of Jet A and Fuel Blending Components

Composition (wt. %)	Jet A	FT-SPK	HEFA	SIP	ATJ
n-paraffins	21.84	0.31	10.67	0.00	0.00
isoparaffins	30.05	94.83	85.51	99.40	99.62
cycloparaffins	29.99	4.22	3.72	0.54[a]	0.37[b]
alkylbenzenes	12.77	0.46	0.00	0.00	0.00
cycloaromatics	2.92	0.16	0.00	0.00	0.00
naphthalenes	2.21	0.02	0.09	0.06	0.00

[a]approximately 0.03 wt. % of trimethyl-dodecanol; [b]aproximetely 0.32 wt. % of olefins

Alternative blending components have much simpler chemical compositions than that of Jet A; hence, they require further mixing with Jet A. FT-SPK contains hundreds of compounds that are primarily isoparaffins. HEFA is a mixture mainly of *n*- and isoparaffins. SIP is composed of only one isoparaffin, namely farnesane (2,6,10-trimethyldodecane). The amount of aromatics in all these blending components is negligibly small. A representative alternative blending component compositions are shown in Table 2.3.

Each group and compound can influence the fuel properties. For instance, linear paraffins (*n*-paraffins) have very poor cold flow properties, which is a clear disadvantage for aviation as aircraft is expected to operate at high altitudes. Therefore, not only the total quantitative analysis of hydrocarbon groups but also qualitative analysis is necessary in order to understand all these correlations. One of the main scopes of this work is to include the interactions between fuel chemistry and properties into a predictive model.

2.4.1 Comprehensive Two-Dimensional Gas Chromatography

Comprehensive two-dimensional gas chromatography (GC×GC) is a technique that was originally described by Liu & Phillips (1991). GC×GC is equipped with two different columns. The entire sample is introduced to both columns. First, the sample is separated on first GC column, then the first-column eluate is "injected" via modulator into the second GC column, which is typically much shorter than the first GC column (Dallüge, Beens, & Udo, 2003). The columns are selected in order to create what is referred to as "orthogonal separation conditions" (Schoenmakers, Oomen, Blomberg, Genuit, & van Velzen, 2000). In order to achieve orthogonal separation, selected columns have to provide independent separation mechanisms. Separation mechanisms of GC columns can be divided into two groups: (a) based on the analyte volatility

and (ii) based on the interaction of the analyte with the stationary phase in the GC column (Dallüge, Beens, & Udo, 2003).

The polarity of the stationary phase of the GC column can be either polar (e.g., polyethylene glycol, cyanopropyl–phenyl-dimethylpolysiloxane), mid-polar (e.g., (50%-Phenyl)-methylpolysiloxane), or nonpolar (e.g., dimethyl polysiloxane, 5% phenylene – 95% dimethylpolysiloxane). The configuration nonpolar×polar/mid-polar is referred to as a normal column configuration and the combination polar/mid-polar×nonpolar is referred to as a reversed phase column configuration (Dallüge, Beens, & Udo, 2003).

2.5 Fuel Properties

Fuel properties, which are parts of Tier 1 and 2, are evaluating the fuel readiness. ASTM standards D1655 (conventional jet fuel) and D7566 (alternative jet fuel) divide properties into the following main groups: volatility (distillation range, distillation residue, and distillation loss, flash point, and density), fluidity (freezing point, viscosity), combustion (net heat of combustion, smoke point, and naphthalenes content), corrosion, thermal stability, contaminants, and additives. Naphthalene content, contaminants, and additives were covered in Chapter 2.4 as they belong to the fuel composition as opposed to the fuel property.

Fuel amount in the aircraft is monitored volumetrically; hence, density plays an important role in determining the total load as well as the aircraft range. Density is also used in flow calculations, fuel gauging, metering device adjustments, fuel loading, and fuel thermal expansion (Handbook of aviation fuel properties, 1983). Fuel composition directly influences the density. For the same carbon number, aromatic hydrocarbons have higher density values than those of normal and iso-paraffins. Viscosity, defined as internal resistance to motion caused by cohesive forces among the fluid molecules (Handbook of aviation fuel properties, 1983), is another important property of the fuel. Viscosity value indicates the fuel flow property. In cases of too high a viscosity, the fuel can clog the filters and prevent efficient atomization; resulting in lagged engine response during the flight. Freezing point together with the viscosity are important factors that determine the fuel pumpability. Freezing point is a “low-temperature property” of the fuel. Low-temperature properties of the fuel are severely restrictive as they define the fuel fluidity; hence the fuel availability in the aircraft. Volatility, tendency to change from liquid to vapor, has effects on multiple criteria of fuel performance: pumping, flammability, entrainment and vapor

losses as well as the engine start (Handbook of aviation fuel properties, 1983). An equally crucial fuel property is the amount of heat released upon its combustion; namely, net heat of combustion. The aviation fuel needs to provide a minimum amount of energy for a continuous thrust and lift during take-off, cruise, and landing. Flash point, defined as the lowest temperature at which the fuel vapors will ignite upon exposure to an ignition source, is a property that concerns the fuel safety. Flash point is a very important criterion for the fire-hazard rating; especially at US Navy aircraft carrier ships. All these fuel properties are monitored to be within the necessary operational limits with an "umbrella property" that determines the cut for the aviation fuel: distillation profile.

2.6 Composition-Property Correlations

During 1980, researchers recognized the value in correlating the fuel chemical composition to its properties. In spite of the technological limitations of the time, the predictive models developed for fuel properties based on fuel composition were very accurate.

In 1985, Cookson, Latten, Shaw, and Smith initiated research on fuel property-composition relationships for gas turbine aviation fuels as well as diesel fuels. The distillation profiles of petroleum diesel (200-350 °C) and kerosene (170-300 °C) resembled each other very closely. This enabled previous researchers to utilize similar equations $P = a_1[n] + a_2[BC] + a_3[Ar]$ (2.1) for both liquid transportation fuels. Two aviation fuel properties extensively studied were the smoke point and aromatics content. The pertinent equation is below:

$$P = a_1[n] + a_2[BC] + a_3[Ar] \quad (2.1)$$

Cookson et al. (1985) stated in this work that a_1, a_2, and a_3 are coefficients, [n], [BC], and [Ar] are wt.% of *n*-paraffins, branched plus cyclic saturates, and aromatics, respectively. Aromatics content was measured using ^{13}C and ^{1}H nuclear magnetic resonance (NMR) spectroscopy method, which was the advanced technology at the time. Consecutive high-pressure liquid chromatography (HPLC) measurements helped distinguish aromatics from saturates.
As of this writing, different methodologies of hydrocarbon group measurements have been developed, such as the state-of-the-art instrument two-dimensional gas chromatography coupled with high-resolution time-of-flight mass spectrometry. This instrument provides a very precise quantitative analysis. Therefore, as of this writing, there is no more a need for the equation for

the calculation of aromatics content. It is also important to mention here that the aviation fuel specifications were quite different in the 1980s than today (2018). Further details on this subject are provided in consecutive chapters.

In a consecutive work (Cookson, Lloyd, & Smith, 1987), the previous model (Equation $P = a_1[n] + a_2[BC] + a_3[Ar]$ (2.1) was expanded to include equations for net heat of combustion, specific gravity, and freezing point. These properties, with the previously studied smoke point and aromatics content, created a strong base for Tier 1. Cookson, Lloyd, and Smith (1987) developed ternary diagrams to represent each fuel property. The vertices of the triangles shown in Figure 2.3 represent the weight composition of each hydrocarbon group, namely a mixture composed of 100 wt. % [n], [BC], and [Ar]. The operational limitations for the aviation fuels require the composition to be kept within a certain range. This range is seen as the shaded area in Figure 2.3. Fuel candidates with hydrocarbon group concentrations that fall out of this range would not be certified. This area, which is denoted as the shaded zone in Figure 2.3, displays the boundaries of a fuel mixture, its performance limitations, and the corresponding constituent hydrocarbon concentrations. For instance, a candidate fuel could only be operational and functional if the following criteria were met: aromatics content (V_{ar}) < 20 vol. %, specific gravity (SG) between 0.7750 and 0.8398 g/cm^3, net heat of combustion (Q_n) > 42.8 MJ/kg, smoke point (SP) > 20 mm, and freezing point (FP) < -40 °C.

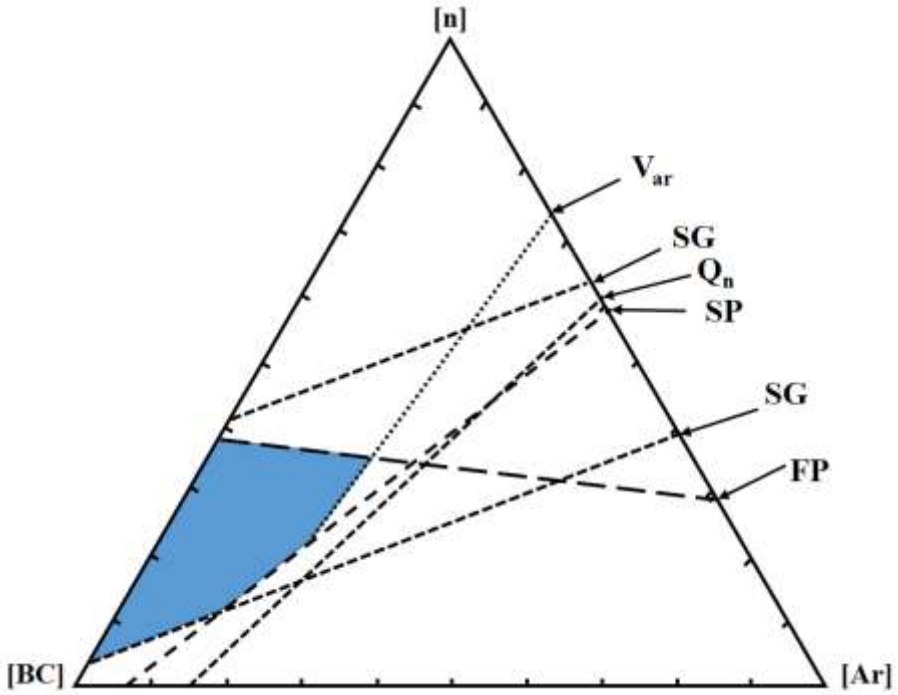

Figure 2.3 Aviation fuel composition region that meets the main Tier 1 properties. Reprinted (adapted) with permission from Cookson, Lloyd, and Smith, 1987. Copyright © (2018) American Chemical Society.

Authors (Cookson, Lloyd, & Smith, 1987) mentioned that this study was limited by the composition, boiling range, and the number of hydrocarbon groups chosen to represent the fuel chemistry. In the case that the fuel composition falls outside the designated area, the predictive model will be inaccurate. Another limitation of this work can be attributed to the oversimplification of the fuel constituents. The authors focused on only three main hydrocarbon groups: *n*-paraffins, branched plus cyclic saturates, and aromatics. Current studies identify nine hydrocarbons groups making up the aviation fuel composition. Further discussions on this subject are provided in further chapters. Still, this simplification (grouping) will not lead to an error in the case that the constituent hydrocarbon compounds behave uniformly (i.e., their physical properties are similar). For example, mono- and di-aromatics can be grouped to form a single group. Similarly, this rule can be applicable to other hydrocarbon groups.

Cookson and Smith (1990) introduced an alternative equation for the cases in which the fuel composition is measured via only ^{13}C NMR as opposed to a combination of ^{13}C NMR and

HPLC. This method can measure only n-alkyl carbons and aromatic carbons as shown in Equation $P = b_1 C_n + b_2 C_{ar} + c$ (2.2).

$$P = b_1 C_n + b_2 C_{ar} + c \quad (2.2)$$

P is the property of interest, Cn and Car are wt. % of n-alkyl carbon and wt. % of aromatic carbon, respectively; while b_1, b_2, and c are the coefficients introduced. Equation $P = b_1 C_n + b_2 C_{ar} + c$ (2.2) produced better results than those from the Equation $P = a_1[n] + a_2[BC] + a_3[Ar]$ (2.1) only for one property: specific gravity.

One significant assumption that this group of researchers made was regarding the boiling range of the test fuel samples. Most of the test samples had similar boiling ranges (190-230 °C). This work did not evaluate the effect of boiling range on the data collected. However, the authors pointed out that modest deviation from this boiling range should not adversely affect their results. This triggered another topic of research interest: composition-property relationships in varying boiling ranges of fuels (Cookson, Iliopoulos, & Smith, 1995). Authors tested Equation $P = b_1 C_n + b_2 C_{ar} + c$ (2.2) from the previous work (Cookson & Smith, 1990) on samples with different boiling ranges (150-250 °C). Results showed that Equation 2.2 worked well for all mentioned properties except for the low-temperature properties (freezing point). This shortcoming was mitigated by the development of the Equation $P = a_1 C_n + a_2 C_{ar} + b_1 T_{10} + b_2 T_{90} + k$ (2.3).

$$P = a_1 C_n + a_2 C_{ar} + b_1 T_{10} + b_2 T_{90} + k \quad (2.3)$$

Cookson, Iliopoulos, and Smith (1995) stated in this work that a_1, a_2, b_1, b_2, and k are coefficients determined by multiple linear regression. T_{10} and T_{90} represent the temperature values (°C) at which 10 and 90% of the fuel boils, respectively. The model based on Equation $P = a_1 C_n + a_2 C_{ar} + b_1 T_{10} + b_2 T_{90} + k$ (2.3) successfully predicted the changes in fuel properties as a function of the boiling range.

The original model was also improved in an additional work (Cookson & Smith, 1992), where alternative aviation fuels derived from Fisher-Tropsch synthesis and coal hydroliquefaction were investigated. This work introduced a major development as it was the premiere one investigating the composition-property relationships in alternative fuel blending components. Four blended samples consisting of coal-derived fuels via hydroliquefaction and Fisher-Tropsch were prepared. Only two of those five samples fell within the composition shown

by the shaded area (Figure 2.3). Hence, this study confirmed one of the limitations of the previous work: if the sample composition falls outside the shaded area, the measured and calculated values for fuel properties were highly discrepant. On the other hand, if the sample compositions were within the shaded area, experimental and theoretical results were in good agreement. Equation $P = a_1[n] + a_2[BC] + a_3[Ar]$ (2.1) was used for this purpose and coefficients a_1-a_3 are displayed in Cookson and Smith (1992).

The fuel property requirements established in the 1980s by the ASTM D1655 were different than the current ones. Additionally, there were no incentives for biofuels. Therefore, the borders of the shaded area from Cookson's model needed to be updated to meet the most recent ASTM D1655 specifications. Table 2.4 displays the changes adopted. Values of net heat of combustion and freezing point did not change in comparison with others. Our updated model (Figure 2.4) has included the physical and chemical fuel properties referred to in ASTM D1655 except for flash point and viscosity (compare with Table 2.1).

Another significant hurdle in modeling fuel properties based on chemical composition is the presence of fuel additives. Additives are used to improve fuel properties (e.g., gum inhibitors, lubricating properties). These additives are added in really trace concentrations; yet, they are capable of bringing along great improvements; hence are necessary components of aviation fuels. Due to this fact, it is important to assure that the correlations between the fuel composition and properties are not affected by the additives. Cookson et al. (1985), Cookson, Lloyd, and Smith (1987), and Cookson and Smith (1990) did not specify which types of aviation fuels were used for their research and especially if those fuels were additive-free. For this reason, some of their equations may not be valid for currently utilized jet fuel prior to doping with additives.

Table 2.4 Previous and Current Values for Specification

Property	Previous	New
Smoke point (mm)	> 20	> 18
Aromatics content (vol.%)	< 20	8-25
Net heat of combustion (MJ/kg)	> 42.8	> 42.8
Specific gravity (g/cm^3)	0.7750-0.8398	0.7750-0.8400
Freezing point (°C)	< -40	< -40

Data taken from (ASTM D1655, 2016; Cookson, Lloyd, & Smith, 1987)

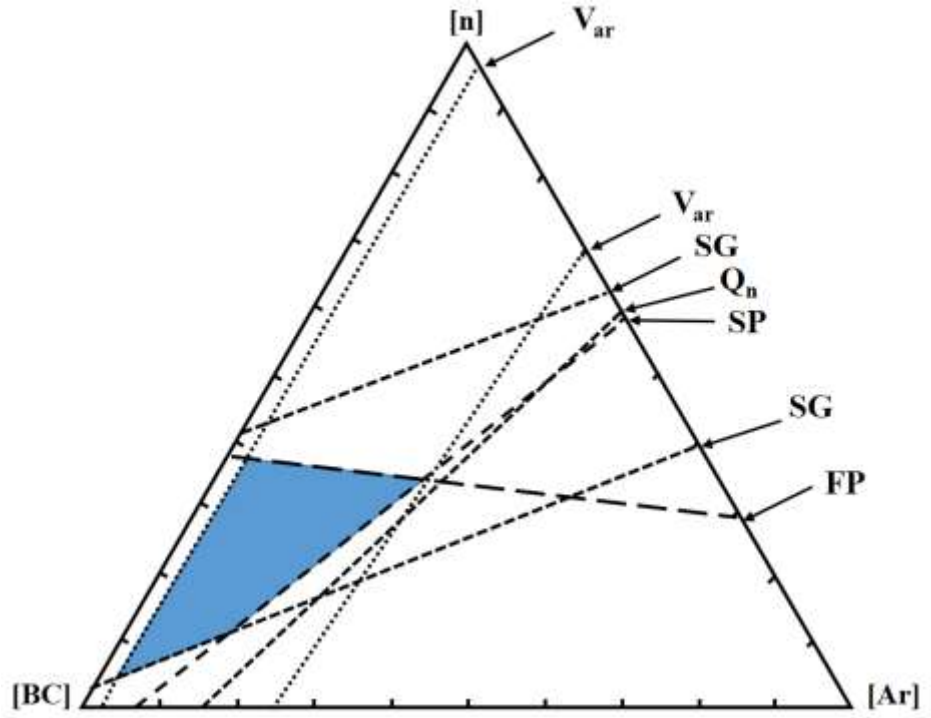

Figure 2.4 Updated Model (Cookson, Lloyd, & Smith, 1987) of Required Aviation Fuel Composition to Meet the Abovementioned Properties

After a long break, in 2007 (Liu, Wang, Qu, Shen, Zhang, Zhang, & Mi, 2007), fuel composition-property correlation focus reemerged in aviation fuels research world. Since then, several papers were published: (Morris, Hammond, Cramer, Johnson, Giordano, Kramer, & Rose-Pehrsson, 2009) in 2009, (Cramer, Hammond, Myers, Loegel, & Morris, 2014) in 2014, and (Braun-Unkhoff, Kathrotia, Rauch, & Riedel, 2016) in 2016. These studies contained the use of GC-MS, Chemometric modeling, and artificial neural networks; however, none mentioned the utilization of two-dimensional gas chromatography.

As of this writing, the most current study (Shi, Li, Song, Zhang, & Liu, 2017) utilizing a comprehensive two-dimensional gas chromatography with mass spectrometry and flame ionization detector was published in July 2017. Researchers utilized all the above-mentioned approaches in this work. Fuel composition was grouped into 10 hydrocarbon classes (C7 to C19) including but not limited to *n*-paraffins, mono-branched paraffins, and highly branched paraffins. A matrix of each group's mass percentage was constructed. Several correlation algorithms, such as weighted average method, partial least squares analysis, genetic algorithm, and modified weighted average method were developed to correlate aviation hydrocarbon fuel compositions to

its properties. In this study, properties of interest were: density, freezing point, flash point, and net heat of combustion. The results showed that the composition-property relationships based on the modified weighted average method enabled a very precise prediction. The reported mean of absolute errors (0.82 °C for the freezing point and 0.0102 MJ/kg for the net heat of combustion predictions) and absolute relative errors (0.2085% for the density and 1.24% for the flash point predictions) were very low.

It should be noted here that this study evaluated only the ASTM approved fuels and fuel blending components. Additionally, the correlations developed did not take into consideration the influence of each hydrocarbon class on each property. Instead, each group was represented by the most abundant molecule within each class.

2.7 Summary

This chapter has displayed a summary of relevant literature pertinent to fuel composition and property analyses, as well as the ASTM standards related to the certification of conventional and alternative aviation fuels. Additionally, a primary model for chemical composition-property correlation was analyzed, adapted to today's specifications, and used as the benchmark for future experiments. Following chapters provide the specifics on the progress made in the development of advanced correlations between fuel chemical composition and properties such as hydrogen content (Chapter 3) and density (Chapter 4). Chapter 5 displays the use of these correlations for alternative blending components (HEFA) and their mixtures with Jet A. In this chapter, correlations were developed for additional properties (e.g., viscosity, flash point). The flash point equation introduced in Chapter 5 was later evaluated by using all approved blending components (Vozka, Vrtiška, Šimáček, & Kilaz, 2019).

CHAPTER 3. MIDDLE DISTILATES HYDROGEN CONTENT VIA GC×CG-FID

 Middle distillates hydrogen content via GC×GC-FID was collaborative work with Dr. Huaping Mo, Prof. Pavel Šimáček, and Prof. Gozdem Kilaz.

3.1 Introduction

Hydrogen content in middle distillates is an important parameter determining the fuel combustion efficiency. The ease of ignition and combustion increases with higher percentages of hydrogen content in the fuels (Ali, Basit, 1993). Moreover, fuels with higher hydrogen content tend to produce less soot during combustion. Hydrogen content strongly influences the net heat of combustion, which determines the vehicle range, a crucial transportation parameter. Similarly, net heat of combustion requires hydrogen content to be calculated from the gross heat of combustion (ASTM D4809).

Liquid transportation fuels such as diesel and aviation jet fuels make up a crucial portion of the middle distillates. The experimental methods for the determination of hydrogen content in fuels can be categorized into multiple techniques based on the criteria of the instrument configurations, detectors, and other operational parameters. However, on a broader scale, there are two main principles of hydrogen content determination. The first principle includes the combustion of the sample and consequent determination of water vapor produced via gravimetry, conductometry, or infrared spectrometry. Combustion methods ASTM D1018 and D5291 are arguably the most widely accepted methods for determination of the hydrogen content in middle distillates. These methods have their limitations as they are destructive and not reliable for low boiling range samples (ASTM D5291, 2016). The second group of methods is through the utilization of Nuclear Magnetic Resonance (NMR). This technique has matured since its first introduction in 1950s; since then, there are multiple ASTM standard test methods published on hydrogen content determination via low-resolution NMR: D3701 in 1987, D4808 in 1988, and D7171 in 2015. NMR data are considered to be accurate and precise. The tolerance deemed necessary by the standard D7171 repeatability is 0.11-0.16 wt.% for a hydrogen content between

10.5 and 15.5 wt. % (ASTM D7171, 2016). The above mentioned low-resolution NMR methods bring the disadvantage of requiring high volumes of the standard, solvent, and test sample (Mondal, Kumar, Bansal, & Patel, 2015).

Several papers have been published on a method to determine the hydrogen content in petroleum products via high-resolution NMR spectroscopy (Modal et al., 2015; Khadim, Wolny, Al-Dhuwaihi, Al-Hajri, & Al-Ghamdi, 2003). The results obtained with high-resolution NMR were reported to be as reliable as those with low-resolution NMR. However, high-resolution NMR technique also carries a few disadvantages. The instrument is expensive to purchase and maintain, and requires a dedicated NMR facility. A solution proposed to mitigate this issue was the utilization of benchtop NMR spectrometers, but they need to be operated by experts with deep knowledge in the field.

There is an alternative pathway for hydrogen content determination based on calculation that is available only for the aviation jet fuels - ASTM D3343. This calculation method requires density, aromatic content, and distillation data. One crucial limitation of this method is it can be less accurate for the alternative fuel blending components or their blends with Jet A/A-1 as the estimation equation was developed almost 70 years ago for only petroleum-derived fuels (ASTM D3343, 2016; AV-23-15, 2017).

Hydrogen content determination via comprehensive two-dimensional gas chromatography (GC×GC) utilizing time-of-flight mass spectrometry (Kehimkar, Hoggard, Marney, Billingsley, Fraga, Bruno, & Synovec, 2014) and flame ionization detector (Freye, Fitz, Billinngsley, & Synovec, 2016) was discussed previously. This study was focused on rocket propulsion fuels with hydrogen content in the range of 14.15 to 14.45 wt. %. GC×GC coupled with partial least-squares analysis (PLS) predicted hydrogen content with root mean squared error of cross validation of 0.05 to 0.06 wt. %. The hydrocarbon classes utilized for the calculations were *n*-paraffins, isoparaffins, cycloparaffins, di-cycloparaffins, tri-cycloparaffins, and aromatics. In spite of the fact that PLS is a fast approach, there are two significant limitations: (1) the cases where the range of the hydrogen content falls out of the range studied and (2) the sample fuel composition falling out of the range studied.

We propose a simple up-to-date alternative method for hydrogen content determination via comprehensive two-dimensional gas chromatography with flame ionization detector (GC×GC-FID) utilizing weighted average method. GC×GC-FID is a very powerful technique,

which is abundantly used in middle distillate (aviation and diesel fuels) chemical composition analysis. This method does not require any additional instruments, and is simple, easy, precise and accurate. High-resolution NMR measurements were used for the validation of the GC×GC-FID method accuracy.

3.2 Experimental

3.2.1 Materials

A total of 28 samples (Table 3.1) were tested including 9 aviation petroleum-derived jet fuels, 7 synthetically and bio-derived aviation jet fuel blending components, 4 diesel fuels, 6 synthetically and bio-derived diesel fuel blending components, 1 aviation jet fuel blend, and 1 diesel fuel blend. This broad range of fuel samples allowed to test the hydrogen content in the range of 12.72 to 15.54 wt. %.

Table 3.1 List of All Tested Samples

Fuel	Composition	Note
aviation jet fuel[a]	Jet A (Exxon Mobil)	petroleum-derived
aviation jet fuel[a]	Jet A (Shell)	petroleum-derived
aviation jet fuel[b]	JP-5	petroleum-derived; military
aviation jet fuel[b]	F-24	petroleum-derived; military
aviation jet fuel[a]	Jet A (Chevron Pillips)	petroleum-derived
aviation jet fuel	Jet A (ASTM, #1)	petroleum-derived
aviation jet fuel	Jet A (ASTM, #2)	petroleum-derived
aviation jet fuel	Jet A-1 (Twin Trans s.r.o.)	petroleum-derived
aviation jet fuel	Jet A-1 (Unipetrol, a.s.)	petroleum-derived
diesel fuel	Diesel fuel (GoLo gas station)	petroleum-derived
diesel fuel[b]	F-76, low sulfur	petroleum-derived; military
diesel fuel[b]	F-76, ultra-low sulfur	petroleum-derived; military
diesel fuel[b]	F-76 (Citgo)	petroleum-derived; military
av. blend component[a]	Alcohol-to-Jet (Gevo)	biofuel

Table 3.1 continued

av. blend component[a]	HEFA from tallow (UOP)	biofuel
av. blend component[a]	HEFA from mixed fats (Dynamic Fuels)	biofuel
av. blend component[a]	HEFA from camelina (UOP)	biofuel
av. blend component[a]	Fischer–Tropsch IPK (Sasol)	synthetic fuel
av. blend component[b]	CHCJ (ARA)	biofuel
av. blend component[c]	SIP Kerosene (Amyris Bio.)	biofuel
diesel blend component[a]	Fischer–Tropsch F-76 (Syntroleum)	synthetic fuel
diesel blend component[a]	Renewable Diesel HRD76 (Dynamic Fuels)	biofuel
diesel blend component[a]	Renewable Diesel DSH 76 (Amyris Bio.)	biofuel
diesel blend component[a]	Green Diesel (Neste Oil, #1)	biofuel
diesel blend component[a]	Green Diesel (Neste Oil, #2)	biofuel
diesel blend component[a]	Green Diesel (UOP)	biofuel
aviation jet blend[a]	50/50 vol. % Jet A/HEFA Camelina	
diesel blend[b]	50/50 vol. % F-76/HRD	

[a]provided by the Wright-Patterson Air Force Base, Dayton, Ohio

[b]provided by the Naval Air Warfare Center Aircraft Division, Patuxent River, MD

[c]provided by the Aircraft Rescue and Firefighting division of Federal Aviation Administration

3.2.2 NMR Experiment Description

^{1}D proton spectra were acquired for all samples in standard 5 mm NMR tubes (without dilution or introduction of any deuterated solvent; sample volume 500 µl at 20.3 +/- 0.2 °C on a Bruker ARX 300 MHz NMR spectrometer equipped with a QNP probe. The sweep width was 14 ppm and acquisition time was 1.93 s. Eight scans were accumulated after four dummy scans. Relaxation delays between successive scans were 5 s. The excitation pulse was chosen as 2 µs in length (about 17° excitation angle) to reduce the detrimental impacts of radiation damping.

All free induction decays were multiplied by exponential window functions with 1 Hz line-broadening, Fourier transformed, phased and base-line corrected. Molar proton

concentration was calculated by total signal integrations, with solvent *n*-decane (99+% pure; Sigma-Aldrich) as the reference (Mo & Raftery, 2008; Mo, Balko, & Colby, 2010). Proton content was calculated from the molar concentration and density, which was measured with SVM 3001 Stabinger Viscometer (Anton Paar) via ASTM D4052.

3.2.3 GC×GC-FID Experiment Description

3.2.3.1 Analysis

In this work, the GC×GC system used for the experiments was composed of an Agilent 7890B gas chromatograph, a flame ionization detector (FID), liquid nitrogen thermal modulator (LECO Corporation, Saint Joseph, MI), an Agilent 7683B series injector, and HP 7683 series auto sampler. Columns were installed in reversed phase mode; the primary column was of midpolarity and secondary column was a non-polar one. The column configuration allowed the sample to be separated according to the polarity followed by the volatility; hence, a better separation among saturates acyclic paraffins, cycloparaffins, and aromatics was achieved than in normal phase configuration. Normal phase is referred to the GC×GC column configuration where the first column separates with respect to volatility, while the second column separates with respect to polarity. The experimental parameters are listed in Table 3.2. The sample preparation consisted of the following: 10 µl of each sample was diluted in 1 ml of dichloromethane (99.9% pure; Acros Organics) in autosampler vial (1:100 dilution). Various columns, columns lengths, volume of sample injected, temperature offset (secondary oven and modulator), modulation times, temperature rates, and hot pulse durations were optimized for the best separation and efficiency.

Table 3.2 Experiment conditions of GC×GC-FID analysis

Columns	DB-17MS (30 m × 0.25 mm × 0.25 µm)
	DB-1MS (0.8 m × 0.25 mm × 0.25 µm)
Injection	0.5 µL
	split 20:1, inlet temperature 280 °C
Oven program	40-250 °C, rate 1 °C/min
Mobile gas	UHP Helium, 1.25 mL/min

Table 3.2 continued

Offsets	secondary oven 55 °C, modulator 15 °C
Modulation	6.5 s, hot pulse 1.06 s
Detector	FID, 300 °C, 200 Hz
Acquisition delay	165 s

3.2.3.2 Classification

ChromaTOF software (version 4.71.0.0 optimized for GC×GC-FID) was used for classification. The classification was developed utilizing hydrocarbon standards (over 50 compounds), GC×GC with high-resolution time-of-flight mass spectrometry (GC×GC-TOF/MS), literature (Gieleciak & Fairbridge, 2013; Striebich, Shafer, Adams, West, DeWitt, & Zabarnick, 2014; Shi, Li, Song, Zhang, & Liu, 2017), and intrinsic features of GC×GC chromatograms. A LECO Pegasus GC-HRT 4D High Resolution TOF/MS was used and experimental parameters can be found in previous paper (Lunning-Prak, Romanczyk Wehde, Ye, McLaughlin, Lunning-Prak, Foley, Kenttämaa, Trulove, Kilaz, Xu, & Cowart, 2017). Figure 3.1 displays the classification established in this study.

Table 3.3 contains the pertinent hydrocarbon classes for each carbon number in the range of C7 to C26.

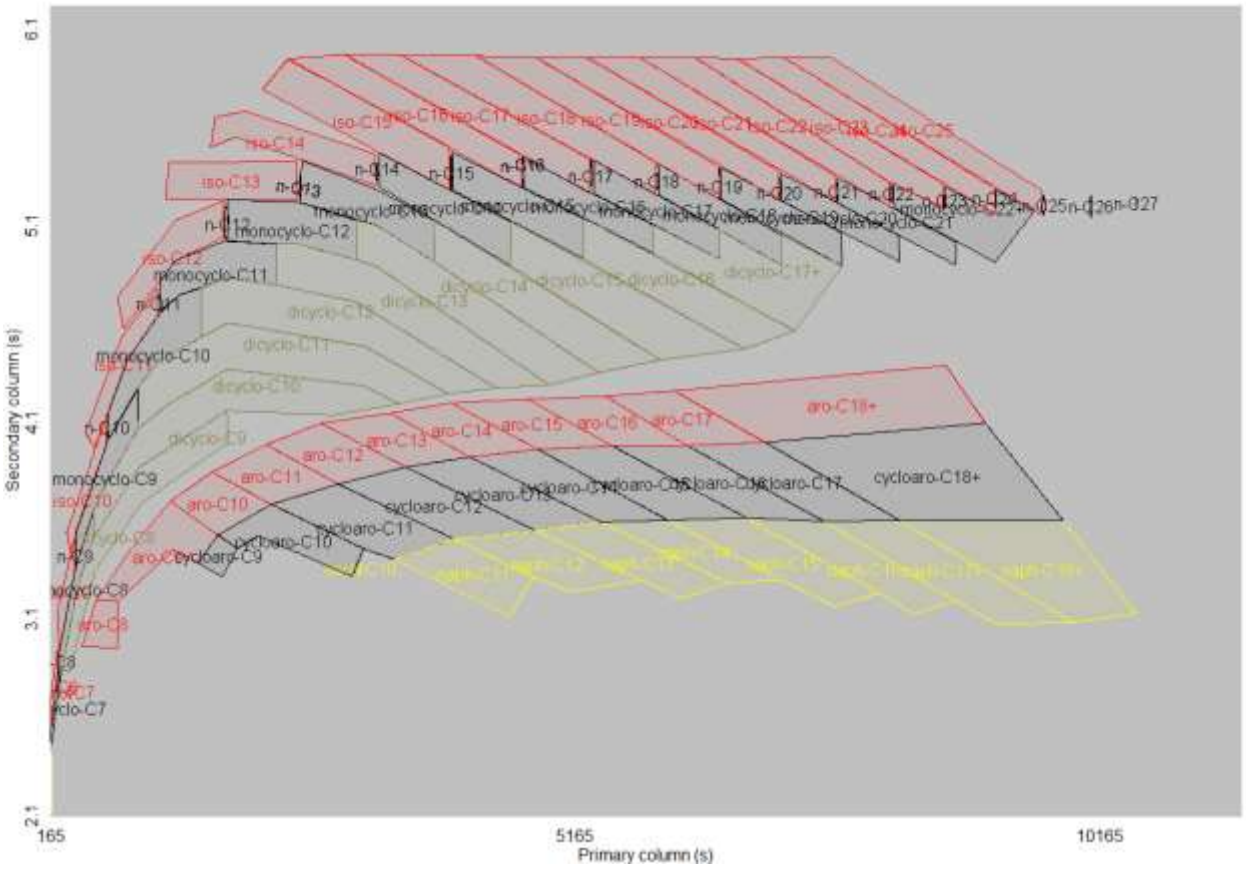

Figure 3.1 GC×GC Classification Developed in ChromaTOF Software for Reversed Phase Separation

Table 3.3 Hydrocarbon Classes Determined for Carbon Number in the Range C7 to C26

Number	Name
Class 1	*n*-paraffins
Class 2	isoparaffins
Class 3	monocycloparaffins
Class 4	di- + tricycloparaffins
Class 5	alkylbenzenes
Class 6	cycloaromatics[a]
Class 7	alkylnaphthalenes

[a]indans, tetralins, indenes, etc.

3.2.3.3 Quantitative Analysis

The FID response is linear over a very wide range of concentrations and the detector response increases with the number of hydrocarbon atoms providing CHO+ ions. Hence, the FID detector is considered as the universal hydrocarbon detector. In this work weight percentage (wt. %) was calculated via normalizing the peak area by integration of the GC×GC chromatograms. As the response factors of all hydrocarbons are approximately the same (1.00±0.05), they were set to 1 for all hydrocarbons. This approach was supported by other researchers in this field (Gieleciak & Oro, 2013).

3.2.4 Weighted Average Method

Liquid transportation fuels contain hundreds of hydrocarbon compounds. Despite this fact, the compounds can be divided into pertinent hydrocarbon classes based on the carbon number. Every hydrocarbon class has its general formula (e.g. *n*-paraffins C_nH_{2n+2}) from which the molecular weight (Table 4 and 5), carbon content, and hydrogen content (Table 6 and 7) can be easily calculated for each constituent.

Table 3.4 Molecular Weight for Hydrocarbons C7 to C17 (g/mol)

Class	C7	C8	C9	C10	C11	C12	C13	C14	C15	C16	C17
1	100.20	114.23	128.26	142.28	156.31	170.33	184.36	198.39	212.41	226.44	240.47
2	100.20	114.23	128.26	142.28	156.31	170.33	184.36	198.39	212.41	226.44	240.47
3	98.19	112.21	126.24	140.27	154.29	168.32	182.35	196.37	210.40	224.43	238.45
4	-	110.20	124.22	138.25	152.28	166.30	180.33	194.36	208.38	222.41	236.44
5	92.14	106.17	120.19	134.22	148.24	162.27	176.30	190.32	204.35	218.38	232.40
6	-	-	118.18	132.20	146.23	160.26	174.28	188.31	202.34	216.36	230.39
7	-	-	-	128.17	142.20	156.22	170.25	184.28	198.30	212.33	226.36

Table 3.5 Molecular Weight for Hydrocarbons C18 to C27 (g/mol)

Class	C18	C19	C20	C21	C22	C23	C24	C25	C26	C27
1	254.49	268.52	282.55	296.57	310.60	324.63	338.65	352.68	366.71	380.73
2	254.49	268.52	282.55	296.57	310.60	324.63	338.65	352.68	366.71	380.73
3	252.48	266.51	280.53	294.56	308.58	322.61	336.64	350.66	364.69	378.72
4	250.46	264.49	278.52	292.54	306.57	320.60	334.62	348.65	362.68	376.70
5	246.43	260.46	274.48	288.51	302.54	316.56	330.59	344.62	358.64	372.67
6	244.41	258.44	272.47	286.49	300.52	314.55	328.57	342.60	356.63	370.65
7	240.38	254.41	268.44	282.46	296.49	310.52	324.54	338.57	352.60	366.62

Table 3.6 Hydrogen Content (wt. %) for Hydrocarbons C7 to C17 (wt. %)

Class	C7	C8	C9	C10	C11	C12	C13	C14	C15	C16	C17
1	16.095	15.883	15.718	15.585	15.476	15.385	15.308	15.242	15.184	15.134	15.090
2	16.095	15.883	15.718	15.585	15.476	15.385	15.308	15.242	15.184	15.134	15.090
3	14.372	14.372	14.372	14.372	14.372	14.372	14.372	14.372	14.372	14.372	14.372
4	-	12.805	12.982	13.123	13.238	13.334	13.415	13.484	13.543	13.596	13.642
5	8.683	9.419	9.984	10.431	10.793	11.093	11.344	11.559	11.744	11.906	12.048
6	-	-	8.462	9.077	9.574	9.984	10.328	10.621	10.873	11.093	11.285
7	-	-	-	6.242	7.032	7.681	8.223	8.683	9.077	9.419	9.719

Table 3.7 Hydrogen Content (wt. %) for Hydrocarbons C18 to C27 (wt. %)

Class	C18	C19	C20	C21	C22	C23	C24	C25	C26	C27
1	15.050	15.015	14.983	14.954	14.928	14.904	14.882	14.861	14.843	14.825
2	15.050	15.015	14.983	14.954	14.928	14.904	14.882	14.861	14.843	14.825
3	14.372	14.372	14.372	14.372	14.372	14.372	14.372	14.372	14.372	14.372
4										
5	12.174	12.286								
6	11.456									
7	9.984									

If the GC×GC classification is completed properly, total hydrogen content can be calculated as the sum of hydrogen contents of each constituent weighted by the weight percentage. This method is known as weighted average (WA) method and can be expressed as Equation $H_{wt.\%} = \sum_{i=1}^{7}\sum_{j=1}^{21}(a_{i,j}b_{i,j})$ (3.1).

$$H_{wt.\%} = \sum_{i=1}^{7}\sum_{j=1}^{21}(a_{i,j}b_{i,j}) \quad (3.1)$$

In Equation $H_{wt.\%} = \sum_{i=1}^{7}\sum_{j=1}^{21}(a_{i,j}b_{i,j})$ (3.1), *a* is the hydrogen content (Table 3.6Table 3.7) and *b* is the weight fraction. The subscript *i* and *j* refer to the hydrocarbon class and carbon number, respectively. Similarly, the average molecular weight can be obtained by substituting the hydrogen content by molecular weight of each component in Equation $H_{wt.\%} = \sum_{i=1}^{7}\sum_{j=1}^{21}(a_{i,j}b_{i,j})$ (3.1). Consecutively, carbon content (wt. %) can be calculated as *100 – hydrogen content*.

3.3 Results and Discussion

3.3.1 GC×GC Quantitative Analysis

The experiments were followed by data processing, visual chromatogram inspection, and exporting raw data to MS Excel. Raw data contained the peak area and pertinent classification for each compound. In MS Excel, peak areas for each group and carbon number were summed. Weight percent for each class and carbon number was obtained through normalizing by the total sum of the sample areas. Figure 3.2 displays an example chromatogram from the set of runs executed. Table 3.8 shows an output after data processing in MS Excel and comparison between four samples from different fuel categories. The GC×GC method was validated by comparing the results with three federal research labs.

There can be trace amounts of sulfur, nitrogen, and oxygen in the fuels tested. In this work, the focus was not concentrated on analysis of heteroatoms, as the total content of these heteroatoms is strictly limited for aviation jet fuels (ASTM D1655), aviation jet fuel blending components (ASTM D7566), and diesel fuels (ASTM D975). One source of oxygen in fuels is fatty acid methyl esters (FAMEs). The maximum allowable FAME concentration in aviation jet fuels is 50 ppm, commensurate with ~10 ppm oxygen. This value is 3,000 ppm for the total sulfur amount. Alternative aviation jet fuel blending components have to contain a minimum 99.5 wt. % of carbon and hydrogen. Sulfur content is limited in these components to 15 ppm,

nitrogen to 2 ppm, and FAME to 5 ppm. Additionally, the amount of non-petroleum jet fuel blending components is limited to a maximum of 50 vol. % in Jet A. Therefore, the total concentration of heteroatoms coming from the blending components is negligibly small. Similarly, diesel fuels have three different limitations for sulfur: 15, 500, and 5000 ppm. FAME is limited by 5 vol. %, commensurate with ~0.6 wt. % oxygen. European Union limit (EN 590) is 10 ppm for sulfur and 7 vol. % for FAME. The limit for nitrogen content is not established in ASTM D975 nor in the EN 590. Generally, for diesel with 15 ppm sulfur limit, the nitrogen content will be of the same order.

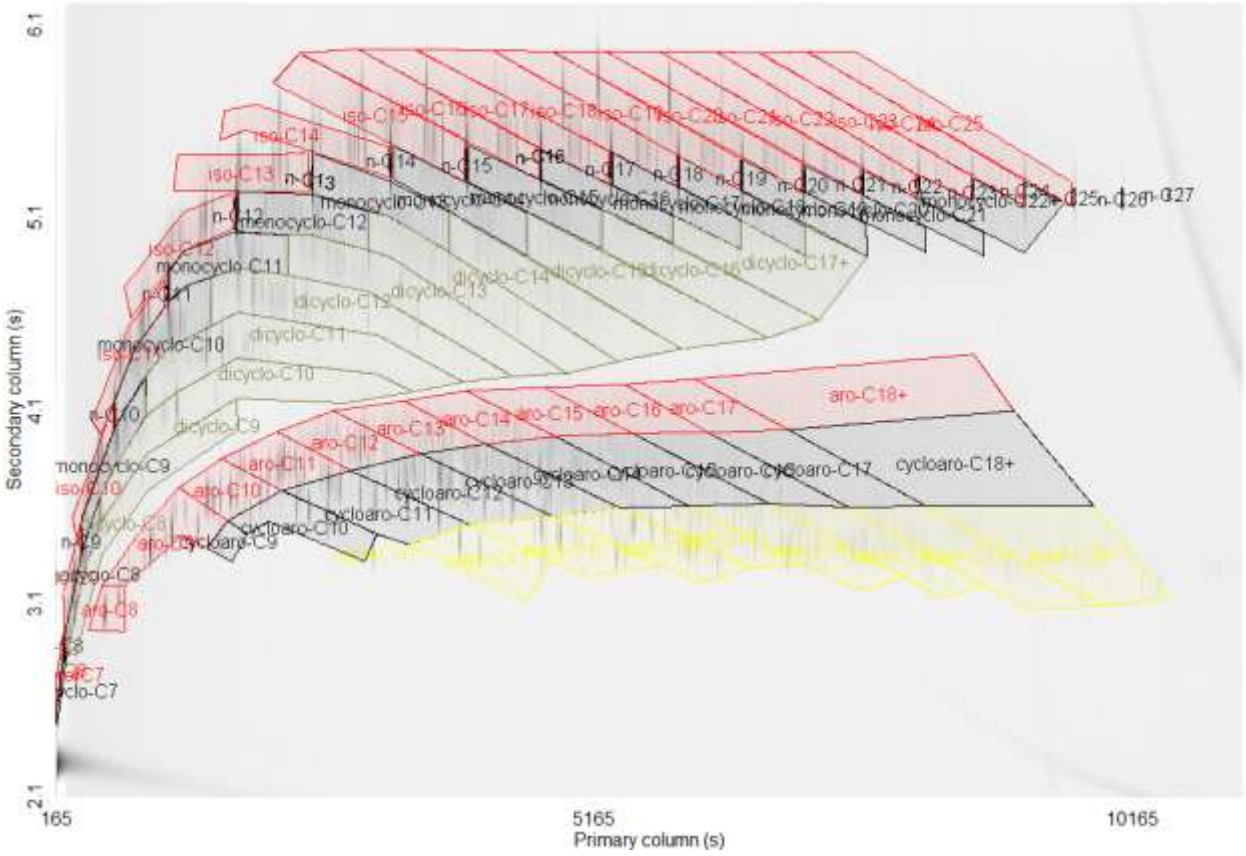

Figure 3.2 F–76 Military Diesel Chromatogram with Classification Obtained from GC×GC-FID

Table 3.8 Fuel Chemical Composition (wt. %) of Low Sulfur F-76, Jet A (Exxon Mobil), Fischer–Tropsch IPK (Sasol), and Green Diesel (Neste Oil, #1) Obtained from GC×GC-FID

n-paraffins	F-76	Jet A	FT-IPK	Green Diesel
C8	0.13	0.83	0.00	0.13
C9	0.42	5.05	0.00	0.20
C10	1.54	4.96	0.10	0.18
C11	2.32	3.36	0.00	0.00
C12	2.22	2.37	0.10	0.18
C13	2.21	1.90	0.08	0.23
C14	2.13	1.27	0.04	0.40
C15	1.93	0.76	0.03	0.88
C16	1.71	0.36	0.01	2.84
C17	1.58	0.10	0.00	1.76
C18	1.32	0.02	0.00	4.40
C19	1.10	0.00	0.00	0.04
C20	0.95	0.00	0.00	0.08
C21	0.72	0.00	0.00	0.00
C22	0.45	0.00	0.00	0.01
C23	0.24	0.00	0.00	0.00
C24	0.11	0.00	0.00	0.00
C25	0.05	0.00	0.00	0.00
C26	0.02	0.00	0.00	0.00
C27	0.00	0.00	0.00	0.00
total *n*-paraffins	21.15	20.97	0.35	11.33

isoparaffins	F-76	Jet A	FT-IPK	Green Diesel
C7	0.00	0.00	0.00	0.00
C8	0.09	0.28	0.52	0.12
C9	0.40	4.97	7.97	0.22
C10	1.32	6.94	19.35	0.32
C11	2.70	5.36	23.48	0.34

Table 3.8 continued

C12	2.70	3.69	27.74	0.41
C13	3.34	3.51	11.78	0.69
C14	3.11	2.63	5.08	1.76
C15	2.87	1.97	1.06	5.41
C16	2.33	0.94	0.00	18.64
C17	1.85	0.23	0.00	14.44
C18	2.23	0.06	0.00	44.41
C19	2.46	0.00	0.00	0.67
C20	1.35	0.00	0.00	1.00
C21	0.69	0.00	0.00	0.03
C22	0.34	0.00	0.00	0.05
C23	0.08	0.00	0.00	0.00
C24	0.02	0.00	0.00	0.00
C25+	0.00	0.00	0.00	0.00
total isoparaffins	27.89	30.58	96.98	88.52

monocycloparaffins	F-76	Jet A	FT-IPK	Green Diesel
C7	0.10	0.22	0.00	0.02
C8	0.62	3.74	0.06	0.02
C9	1.82	4.47	0.39	0.00
C10	2.71	4.10	0.77	0.03
C11	2.64	2.85	0.83	0.00
C12	2.64	2.25	0.33	0.00
C13	2.89	1.67	0.00	0.00
C14	2.01	0.69	0.00	0.00
C15	1.47	0.12	0.00	0.00
C16	1.36	0.00	0.00	0.01
C17	1.41	0.00	0.00	0.05
C18	1.05	0.00	0.00	0.00
C19	0.83	0.00	0.00	0.00

Table 3.8 continued

C20	0.15	0.00	0.00	0.00
C21	0.00	0.00	0.00	0.00
C22+	0.00	0.00	0.00	0.00
total monocycloparaffins	21.70	20.12	2.37	0.13

di- + tricycloparaffins	F-76	Jet A	FT-IPK	Green Diesel
C8	0.07	0.23	0.00	0.00
C9	0.53	0.78	0.00	0.00
C10	1.18	1.01	0.00	0.00
C11	1.00	1.07	0.00	0.00
C12	0.99	0.80	0.00	0.00
C13	0.33	0.27	0.00	0.00
C14	0.57	0.14	0.00	0.00
C15	0.13	0.00	0.00	0.00
C16	0.03	0.00	0.00	0.00
C17+	0.00	0.00	0.00	0.00
total di- + tricycloparaffins	4.83	4.30	0.00	0.00
total cycloparaffins	26.53	24.41	2.37	0.13

alkylbenzenes	F-76	Jet A	FT-IPK	Green Diesel
C7	0.06	0.07	0.00	0.03
C8	0.26	1.79	0.01	0.00
C9	1.30	4.86	0.07	0.00
C10	1.75	3.27	0.08	0.00
C11	1.33	2.15	0.04	0.00
C12	0.94	1.72	0.00	0.00
C13	0.63	1.04	0.00	0.00
C14	0.33	0.35	0.00	0.00
C15	0.25	0.19	0.00	0.00
C16	0.20	0.02	0.00	0.00

Table 3.8 continued

C17	0.19	0.00	0.00	0.00
C18+	0.14	0.00	0.00	0.00
total alkylbenzenes	7.40	15.46	0.20	0.03

cycloaromatics	F-76	Jet A	FT-IPK	Green Diesel
C9	0.05	0.14	0.00	0.00
C10	0.44	0.78	0.00	0.00
C11	1.29	1.73	0.01	0.00
C12	1.68	2.24	0.05	0.00
C13	1.52	1.26	0.01	0.00
C14	1.19	0.73	0.00	0.00
C15	1.02	0.01	0.00	0.00
C16	0.36	0.00	0.00	0.00
C17	0.03	0.00	0.00	0.00
C18+	0.00	0.00	0.00	0.00
total cycloaromatics	7.58	6.89	0.08	0.00

alkylnaphthalenes	F-76	Jet A	FT-IPK	Green Diesel
C10	0.25	0.11	0.00	0.00
C11	1.06	0.41	0.02	0.00
C12	1.79	0.64	0.00	0.00
C13	1.78	0.43	0.00	0.00
C14	0.81	0.09	0.00	0.00
C15	1.24	0.01	0.00	0.00
C16	1.18	0.00	0.00	0.00
C17	0.97	0.00	0.00	0.00
C18+	0.36	0.00	0.00	0.00
total alkylnaphthalenes	9.44	1.69	0.02	0.00
total aromatics	24.42	24.05	0.30	0.03
total	100.00	100.00	100.00	100.00

3.3.2 GC×GC Linearity

The linearity of the GC×GC instrument was determined utilizing two standards: *n*-nonane and naphthalene. The concentration values for the standards were within the range of 1 to 500 ppm. The calibration graphs obtained yielded R^2 values of 0.9999 and 0.9998 for *n*-nonane and naphthalene, respectively; suggested good linearity.

3.3.3 Hydrogen Content (GC×GC vs. NMR)

Data acquired by the researchers responsible for the two analytical instruments utilized in this study were not communicated nor shared until the end of runs. Selected NMR data were collected in triplicates, presented standard deviation values below 0.020 wt. %. GC×GC data were collected in triplicates yielding a standard deviation value of 0.005 wt. %. The average values were considered for the comparison of the two methods to measure the total hydrogen content. NMR and GC×GC standard deviation values exhibited high precision of both instruments.

As mentioned above, during the classification process, over 50 hydrocarbon standard compounds were measured. Hydrogen content for these standards can be easily calculated. These standards were used as the basis for the method development; hence, pertinent results were omitted in Figure 3.3. Two of these standards were measured by NMR as an additional blind test to reassure the accuracy. *n*-Heptane (HPLC grade pure; Fisher Chemical) with hydrogen content 16.10 wt. % and 1-methylnaphthalene (97+% pure; Acros Organics) with hydrogen content 7.09 wt. % yielded the total hydrogen content via NMR 16.13 and 7.09 wt. %, respectively.

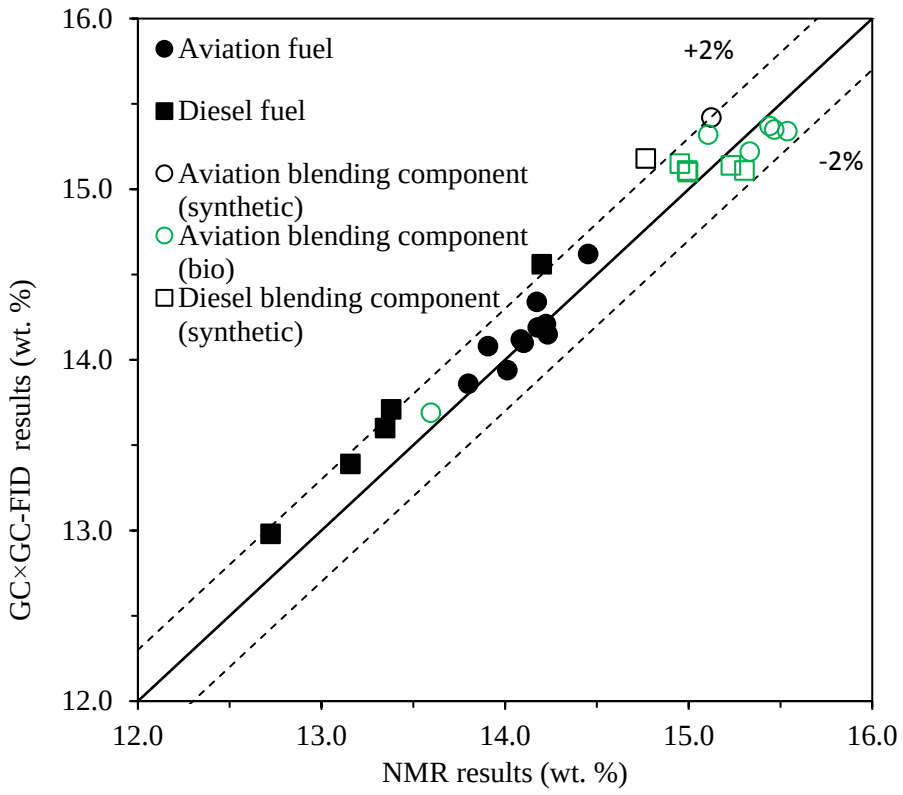

Figure 3.3 Plot of GC×GC-FID versus NMR hydrogen content with weight average (WA) method

Figure 3.3 depicts a plot of GC×GC-FID versus NMR hydrogen content results with WA method. There was only a small number of data points (3) collected that fell out of the ±2% relative error range. The three outlier samples, 50/50 F-76/HRD, Low Sulfur F-76 (Exxon Mobil), and Fischer–Tropsch F–76 (Syntroleum), still stayed within the envelope of ±3% relative error range. The correlation coefficient (R^2) of 0.9617 proved the effectiveness of the WA method.

There are three potential reasons that can explain the differences observed in the data sets obtained from two techniques: the systematic over reporting by GC×GC can be due to not taking FID response factors into consideration. This method relies heavily on the accuracy of the classification template. Once the classification borders are accurately set, each compound elutes within its hydrocarbon class and carbon number. However, this is very challenging process especially for compounds with higher carbon numbers. This challenging can introduce an additional reason to the differences between these two techniques. The third reason can be the

systematic under reporting of the NMR output due to the Lorentzian peak shape that overextends to infinite horizontal asymptotes parallel to the positive and negative x-axes. It was assumed that ~99% of the peak area was included in the data evaluation. As an added validation of the results obtained from the two techniques studied, a third method to determine the fuel hydrogen content: ASTM D3343 method was utilized.

3.3.4 Hydrogen Content (GC×GC and D3343 vs. NMR)

The hydrogen content was calculated via ASTM D3343 for selected samples. The comparison of results obtained from GC×GC and D3343 to NMR is displayed in Figure 3.4 below. For conventional aviation jet fuels, the results obtained from the GC×GC were closer to those obtained from NMR when compared to D3343. For diesel fuels, D3343 gave data closer to NMR results compared to those of GC×GC. As for the alternative aviation jet fuel blending components, the results obtained from GC×GC and D3343 showed similar proximity to those obtained from NMR. It should be noted here, that in spite of the fact this method has been approved only for aviation fuels, the hydrogen content was also calculated for the other fuel types utilized in this study.

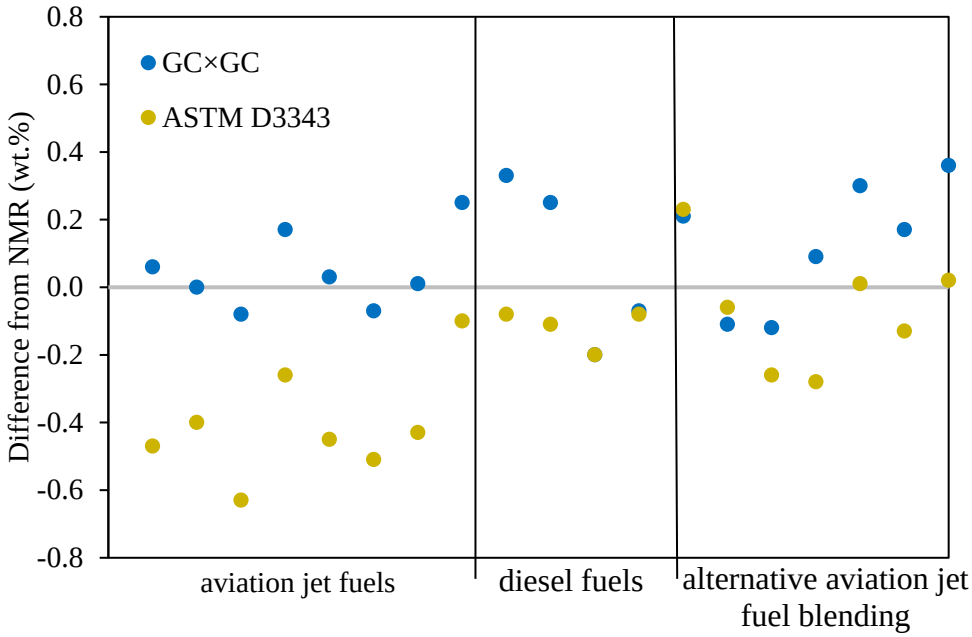

Figure 3.4 A Representative Comparison of Bias of GC×GC and D3343 Methods and Hydrogen Content Obtained by NMR

3.4 Conclusion

In this study, a method for simple and fast hydrogen content calculation via comprehensive two-dimensional gas chromatography with FID was developed for middle distillates. This approach can easily be utilized to determine the carbon content as well as the average molecular weight. Currently, NMR is accepted by the subject matter experts as the accurate analytical technique for hydrogen content determination. GC×GC-FID, in comparison to NMR yielded results with 2% relative error. Additionally, GC×GC provided results closer to those of ASTM D3343 for aviation fuels, which the standard D3343 was originally developed for. Therefore, GC×GC FID method can be concluded as accurate. It should be noted here, that different correlation algorithms (partial least square, etc.) were not applied nor tested. These methods have the potential to decrease the relative error between GC×GC-FID and NMR measurements; however, the scope of this work was not optimizing the proximity (correlating) of the results obtained by the two techniques, but rather evaluate GC×GC-FID efficiency. Future work should focus on better classification for higher carbon numbers, due to the fact the relative error was increasing with increasing complexity of the samples.

CHAPTER 4. JET FUEL DENSITY VIA GC×GC-FID

 Jet fuel density via GC×GC-FID was collaborative work with Brent Modereger (who prepared Table 4.3), Anthony Park (who created PLS and SVM correlations in MATLAB), Jeff Zhang (who found density values in literature), Prof. Rodney Trice, Prof. Hilkka Kenttämma, and Prof. Gozdem Kilaz.

4.1 Introduction

Density of (alternative) aviation fuels is one of the main parameters indicative of fuel quality. Fuel is filled into aircraft volumetrically; hence, density plays an especially important role in determining the total aircraft load as well as the aircraft range. Density is also used in flow calculations, fuel gaging, metering device adjustments, and fuel thermal expansion calculations (CRC No. 530, 1983).

Currently, five alternative aviation fuel blending components have been approved for use in gas turbine engines. These blending components are produced via several pathways: Fischer-Tropsch (FT) process using coal, natural gas, or biomass as feedstock (De Klerk, 2014); hydroprocessing (hydrotreatment and hydroisomerization) of vegetable oils or animal fats (Gupta, Rehman, & Sarviva, 2010); sugar fermentation; and via an Alcohol-to-Jet (ATJ) process that is composed of three-steps (alcohol dehydration, oligomerization, and hydrogenation), utilizing corn, unrefined sugars, switchgrass, corn stover, corn fiber, glucose, wheat straw, liquefied corn starch, barley straw, sweet potato slurry, whey permeate, unrefined sugarcane, or woody biomass as a feedstock (Wang & Tao, 2016; ICAO, 2011). The chemical composition of the product obtained from each process is different, which requires attention as the constituents of these fuel blending components affect the fuel properties. These are expected to fall within a specific range as deemed necessary by fuel standards. One of the important properties for aviation fuels is the density at 15 °C. It is known that density increases in the order of paraffins < cycloparaffins < aromatics for the same carbon number. Density of *n*-paraffins is in most cases slightly higher than isoparaffins of the same carbon number. Establishing accurate fuel chemistry-property correlations is a still major subject of interest by multiple researchers.

Research focused on correlating the fuel chemical composition to its properties began in the 1980s (Cookson et al., 1985, 1987, 1990, 1992, 1995). First correlations between petroleum-based jet fuel composition and density were published in 1985 (Cookson et al., 1985). These studies used gas chromatography (GC), nuclear magnetic resonance (NMR) spectroscopy, and high-pressure liquid chromatography (HPLC) to determine the fuel chemical composition. Density predictions were based on the total content of *n*-paraffins and aromatic compounds. Later efforts focused on improving these models by adding distillation profile information into the calculations, which allowed for the prediction of the density of alternative aviation fuels (Cookson et al., 1995). Alternative fuels used in these studies were obtained via hydroliquefaction and FT process of coal. Liu et al. (2007) were the first to use an artificial neural network in 2007 to predict the density of aviation jet fuels based on their chemical composition determined via GC-MS. An alternative chemometric modeling (partial least square) of near-infrared absorption spectra was first mentioned in the literature by Morris et al. (2009). This approach was later updated by utilizing GC-MS (Cramer et al., 2014).

A comprehensive two-dimensional gas chromatograph (GC×GC) capable of simultaneous mass spectrometry and flame ionization (FID) detection was used in 2017 for the development of quantitative chemical composition-property relationships for petroleum-based jet fuels and one FT synthetic fuel, as described by Shi et al. (2017). These authors tested several algorithms to correlate the density to fuel chemical composition. Partial least squares and modified weighted average methods yielded the most accurate results. However, these correlations were developed only for density values at 20 °C. Therefore, this study explores the use of different algorithms and approaches, which all potentially increase the predictive capability of the models studied. Additionally, this paper focuses on utilizing these methods to predict the density of aviation jet fuels at 15 °C, a capability pertinent to the field of aviation (D1655, 2018). Furthermore, this is the first reported use of two-dimensional gas chromatography with flame ionization detector (GC×GC-FID) for determining fuel density at 15 °C.

4.2 Experimental

4.2.1 Materials

Total sample set contained 50 samples composed of calibration and validation samples. Calibration sample set was comprised of 38 samples (Table 4.1), including 25 military petroleum-derived aviation jet fuels, 4 petroleum-derived Jet A fuels, 2 petroleum-derived Jet A-1 fuels, 6 synthetic or bio-derived alternative jet fuel blending components, and 1 jet fuel blend. Validation sample set was prepared manually by blending jet fuel and alternative aviation blending component from Table 4.1 in various ratios. Validation set contained 12 samples following the blending limitations of ASTM D7566: HEFA from tallow, HEFA from mixed fats, HEFA from camelina, and Fischer–Tropsch IPK were blended in 20 and 50 vol. % with Jet A. Alcohol-to-Jet was blended in 10 and 30 vol. % with Jet A. SIP Kerosene was blended in 5 and 10 vol. % with Jet A.

Table 4.1 List of Tested Samples

Fuel	Composition	Note
aviation jet fuel[a]	25 different samples of F-24	petroleum-derived; military
aviation jet fuel	Jet A (ASTM)	petroleum-derived
aviation jet fuel[b]	Jet A (Chevron Pillips)	petroleum-derived
aviation jet fuel[b]	Jet A (Exxon Mobil)	petroleum-derived
aviation jet fuel[b]	Jet A (Shell)	petroleum-derived
av. blend component[b]	Alcohol-to-Jet (Gevo)	biofuel
av. blend component[b]	HEFA from tallow (UOP)	biofuel
av. blend component[b]	HEFA from mixed fats (Dynamic Fuels)	biofuel
av. blend component[b]	HEFA from camelina (UOP)	biofuel
av. blend component[b]	Fischer–Tropsch IPK (Sasol)	synthetic fuel
av. blend component[c]	SIP Kerosene (Amyris Bio.)	biofuel
aviation jet fuel	Jet A-1 (Twin Trans s.r.o.)	petroleum-derived
aviation jet fuel	Jet A-1 (Unipetrol, a.s.)	petroleum-derived
aviation jet blend[b]	50/50 vol. % Jet A/HEFA Camelina	

[a]provided by the Naval Air Warfare Center Aircraft Division, Patuxent River, MD
[b]provided by the Wright-Patterson Air Force Base, Dayton, Ohio
[c]provided by the Aircraft Rescue and Firefighting division of Federal Aviation Administration, Egg Harbor Township, NJ

In addition to above samples, density was measured for the following compounds: n-heptane (99% pure; Sigma-Aldrich), n-octane (≥99.5% pure; Sigma-Aldrich), n-nonane (≥95% pure; Fluka), n-decane (98% pure; ETI Science), n-dodecane (≥99% pure; Sigma-Aldrich), n-pentadecane (≥99% pure; Sigma-Aldrich), 2,2,4,4,6,8,8-heptamethylnonane (98% pure; Acros Organics), 1-ethyl-1-methylcyclohexane (>99% pure; TCI), n-butylcyclohexane (≥99% pure, Sigma-Aldrich), decahydronaphthalene (≥99% pure; Fluka), toluene (99.8% pure, Acros Organics), 1,3-dimethylbenzene (99% pure; Alfa Aesar), 1,2,3,4-tetrahydronaphthalene (99% pure; Sigma-Aldrich), and 1-methylnaphthalene (97+% pure; Acros Organics).

4.2.2 Density Measurements

The density of all samples was measured using an SVM 3001 Stabinger Viscometer (Anton Paar) via ASTM D4052. The instrument was cleaned, calibrated, and checked for accuracy per instructions provided by the vendor. Anton Paar-certified standards (APN7.5 and APN26) were utilized. Samples were measured five times at 15 °C, and standard deviations were calculated automatically by the instrument. The average standard deviation value was -0.00003 g/cm^3, demonstrating a high precision for the measurements. Petroleum-based aviation fuel density value is required to be in the range between 0.775 and 0.840 g/cm^3 (D1655, 2018), while for alternative fuel blending components (ASTM D7566), the density value is required to be in the range of 0.730-0.770 g/cm^3 for Fischer-Tropsch Hydroprocessed Synthesized Paraffinic Kerosine, Synthesized Paraffinic Kerosine from Hydroprocessed Esters and Fatty Acids (HEFA), and Alcohol-to-Jet Synthetic Paraffinic Kerosene (ATJ), and between 0.765 and 0.780 g/cm^3 for Synthesized Iso-Paraffins from Hydroprocessed Fermented Sugars (SIP). Samples utilized in this study were selected to cover the complete density range.

4.2.3 Analysis of the chemical composition of the fuel samples

4.2.3.1 GC×GC-TOF/MS analysis

Qualitative analysis of the samples was performed using two-dimensional gas chromatography with electron ionization high resolution time-of-flight mass spectrometry (GC×GC-TOF/MS). LECO Pegasus GC-HRT 4D (EI) High Resolution TOF/MS (LECO

Corporation, Saint Joseph, MI) was equipped with an Agilent 7890B gas chromatograph and a thermal modulator cooled with liquid nitrogen. The system was also equipped with an Agilent G4513A auto injector. Primary mid-polar column Rxi-17Sil ms (60 m × 0.25 mm × 0.25 µm) was connected to a secondary nonpolar column Rxi-1 ms (2.0 m × 0.25 mm × 0.25 µm). Both columns were procured from Restek (Bellefonte, PA). The transfer line, ion source, and inlet temperatures were maintained at 300, 250, and 280 °C, respectively. Oven temperature program started at 40 °C (hold time 0.2 min) and ended at 160 °C (hold time 5 min) with a temperature ramp rate of 3 °C/min. The offsets in the temperature of the secondary oven and modulator were 15 and 15 °C, respectively. Modulation period was set to 1.2 s, with hot pulse duration of 0.20 s. Each sample (10 µl) was diluted in 1 ml of *n*-hexane (≥99.0% pure; Acros Organics) in an autosampler vial (1:100 dilution). Injection volume was 0.5 µL with a 20:1 split ratio. Acquisition delay was 400 s. Ionization was achieved using 70 eV EI. The acquisition rate of mass spectra was 200 Hz with a detector gain voltage of 1750 V. ChromaTOF (Version 1.90.60.0.43266) was utilized for data collection (with an m/z of 45-550), processing, and analysis. Identification of the compounds was performed by matching the measured mass spectra (match threshold of >700) with Wiley (2011) and NIST (2011) mass spectral databases.

4.2.3.2 GC×GC-FID analysis

For quantitative analysis, a comprehensive two-dimensional gas chromatograph (Agilent 7890B GC) with a flame ionization detector (FID) and a thermal modulator (LECO Corporation, Saint Joseph, MI) cooled with liquid nitrogen was used. This system was also equipped with an Agilent 7683B series injector and an HP 7683 series auto sampler. Primary mid-polar column DB-17MS (30 m × 0.25 mm × 0.25 µm) was connected to a secondary nonpolar column DB-1MS (0.8 m × 0.25 mm × 0.25 µm). This column setup is known as a reversed phase setup and it allows for the improved separation of saturated and aromatic compounds. Both columns were provided by Agilent (Santa Clara, CA). FID and inlet temperatures were 300 and 280 °C, respectively. Oven temperature program started at 40 °C (hold time 0.2 min) and ended at 160 °C (hold time 5 min) with a temperature ramp rate of 1 °C/min. Secondary oven and modulator temperature offsets were 55 and 15 °C, respectively. Modulation period was set to 6 s with a hot pulse duration of 1.06 s. Each sample (10 µl) was diluted in 1 ml of dichloromethane

(99.9% pure; Acros Organics) in an autosampler vial (1:100 dilution). Injection volume was 0.5 µL with a 20:1 split ratio. Acquisition delay was 165 s. FID data were collected at an acquisition rate of 200 Hz. GC×GC-FID classification utilizing ChromaTOF software (version 4.71.0.0 optimized for GC×GC-FID) has been described in detail in a previous publication (Vozka et al., 2018). Figure 4.1 displays the fuel constituent classification established in this study. Classification is based on seven hydrocarbon classes (*n*-paraffins, isoparaffins, monocycloparaffins, di- and tricycloparaffins, alkylbenzenes, cycloaromatic compounds (indans, tetralins, indenes, etc.), and alkylnaphthalenes) with 7 – 20 carbon atoms. The weight percentage of each compound in the sample was calculated by utilizing the ratio of the compound peak area to the sum of all peak areas measured for the sample.

4.2.3.3 Chemical composition-density correlation algorithms

Three statistical modeling methods were used in order to process the compound weight percent data obtained from GC×GC-FID: weighted average (WA) method, partial least squares (PLS) regression, and a high dimensional method using regularized support vector machines (SVM).

WA has been described in a previous paper where middle distillates were studied (Martens, Tondel, Tafintseva, Kohler, Plahte, Vik, & Omholt, 2013). Briefly, the density of the sample can be determined by calculating the sum of density of each compound group weighted by the weight percentage of each group as expressed in Equation $D_{(g/cm^3)} = \sum_{i=1}^{7}\sum_{j=1}^{7}(a_{i,j}b_{i,j})$ (4.1).

$$D_{(g/cm^3)} = \sum_{i=1}^{7}\sum_{j=1}^{7}(a_{i,j}b_{i,j}) \quad (4.1)$$

where *a* is the density Table 4.3 and *b* is the weight fraction. The subscripts *i* and *j* refer to the hydrocarbon class and number of carbon atoms, respectively.

PLS is a common methodology in linear multivariate regression. This method is commonly used in chemometrics. It is derived from principal component regression and acts as its "successor". PLS avoids the errors in linear regression that occur in cases where the input data matrix *X* is not full rank (more predictors than observations or more observations than predictors). This is avoided by creating a lower dimensional projection in order to capture linear correlations and variability, which is the foundation of principal component analysis. This still

does not encompass the relevance of principal components that may influence the response variable at different levels. To fix this problem, PLS incorporates collinearities between input matrix *X* and response matrix *Y*. The general underlying model is as follows: let *X* be an *n x p* matrix of predictor variables and *Y* be an *n x q* matrix of response variables. The response matrix can then be approximated as stated in Equation $Y = y_0 + T_A Q_A^T + F_A$

(4.2).

$$Y = y_0 + T_A Q_A^T + F_A \tag{4.2}$$

This can be rewritten via substitution of variables into Equation $Y = b_{0A} + XB_A + F_A$

(4.3)

$$Y = b_{0A} + XB_A + F_A \tag{4.3}$$

where $B_A = V_A Q_A^T$, $b_{0A} = y_0 - x_0 B_A$, and F_A is the vector of residuals. The vector of residuals and intercepts can be added together into one intercept value. Here, Q_A is the coupling between individual variables in *Y* and the *A* orthogonal components in the matrix $T_A = (X - x_0)V_A$. T_A can be thought of as scaled scores which define the covariance of the rows of X. What differentiates PLS from a principal component regression method is the definition of V_A. While this term refers to the maximal covariance in *X*, the term references the maximal covariance between *X* and *Y* in PLS. When considering each hydrocarbon class as a single predictor, PLS is a very powerful tool with great predictive capabilities. However, in very highly underdetermined systems, PLS may not perform as effectively. Despite this, PLS is capable of compensating for these systems to some extent (Martens at al., 2013; Vincenzo, 2010; Haenlein & Kaplan, 2004; Suykens, Van Gestel, & De Brabanter, 2002).

The final model relies heavily on Support Vector Machines (SVM). The philosophy behind SVM is to apply a machine learning method onto creating a linear regression model (Suykens et al., 2002). This model can be derived by applying a least squares regression formula on a derived SVM model, Equation $y(x) = \sum_{k=1}^{N} a_k K(x, x_k) + b$ (4.4).

$$y(x) = \sum_{k=1}^{N} a_k K(x, x_k) + b \tag{4.4}$$

which is then considered given a training set $\{x_k, y_k\}_{k=1}^{N}$. Consecutively, these parameters can be estimated using stochastic gradient descent (SGD) or dual coordinate descent (DCD) method. While both can be used for large scale optimization of the SVM model, the SGD method

depends on a stochastic factor z_i added to a gradient descent method expressed in Equation $w_{t+1} = w_t - \gamma_t \nabla_w Q(z_t, w_t)$ (4.5).

$$w_{t+1} = w_t - \gamma_t \nabla_w Q(z_t, w_t) \quad (4.5)$$

In spite of the fact that above model is drastic simplification of the gradient descent method, this results in an approximation of the true gradient that can include a lot of noise (Bottou, 2010). Alternatively, the DCD method is a newer method, which can more efficiently solve linear SVM methods (Ho & Lin, 2012; Hsieh, Chang, Lin, Keerthi, & Sundarajan, 2008). Both methods were observed to be capable for cases with underdetermined systems, which is useful in creating a predictive model that accounts for each compound.

4.3 Results and discussion

4.3.1 GC×GC qualitative analysis

When calculating the density of a group of compounds two approaches can be used. An average density can be calculated by considering the density of every compound of a particular hydrocarbon class and carbon number. However, this process can become very cumbersome as the number of isomers in a given compound group increases. For example, finding the density of *n*-paraffin with eight carbons involves finding the density of only a single compound: *n*-octane. However, determining the average density of all alkylbenzenes with eight carbons requires involving five isomers (ethylbenzene, 1,1-dimethylbezene, 1,2-dimethylbezene, 1,3-dimethylbezene, and 1,4-dimethylbezene). The number of structural isomers (not including enantiomers) for dodecane, tridecane, and tetradecane are 355, 802, and 1,858, respectively. The complexity of this approach is avoided by using the second approach, which is based on a singular compound used to represent each hydrocarbon class and carbon number. Therefore, the GC×GC-TOF/MS chromatograms was studied for all 38 samples. After considering only those peaks with a minimum similarity score of 700 and excluding any peaks that were identified as the same compound (except that with the greatest peak area), a total of 10,667 peaks were detected with peak area percent over 0.000672%. The representative compound was selected as the compound with the greatest peak area percent for each compound class, only if the density

for that compound could be found in the literature. The approach for the cases where density was not found is explained in Section 4.3.3.

4.3.2 GC×GC quantitative analysis

The standards utilized for the determination of the linear range of the signal obtained using the GC×GC instrument were *n*-nonane and naphthalene with concentration values in the range of 1 to 500 ppm. The regression coefficient (R^2) values of 0.9999 and 0.9998 for *n*-nonane and naphthalene, respectively, validated linearity. Reliability of the GC×GC method was validated by comparing the results to those from three US military research labs. A sample chromatogram of the set of experiments is displayed in Figure 4.1. Table 4.2 provides the comparative data obtained for the four samples representing different fuel types.

Petroleum-derived jet fuels contain approximately 2000 hydrocarbon compounds. For the purpose of classification, these compounds were divided into pertinent groups based on their hydrocarbon classes and carbon number (GC×GC-FID classification). After this division, depending on the number of possible isomers, each compound group contained one (*n*-paraffins, naphthalene, etc.) or several compounds. Jet fuels can also contain trace amounts (ppm) of heteroatoms (S, N, O), which are strictly limited for aviation jet fuels (ASTM D1655) and aviation jet fuel blending components (ASTM D7566). Therefore, the classification did not take heteroatoms into consideration.

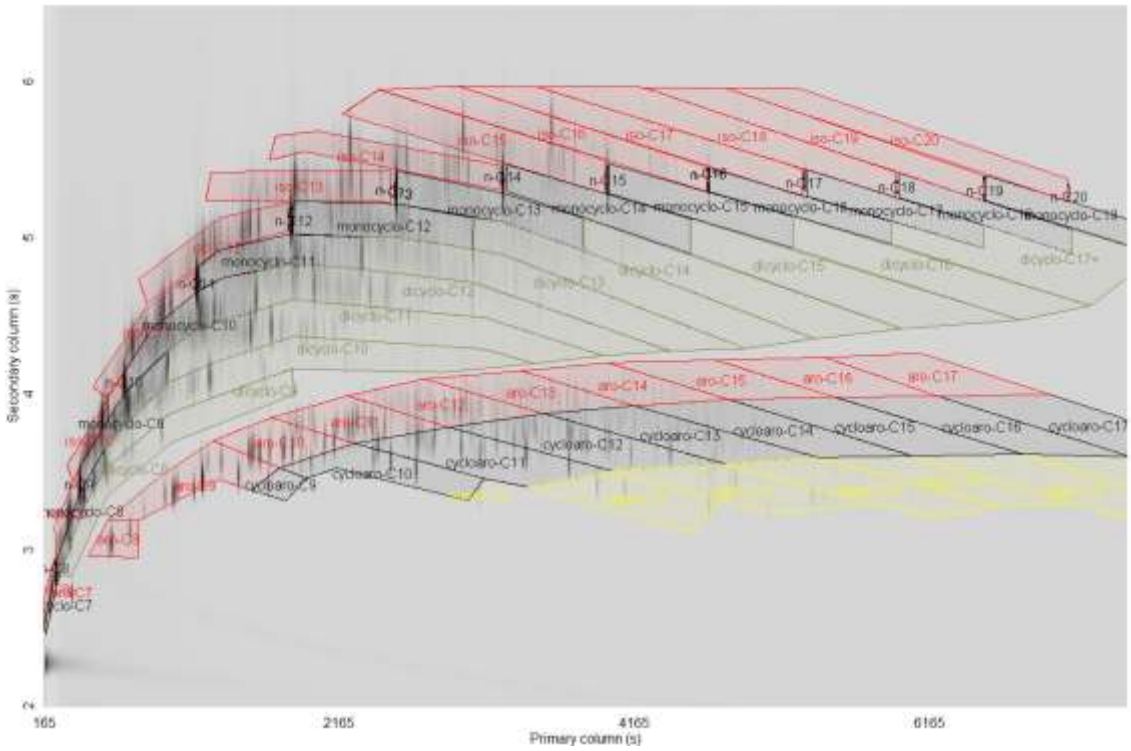

Figure 4.1 F-24 (Luke AFB, AZ) GC×GC-FID Chromatogram Showing Classification Regions Used

Table 4.2 The Chemical Compositions (wt. %) of SIP Kerosene (Amyris Bio.), HEFA from Camelina (UOP), Jet A-1 (Unipetrol, a.s.), and F-24 (Luke AFB, AZ) Obtained by Using GC×GC-FID.

n-paraffins	SIP	HEFA	Jet A-1	F-24
C8	0.00	1.56	0.79	0.28
C9	0.00	2.15	1.45	2.61
C10	0.00	1.38	4.66	3.30
C11	0.00	0.96	6.81	3.22
C12	0.00	0.83	5.59	2.63
C13	0.00	0.65	3.50	2.27

Table 4.2 continued

	C14	0.00	0.25	0.58	1.72
	C15	0.00	0.51	0.04	1.18
	C16	0.00	0.13	0.00	0.68
	C17	0.00	0.10	0.00	0.27
	C18	0.00	0.00	0.00	0.11
	C19	0.00	0.00	0.00	0.04
	C20	0.00	0.00	0.00	0.01
total *n*-paraffins		0.00	8.53	23.41	18.32

isoparaffins		SIP	HEFA	Jet A-1	F-24
	C8	0.00	1.48	0.48	0.41
	C9	0.00	11.18	1.57	2.60
	C10	0.00	11.36	3.48	5.39
	C11	0.00	9.88	7.12	4.91
	C12	0.00	8.48	6.07	4.18
	C13	0.00	8.17	5.86	4.41
	C14	0.05	6.29	2.57	3.35
	C15	99.43	5.59	0.32	2.84
	C16	0.03	2.35	0.03	1.70
	C17	0.00	21.26	0.00	0.87
	C18	0.00	3.66	0.00	0.49
	C19	0.00	0.00	0.00	0.21
	C20	0.00	0.00	0.00	0.05
total isoparaffins		99.52	89.71	27.50	31.39

Table 4.2 continued

monocycloparaffins		SIP	HEFA	Jet A-1	F-24
	C8	0.00	0.81	2.03	3.48
	C9	0.00	0.51	4.00	4.09
	C10	0.00	0.29	6.88	4.58
	C11	0.00	0.08	4.97	3.71
	C12	0.00	0.03	3.86	3.65
	C13	0.00	0.00	0.83	2.74
	C14	0.42	0.00	0.00	1.79
	C15	0.00	0.00	0.00	0.97
	C16	0.00	0.00	0.00	0.35
	C17	0.00	0.00	0.00	0.03
	C18	0.00	0.00	0.00	0.00
	C19+	0.00	0.00	0.00	0.00
total monocycloparaffins		0.42	1.73	22.58	25.38

di- and tricycloparaffins		SIP	HEFA	Jet A-1	F-24
	C8	0.00	0.00	0.22	0.30
	C9	0.00	0.00	1.13	0.95
	C10	0.00	0.00	1.80	1.44
	C11	0.00	0.00	1.61	1.54
	C12	0.00	0.00	0.99	1.42

Table 4.2 continued

	C13	0.00	0.00	0.08	0.60
	C14	0.00	0.00	0.00	0.33
	C15	0.00	0.00	0.00	0.10
	C16	0.00	0.00	0.00	0.00
	C17+	0.00	0.00	0.00	0.00
total di- and tricycloparaffins		0.00	0.00	5.82	6.68
total cycloparaffins		0.42	1.73	28.40	32.06

alkylbenzenes		SIP	HEFA	Jet A-1	F-24
	C8	0.00	0.01	1.27	1.30
	C9	0.00	0.02	4.83	3.16
	C10	0.00	0.00	4.30	3.42
	C11	0.00	0.00	2.45	1.76
	C12	0.00	0.00	1.23	1.43
	C13	0.00	0.00	0.42	0.89
	C14	0.00	0.00	0.01	0.40
	C15	0.06	0.00	0.00	0.26
	C16	0.00	0.00	0.00	0.13
	C17+	0.00	0.00	0.00	0.02
total alkylbenzenes		0.06	0.03	14.51	12.78

cycloaromatic compounds		SIP	HEFA	Jet A-1	F-24
	C9	0.00	0.00	0.21	0.07
	C10	0.00	0.00	0.98	0.45
	C11	0.00	0.00	2.43	1.24
	C12	0.00	0.00	1.30	1.14
	C13	0.00	0.00	0.17	0.75
	C14	0.00	0.00	0.00	0.40

Table 4.2 continued

	C15	0.00	0.00	0.00	0.21
	C16	0.00	0.00	0.00	0.01
	C17 +	0.00	0.00	0.00	0.00
total cycloaromatic compounds		0.00	0.00	5.10	4.27

alkylnaphthalenes		SIP	HEFA	Jet A-1	F-24
	C10	0.00	0.00	0.21	0.07
	C11	0.00	0.00	0.76	0.30
	C12	0.00	0.00	0.11	0.42
	C13	0.00	0.00	0.00	0.26
	C14	0.00	0.00	0.00	0.09
	C15	0.00	0.00	0.00	0.04
	C16 +	0.00	0.00	0.00	0.00
total alkylnaphthalenes		0.00	0.00	1.08	1.18
total aromatic compounds		0.06	0.03	20.69	18.23
Total		100.00	100.00	100.00	100.00

4.3.3 WA Method

Stemming from the fact that volume is an additive property for hydrocarbon mixtures, it is reasonable to assume that density is also an additive property. Thus, the WA method can be considered as an effective approach for fuel (hydrocarbon mixture) density calculations. In order to utilize the WA method for correlation of the chemical composition and density, a representative compound was selected for groups that contained more than one compound, as discussed above. In some cases, (C18- and C19-isoparaffins, C16- and C18-monocycloparaffins, and C15-alkylnaphthalenes), the density of representative compounds could not be found in literature. For these compound groups, a different representative compound was chosen for

which the density could be found in literature. New representative compounds were chosen to have only methyl- alkyl groups for isoparaffins; and only a single alkyl chain for monocycloparaffins and alkylnaphthalenes. Representative compounds and their measured or estimated densities obtained from literature are shown in Table 4.3.

. The density values of these compounds were subsequently used in the calculations. Utilizing the 14 values measured here and the 55 values found in literature, a density matrix was composed. It should be noted that if density values at 15 °C were not available in literature, values at two separate temperatures were utilized to intra- or extrapolate, assuming a linear relationship between density and temperature in that temperature range. Density values taken from literature for temperatures different from 15 °C can be found in Appendix A (Table A.1). In cases where none of the above steps were possible, the representative compound was assigned to be the one having the next greatest peak area percentage (quotient of peak area and total peak area of chromatogram).

Above approach is different from the one published previously (Shi et al., 2017), where authors used the average density of the most abundant compounds in each group. The advantage of the current method (representative compound as opposed to density average) lies in the fact that all compounds in a given class have similar densities (Shi et al., 2017). Therefore, using the density values of compounds with the greatest peak area percent offers a simpler and faster approach. Additionally, this method has the potential to produce more accurate results than using the average density values of some compounds within the group.

Table 4.3 Selected compounds and their density values at 15 °C; pertinent citations for each density value can be found in Vozka et al. (2019).

compound	hydrocarbon class[a]	carbon number	density (g/cm^3)
n-heptane	A	7	0.6884
n-octane	A	8	0.7072
n-nonane	A	9	0.7221
n-decane	A	10	0.7341
n-undecane	A	11	0.7443
n-dodecane	A	12	0.7528
n-tridecane	A	13	0.7601
n-tetradecane	A	14	0.7669
n-pentadecane	A	15	0.7726
n-hexadecane	A	16	0.7768
n-heptadecane	A	17	0.7815
n-octadecane	A	18	0.7852
n-nonadecane	A	19	0.7889
3,3-dimethylpentane	B	7	0.6973
2,4-dimethylhexane	B	8	0.7083
4-ethyl-2-methylhexane	B	9	0.7270
2-methylnonane	B	10	0.7247
2-methyldecane	B	11	0.7407
2,2,4,6,6-pentamethylheptane	B	12	0.7508
3-methyldodecane	B	13	0.7618
3-methyltridecane	B	14	0.7685
2,6,10-trimethyldodecane	B	15	0.7810
2,2,4,4,6,8,8-heptamethylnonane	B	16	0.7881
4-methylhexadecane	B	17	0.7824
2-methylheptadecane	B	18	0.7837
2,6,10,14-tetramethylpentadecane	B	19	0.7865
ethylcyclopentane	C	7	0.7708

Table 4.3 continued

ethylcyclohexane	C	8	0.7923
1-ethyl-1-methylcyclohexane	C	9	0.8063
butylcyclohexane	C	10	0.8032
pentylcyclohexane	C	11	0.8086
hexylcyclohexane	C	12	0.8118
heptylcyclohexane	C	13	0.8144
octylcyclohexane	C	14	0.8172
1-(1,5-dimethylhexyl)-4-methylcyclohexane	C	15	0.8280
decylcyclohexane	C	16	0.8220
undecylcyclohexane	C	17	0.8240
dodecylcyclohexane	C	18	0.8256
octahydropentalene	D	8	0.8702
octahydro-1H-Indene, cis-	D	9	0.8839
decahydronaphthalene	D	10	0.8734
2-syn-methyl-cis-decalin	D	11	0.8823
2-ethyldecahydronaphthalene	D	12	0.8842
2-methyl-1,1'-bicyclohexyl, cis-	D	13	0.8881
1-(cyclohexylmethyl)-2-methylcyclohexane, trans-	D	14	0.8879
decahydro-1,6-dimethyl-4-(1-methylethyl)naphthalene	D	15	0.8883
1,1'-(1-methyl-1,3-propanediyl)bis-cyclohexane	D	16	0.8833
toluene	E	7	0.8715
1,3-dimethylbenzene	E	8	0.8685
1,2,3-trimethylbenzene	E	9	0.8984
1,2,3,4-tetramethylbenzene	E	10	0.9077
1-sec-butyl-4-methylbenzene	E	11	0.8700
hexylbenzene	E	12	0.8615
heptylbenzene	E	13	0.8604
octylbenzene	E	14	0.8599
1-(1,5-dimethylhexyl)-4-methylbenzene	E	15	0.8524

Table 4.3 continued

indane	F	9	0.9680
1,2,3,4-tetrahydronaphthalene	F	10	0.9727
2,3-dihydro-1,6-dimethyl-1H-indene	F	11	0.9313
1,2,3,4-tetrahydro-5,7-dimethylnaphthalene	F	12	0.9629
1,2,3,4-tetrahydro-1,1,6-trimethylnaphthalene	F	13	0.9362
6-(1,1-dimethylethyl)-1,2,3,4-tetrahydronaphthalene	F	14	0.9463
6-(1-ethylpropyl)-1,2,3,4-tetrahydronaphthalene	F	15	0.9321
naphthalene	G	10	1.0168
1-methylnaphthalene	G	11	1.0278
1,7-dimethylnaphthalene	G	12	1.0060
1-propylnaphthalene	G	13	0.9916
1-methyl-7-(1-methylethyl)naphthalene	G	14	0.9797
pentylnaphthalene	G	15	0.9716

[a]A – *n*-paraffins, B – isoparaffins, C – monocycloparaffins, D – di- and tricycloparaffins,
E – alkylbenzenes, F – cycloaromatic compounds, and G – alkylnaphthalenes.

Figure 4.2 depicts a plot of measured density versus density obtained using GC×GC-FID and the WA method. In general, the WA method predicted slightly lower density values than the empirical values. Both data sets (calibration and validation) were measured. In this case, validation set served rather to expand the total sample set than validation. However, all data points were within a range of ±2% relative error. The mean absolute percentage error (MAPE) was 0.6855% and correlation coefficient (R^2) was 0.9327. The repeatability and reproducibility of ASTM D4052 is 0.00045-0.00031 and 0.0019-0.0344 g/cm^3, respectively. Therefore, WA method gave some results with relative error that were higher than the repeatability and/or

reproducibility of ASTM D4052. Therefore, utilizing a more effective algorithm has the potential to decrease the error observed for the WA method.

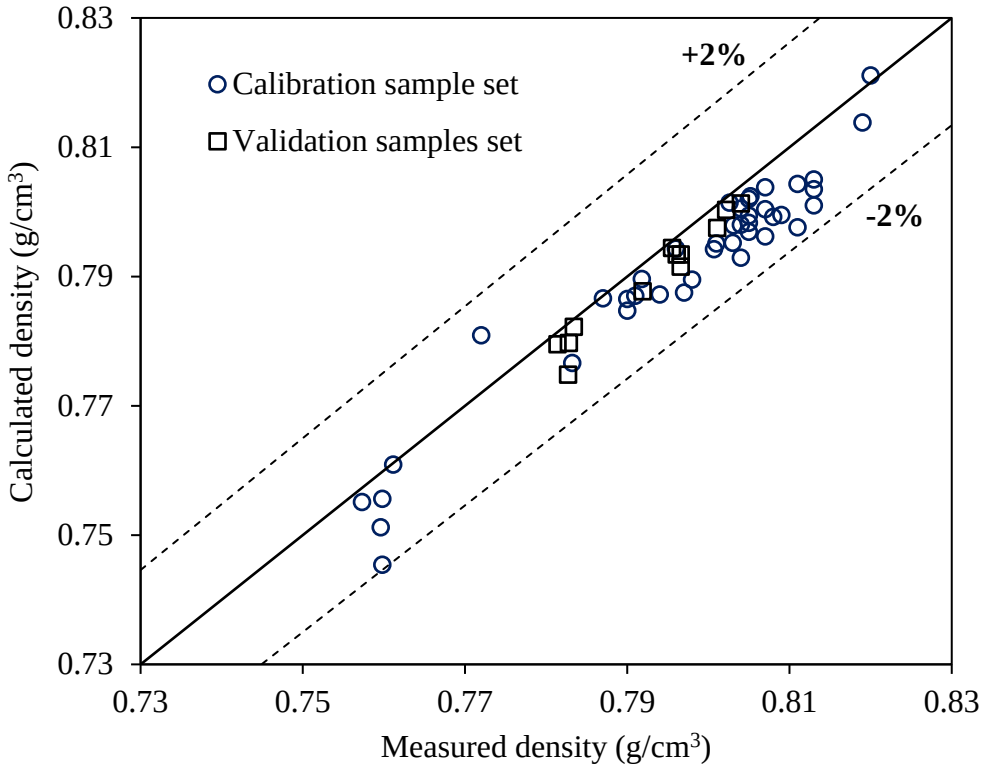

Figure 4.2 Measured Density Versus Density Obtained Using GC×GC-FID Data and the WA Method

4.3.4 PLS and SVM method

In this study, composition matrix refers to the matrix of weight fraction data generated by GC×GC-FID. The algorithms utilized the composition matrix in one of two ways: (i) weight fractions of each carbon number in per hydrocarbon class were summed and used as a predictor; seven predictors total, or (ii) the weight fraction of each compound in the compositional matrix was used; 98 predictors in total. Density matrix is the matrix of density values of the representative compounds for each group. The product matrix is the result of an elementwise

multiplication of composition and density matrices. The product matrix was used in the same way as the composition matrix to improve predictive capabilities of the model.

PLS and SVM methods were applied to the compositional matrix as well as the product matrix. When using 98 predictors, 25 predictors were disregarded due to one of three reasons: (i) compound of that compound group does not exist (e.g., C8-alkylnaphthalenes), (ii) no members of that compound group were detected in any fuel samples, or (iii) the model placed insignificant weight on the predictor. For the product matrix, 30 predictors were disregarded for the same reasons.

A disadvantage to above approach is the underdetermination of the predictor matrix. However, PLS method can prevent the overfitting problem that occurs with an underdetermined system through maximizing covariance. Unlike PLS, SVM is capable of regulating the data during the "learning" procedure. This is an alternative way to prevent overfitting. In order to prevent overfitting for the underdetermined case, the ridge method (Tikhonov regularization) was used for regulation.

Table 4.4 shows the model coefficients of different composition-density correlations for the approach with seven predictors. In Table 4.4, the first coefficient stands for intercept, while the other coefficients correspond to the sum of each hydrocarbon class in the order aforementioned. The coefficients for the approach with 98 predictors can be found in Appendix B (Table A.2). $\rho = \beta_0 + (\sum_{a=1}^{n} \beta_a W_a)$ (4.6) was used for calculating density by using seven predictors (n = 7) or 98 predictors (n = 98). Table 4.5 presents a comparison of the results obtained using each correlation and the product matrix (product) or the composition matrix (composition) for calibration and validation set. The PLS method predicted the density values of aviation jet fuels (at 15 °C) with the lowest mean absolute percentage error and the highest R^2 value when seven predictors were used. However, the SVM method predicted the density values of jet fuels most accurately when 98 predictors were used. The product matrix improved the results for both models. Figure 4.3 and Figure 4.4 display plots of measured density values versus density values derived from GC×GC-FID data output utilizing PLS and SVM methods for both calibration and validation sets, respectively.

$$\rho = \beta_0 + (\sum_{a=1}^{n} \beta_a W_a) \quad (4.6)$$

Where β_0 is the intercept, β_a is the coefficient of compound group a, and W_a is the wt.% of compound group a.

Table 4.4 Correlation Coefficients for PLS and SVM Using Seven Predictors

Correlation	Coefficients
PLS *product*	β_0 = 0.38293, β_a = [0.00470, 0.00500, 0.00596, 0.00508, 0.00519, 0.00614, 0.00637]
PLS *composition*	β_0 = 1.55109, β_a = [-0.00831, -0.00788, -0.00683, -0.00722, -0.00711, -0.00573, -0.00504]
SVM *product*	β_0 = 0.40919, β_a = [0.00423, 0.00466, 0.00582, 0.00451, 0.00512, 0.00533, 0.00574]
SVM *composition*	β_0 = 0, β_a = [0.00727, 0.00760, 0.00885, 0.00797, 0.00836, 0.00936, 0.00951]

Table 4.5 Comparison of Mean Absolute Percentage Errors (MAPE) and Correlation Coefficients (R^2)

Correlation	Calibration set		Validation set		Total set	
	MAPE (%)	R^2	MAPE (%)	R^2	MAPE (%)	R^2
PLS *product* (7)	0.2575	0.9769	0.2508	0.9938	0.2559	0.9746
PLS *composition* (7)	0.3493	0.9584	0.4884	0.9842	0.3827	0.9459
SVM *product* (7)	0.2425	0.9742	0.1970	0.9964	0.2315	0.9744
SVM *composition* (7)	0.3231	0.9530	0.1304	0.9873	0.2769	0.9546
WA (98)	0.7672	0.9330	0.4064	0.9536	0.6855	0.9327
PLS *product* (98)	0.1914	0.9879	0.1621	0.9947	0.1844	0.9869
PLS *composition* (98)	0.1912	0.9877	0.1193	0.9940	0.1740	0.9874
SVM *product* (98)	0.1068	0.9970	0.1299	0.9972	0.1124	0.9961
SVM *composition* (98)	0.1130	0.9967	0.0522	0.9976	0.0984	0.9967

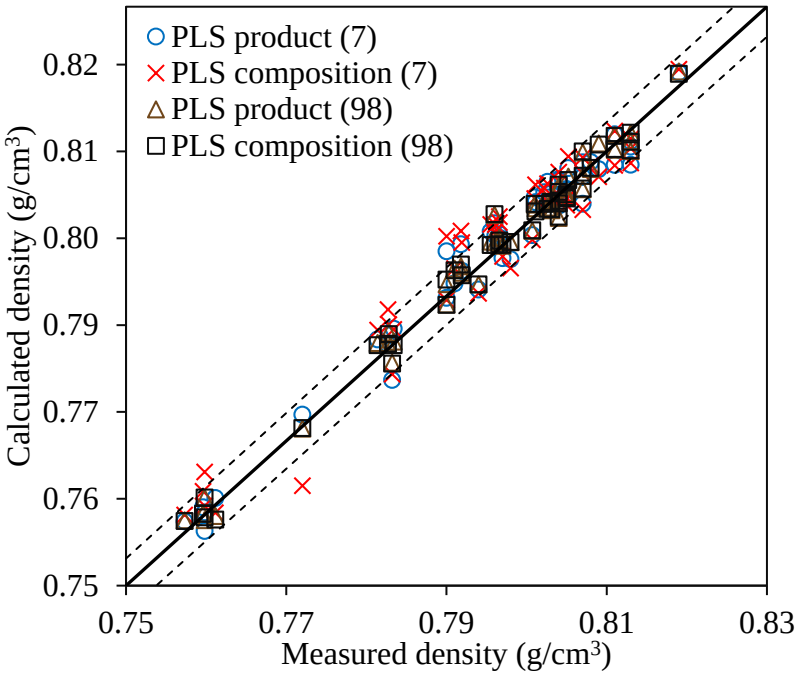

Figure 4.3 Measured Density Versus Density Derived from GC×GC-FID Data and the PLS Method

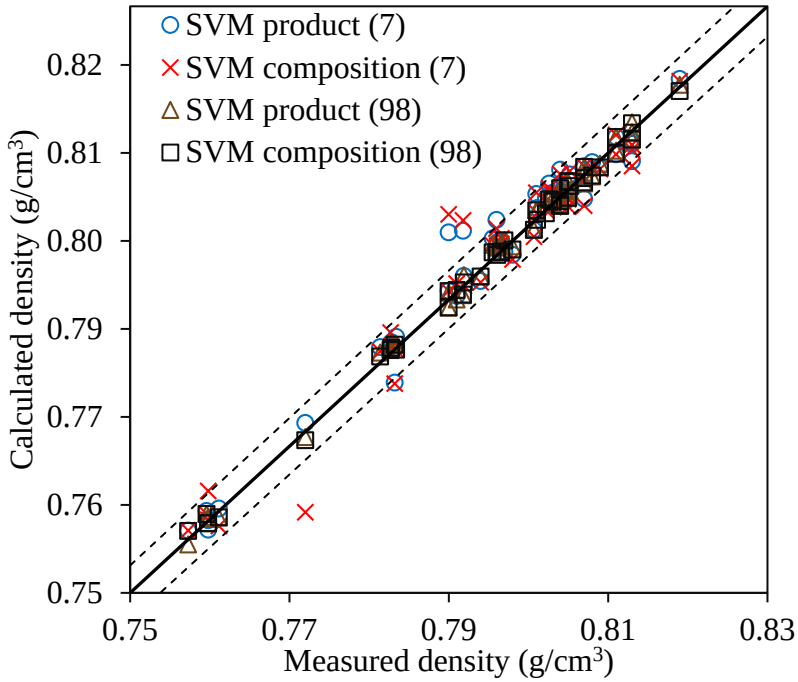

Figure 4.4 Measured Density Versus Density Derived from GC×GC-FID Data and the SVM Method

4.4 Conclusion

In this study, a method for the determination of density from chemical compositions determined via two-dimensional gas chromatography with FID was developed for aviation fuels and alternative fuel blending components. This work focused on density values at 15 °C, which is a standard in the aviation industry. Three correlation algorithms were explored: weighted average method (WA), partial least squares regression (PLS), and a high dimensional algorithm using regulated support vector machines method (SVM). Density results derived this way were compared to those obtained empirically from a Stabinger Viscometer via ASTM. When using the summed wt.% of each hydrocarbon class, the SVM method yielded the most accurate prediction with a mean absolute percentage error (MAPE) of 0.2315%. Alternatively, when 98 predictors were used, the SVM method was observed to yield most accurate results with a MAPE of 0.0984%. Additionally, use of the product matrix improved the results for both models. Moreover, these methods were validated utilizing uncalibrated validation samples. This work can be expanded to additional fuel properties that will enable the manufacturing of alternative aviation fuels with the specific chemistry composition.

CHAPTER 5. IMPACT OF HEFA FEEDSTOCK ON FUEL COMPOSITION AND PROPERTIES IN BLENDS WITH JET A

 Impact of HEFA feedstock on fuel composition and properties in blends with Jet A was collaborative work with Prof. Pavel Šimáček and Prof. Gozdem Kilaz.

5.1 Introduction

One of the biggest challenges in the field of aviation fuels is that deployment of alternative aviation fuels requires a cumbersome and cost intensive fuel certification process. Out of the two aviation fuels utilized in aircraft, the kerosene-type fuel (Jet A/A-1) is much more abundantly used as aviation gasoline (avgas) can power only piston engine aircraft. Hence, avgas has only minor importance on a global scale (Diniz, Sargeant, & Millar, 2018). This can be illustrated by comparing the consumption rates of avgas and jet fuel in 2017 that were 4,120 and 613,790 Mbbl, respectively. Since the demand for avgas production is only about 0.67% of jet fuel, it is not surprising that great emphasis is put on alternative jet fuels as opposed to avgas. The guideline for evaluation and approval of jet fuel blending components from non-petroleum sources is described in ASTM D4054 (*Standard Practice for Qualification and Approval of New Aviation Turbine Fuels and Fuel Additives*). Certification of alternative aviation fuels and blending components was described previously (Wilson, Edwards, Corporan, & Freerks, 2013; Rand, Verstuyft, & Eds, 2016; ASTM D4054, 2017). Once a candidate fuel or blending component is approved, it is incorporated into ASTM D7566 (*Standard Specification for Aviation Turbine Fuel Containing Synthesized Hydrocarbons*) which was first introduced in 2009 (ASTM D7566, 2018). ASTM D7566 regulates the use of non-petroleum source derived blending components in jet fuel (Rand et al., 2016; ASTM D7566, 2018). As of this writing, the ASTM D7566 contains five Annexes; each Annex covers an individual fuel blending component approved for use up to a specified blending ratio with the conventional petroleum-derived jet fuel. Annex A1 covers Fisher-Tropsch Hydroprocessed Synthesized Paraffinic Kerosene (FT-SPK) that was a part of the standard in 2009. Annex A2, added in 2011, covers Synthesized Paraffinic Kerosene from Hydroprocessed Esters and Fatty Acids (HEFA) and Annex A3,

developed in 2014, includes Synthesized Iso-Paraffins (SIP) from Hydroprocessed Fermented Sugars. A similar chemistry to the FT-SPK (Annex A1) has Synthesized Paraffinic Kerosene with Aromatics (FT-SPK/A) derived by alkylation of light aromatics from non-petroleum sources specified by Annex A4 developed in 2015. The most recent Annex A5, added in 2016, covers Alcohol-to-Jet Synthetic Paraffinic Kerosene (ATJ) (Rand et al., 2016; ASTM D7566, 2018).

The key problem is that due to the high risk of investing in alternative aviation fuels, there are only a few technologies currently producing alternative blending components at a commercial scale (DOE/EE-1515 7652, 2017). ATJ and FT-SPK/A are currently not produced on a commercial scale. Amyris is the only company that manufactures farnesane; however, most farnesane produced is sold to competing markets as opposed to aviation fuel (SIP). Similarly, FT-SPK is not produced on a commercial scale. Currently the only alternative blending component produced on a commercial scale is HEFA with a capacity of 4.3 B L/y (Radich, 2015; IRENA, 2018). HEFA production has been adopted by many companies, here are some to name a few: AltAir (USA), UOP (USA), SG Preston (USA), Solazyme (USA), Cetane Energy (USA), Neste Oil (Finland), Pertamina (Indonesia), Sinopec (China), and Total (France).

HEFA fuel was originally referred to as Bio-derived Synthetic Paraffinic Kerosene (Bio-SPK) or Hydroprocessed Renewable Jet (HRJ). During the evaluation and approval process, HRJ fuels were renamed as Hydroprocessed Esters and Fatty Acids (HEFA) since HEFA is more descriptive of the feedstock and the manufacturing process (Wilson et al., 2013). Hydrotreating of vegetable oils can produce high quality hydrocarbon fuels with compositions that closely resemble that of FT-SPK. HEFA is produced by the same technology as renewable diesel called traditionally HVO (Hydrotreated Vegetable Oil) or Green Diesel. Regardless to particulate feedstock (mainly vegetable oils and animal fats), the technology providing HEFA as well as HVO is composed of two steps – hydrotreatment and hydroisomerization. The hydrotreatment step consists of oxygen removal during which primarily saturated hydrocarbons are formed from triglycerides. These saturated hydrocarbons have either the same (hydrodeoxygenation - HDO) or one less carbon number (hydrodecarbonylation - HDCN and/or hydrodecarboxylation - HDCX) than the triglycerides fatty acid chain (Kochetkova, Blažek, Šimáček, Staš, & Beňo, 2016; Starck, Pidol, Jeuland, Chapus, Bogers, & Bauldreay, 2016). The desired fuel product yield may be maximized if the HDO pathway is favored over HDCN and/or HDCX since no

carbon atoms are lost (Starck et al., 2016). A more detailed description of the reaction steps can be found in literature (Kochetkova et al., 2016). Hydrotreatment step yields primarily *n*-paraffins enabling the fuel product with a very high cetane number. On the other hand, the n paraffins also cause the product to have very poor cold flow properties, which is a clear disadvantage for aviation and even for diesel fuel. Another, more serious disadvantage is that the hydrogenation step produces a product, which is rather in the diesel boiling range (> 250 °C), the yield of kerosene is relatively low. Moreover, there is competition between diesel and kerosene producers, which accentuates the importance of HEFA process optimization. The facilities for bio-derived kerosene need to be designed in a way that further processing a product that is already in fuel range makes sense in terms of economic feasibility (Starck et al., 2016). The cold flow properties may be improved by hydroisomerization (HIS) via which *n*-paraffins are converted into isoparaffins. After the HIS, HEFA is obtained as a desired distillation cut. Distillation can also affect the final product properties.

In principle, any vegetable oil, animal fat or used cooking oil can be utilized as HEFA feedstock. Camelina, tallow, reprocessed tallow, mixed fat (Syntroleum R-8), and halophyte Salicornia oil from sea plants are to name a few that were tested by the U. S. Air Force Research Laboratory (AFRL) (Edwards, Shafer, & Klein, 2012). HEFA fuels have similar distillation profile to that of the petroleum-derived jet fuels (C8 to C16 hydrocarbons), but their distribution may differ (Dancuart, 2000). In terms of chemical composition, HEFA fuels are closer to synthetic SPK than conventional petroleum-derived kerosene. The HEFA hydrocarbon mixtures are primarily composed of saturated *n*-paraffins and isoparaffins and do not contain any aromatics. Similarly, cycloparaffins content is negligibly low (Rand et al., 2016; Edwards, 2003). Current jet fuel specifications (ASTM D7566, Defense Standard 91-91, and MIL-DTL-83133 H) permit up to 50 vol.% of HEFA blending in Jet A/A-1 (ASTM D7566, 2018; Def. 91-91, 2015; MIL-DTL-83133H, 2011).

AFRL report, which served as a supplements for the ASTM Research Report for Bio-SPK (HRJ/HEFA), compared several HEFA samples from different feedstocks and in different blends with Jet A (Edwards et al., 2012). This report presented chemical compositional data from ASTM D6379 (mono- and di-aromatics), ASTM D1319 (aromatics, olefins, and saturates), ASTM D2425 (paraffins, cycloparaffins, alkylbenzenes, indanes and tetralins, indenes, and naphthalenes), and *n*-paraffins distribution obtained from GC-FID. Another report analyzed the

properties of HEFA kerosene blends with various samples of conventional petroleum-derived kerosene, with a focus on blends of HEFA up to 60 vol.% in Jet A-1 (Zschocke, Scheuermann, & Ortner, 2017). This report did not present any compositional data, authors only mentioned one dimensional gas chromatography and visual comparison of HEFA and Jet A-1 chromatograms. An additional work that compared chemical composition and fuel properties of two HEFA samples (from tallow and camelina) used gas chromatography mass spectrometry (GC-MS) with the focus on quantitative analyses on *n*-paraffins, isoparaffins, olefins, cycloparaffins, and aromatics (Pieres, Han, Kramlich, & Garcia-Perez, 2018). Other studies focused more on property testing than chemical composition (Luning Prak, Brown, & Trulove, 2013; Gawron, & Bialecki, 2018). One of this study focused on developing surrogate mixtures for HEFA from camelina and tallow (Gawron, & Bialecki, 2018). The chemical composition was obtained also from GC-MS and density, viscosity, and speed of sound were measured.

The first set of studies focusing on the correlations between petroleum-based jet fuel composition and fuel properties was introduced in 1980's (Cookson et al., 1985, 1987, 1995). The analytical techniques utilized in these studies were: gas chromatography (GC), nuclear magnetic resonance (NMR) spectroscopy, and high-pressure liquid chromatography (HPLC). Specific gravity, smoke point, net heat of combustion, and freezing point values were predicted from the total content of *n*-paraffins, branched plus cyclic compounds, and aromatics. These predictions were further broadened to include the alternative aviation fuels (hydroliquefaction and FT process of coal) by utilizing the distillation profile information in the calculations to predict the properties from chemical composition (Cookson et al., 1995). Artificial neural network enabled the prediction of more fuel properties (density, freezing point, net heat of combustion, flash point, and aniline point) from the chemical composition determined via GC–MS (Liu et al., 2007). The hydrocarbon classes focused in this study were: *n*-paraffins, isoparaffins, monocyclopraffins, dicyclopraffins, alkylbenzens, naphthalenes, tetralins, and hydroaromatics. Morris et al. (2009) was the first group that applied a chemometric modeling of near-infrared absorption spectra, which expanded the number of properties predicted. The additional properties were refractive index, viscosity, distillation profile, conductivity, and acid number. The use of GC–MS in a consecutive work (Cramer et al., 2014) assisted in improving these models. The first use of a comprehensive two-dimensional gas chromatography (GC×GC) with mass spectrometry (MS) and flame ionization (FID) detection was achieved in 2017 by Shi

et al. (2017). Shi et al. (2017) correlated the fuel properties to the chemical composition via several algorithms. Out of those, modified weighted average algorithm yielded results with the lowest mean absolute error. The properties of interests were density at 20 °C, freezing point, flash point, and net heat of combustion. Aviation fuel standards require measuring the density at 15 °C. Correlation of fuel chemistry to density at this temperature was later achieved by Vozka et al. (2019).

This work focuses on comparison of three HEFA fuels produced from different feedstocks (camelina, tallow, and mixed fat) based on the detailed chemical composition obtained from GC×GC-MS and FID. For this purpose, blends of HEFA with Jet A in various blend ratios (10-60 vol.%) were prepared. The objective of this study was to determine the changes in fuel properties caused by the changes in chemical composition brought upon blending. The properties of interest were distillation profile, density, viscosity, flash point, freezing point, and net heat of combustion. Our key observation was that distillation profile had the main impact on the final fuel properties. Additionally, the selection of the feedstock or the process conditions yielding final HEFA fuel composition can adversely affect properties, such as viscosity and/or freezing point. Moreover, this work contains very detailed analyses on the chemical compositions of all HEFA samples based on each carbon number and hydrocarbon class. This database established has the potential to be the first step in filling the knowledge gap on how fuel properties are influenced by fuel composition.

5.2 Experimental Section

5.2.1 Materials

The petroleum-derived jet fuel Jet A (POSF 9326) and Hydroprocessed Esters and Fatty Acids (HEFA) from camelina (POSF 10301), tallow (POSF 6308), and mixed fat (POSF 7635) were provided by the Wright-Patterson Air Force Base, Dayton, Ohio. HEFA was produced by Honeywell UOP with camelina and tallow as the feedstock and by Dynamic Fuels with mixed fat (presumably mostly chicken fat) as a feedstock. Mixtures of each HEFA sample with varying concentrations in the range of 10-60 vol.% in Jet A were prepared. Designation of all analyzed samples and mixtures is displayed in Table 5.1. Dichloromethane (DCM; 99.9% pure; Acros Organics) was used as a solvent for GC×GC-FID analysis.

Table 5.1 Mixture Compositions and Designations

Jet A (vol.%)	Blending component (vol.%)	HEFA Camelina	HEFA Tallow	HEFA Mixed fat
0	100	CAME	TALL	MFAT
90	10	C-10	T-10	M-10
80	20	C-20	T-20	M-20
70	30	C-30	T-30	M-30
60	40	C-40	T-40	M-40
50	50*	C-50	T-50	M-50
40	60	C-60	T-60	M-60

*maximum allowable concentration for blending with petroleum jet fuels (ASTM D7566)

5.2.2 GC×GC analyses

Qualitative analysis of the samples was performed using a two-dimensional gas chromatography with electron ionization and high resolution time-of-flight mass spectrometry detection (GC×GC-TOFMS). A LECO Pegasus GC-HRT 4D (EI) High Resolution TOF MS was used under chromatographic conditions listed in a previous work (Luning Prak et. al, 2017). Quantitative analysis of the samples was performed using a two-dimensional gas chromatography with flame ionization detector (GC×GC-FID). An Agilent 7890B gas chromatograph was used with a non-moving quad-jet dual stage thermal modulator, liquid nitrogen for modulation, and He as the carrier gas. Chromatographic conditions for GC×GC-FID are shown in Table 5.2. Data were processed using the ChromaTOF software version 4.71.0.0 optimized for GC×GC-FID. All samples were also analyzed using different column setup (60 m Rxi-17Sil MS and 1.1 m Rxi-1ms) in order to assure the column selected did not produce any bias. Detailed description of the secondary method and results obtained from this column configuration can be found in Appendix B (Table B.). For both column setups, 10 µL of sample was diluted in 1 mL of DCM. 0.5 µL of the sample solution was injected using an Agilent 7683B series injector with 20:1 split ratio. Acquisition delay was set to 165 s. Inlet and FID temperature values were 280 and 300 °C, respectively.

Table 5.2 Chromatographic Conditions for GC×GC-FID Using DB-17MS and DB-1 MS Columns

Parameters	Description
Columns	Primary: DB-17MS Agilent (30 m × 0.25 mm × 0.25 μm) Secondary: DB-1 MS Agilent (0.8 m × 0.25 mm × 0.25 μm)
Carrier gas	UHP helium, 1.25 mL/min
Oven temperature	isothermal 40 °C for 0.2 min, followed by a linear gradient of 1 °C/min to a temperature of 160 °C being held isothermally for 5 min
Modulation period	6.5 s with 1.06 s hot pulse time
Offsets	Secondary oven: 55 °C Modulator: 15 °C

GC×GC-TOFMS was used as a baseline for developing a classification on the GC×GC-FID (Figure 5.1). Classification included the following hydrocarbon classes: *n*-paraffins (C7 to C18), isoparaffins (C7 to C19), monocycloparaffins (C7 to C16), di- and tricycloparaffins (C8 to C15), alkylbenzenes (C6 to C17), cycloaromatics (C9 to C16), and alkylnaphthalenes (C10 to C15). The first step of the quantification was to sum the peak areas of the compounds in each group. Group in this study is referred to all compounds with the same carbon number for the same hydrocarbon class. Consecutively, the weight percent of each group was calculated by dividing the total peak area of the group by the total peak area of the sample (Gieleciak et al., 2013).

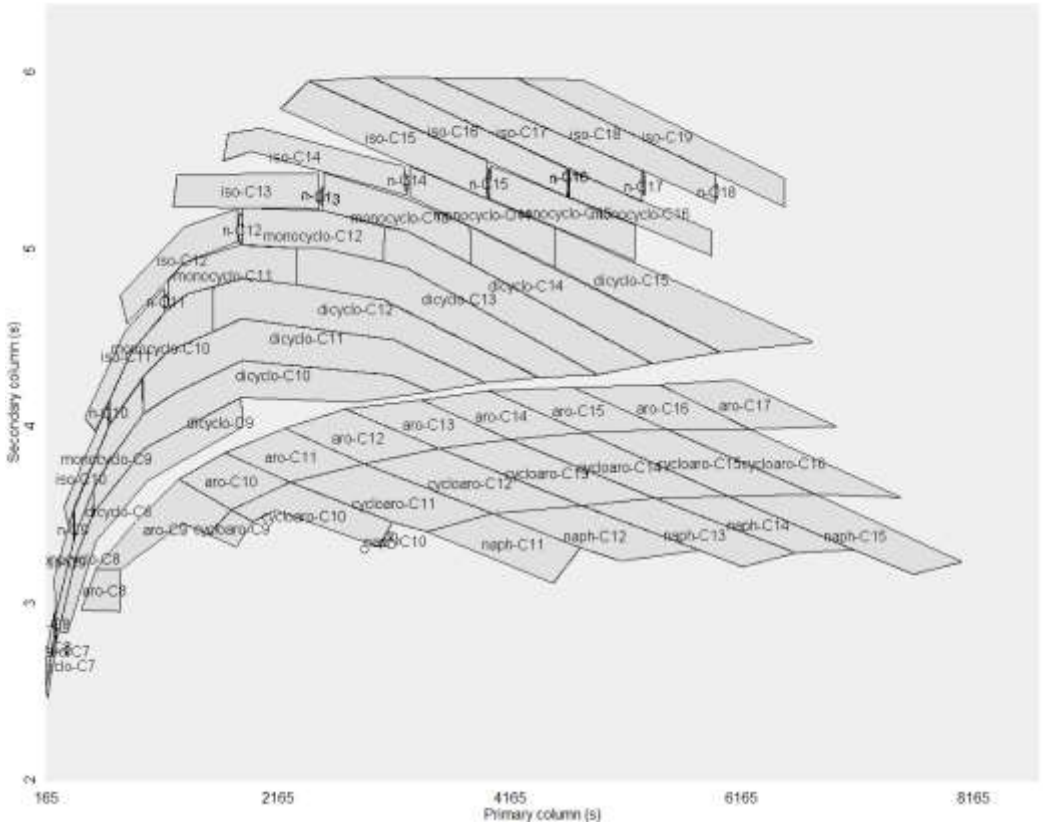

Figure 5.1 GC×GC-FID Chromatogram Illustrating the Jet Fuel Classification for Analyzed Samples with the Following Classes:
isoparaffins (iso-), *n*-paraffins (n-), monocycloparaffins (monocyclo-), di- + tricycloparaffins (dicyclo-), alkylbenzenes (aro-), cycloaromatics (cycloaro-), and alkylnaphthalenes (naph-)

5.2.3 Physical Properties

A Trace GC Ultra gas chromatograph was utilized for the simulated distillation (SIM DIST) of the samples using a method covering the ASTM standard D2887. Simulated distillation parameters are listed in a previous work (Šimáček, Kubička, Pospíšil, Rubáš, Hora, & Šebor, 2013). SIM DIST data were converted to ASTM D86 test data following the protocol displayed in the ASTM D2887. Density and viscosity were determined using a Stabinger Viscometer SVM 3001 (Anton Paar) via ASTM D4052 and ASTM D7042 methods, respectively. Freezing point was measured using a manual freezing point apparatus (K29700, Koehler Instrument) following ASTM D2386. Flash point was measured using a Tag 4 Flash Point Tester (Anton Paar) according to ASTM D56. Hydrogen content was measured via a high-resolution NMR following ASTM method D3701 as described in a previous work (Vozka et al., 2018). Gross heat of

combustion was measured with a 6200 Isoperibol Calorimeter (Parr Instrument Co.) via ASTM D4809. Net heat of combustion was calculated from gross heat of combustion and hydrogen content. All measurements were in compliance with techniques listed in ASTM D1655 and ASTM D7566 except for the case where the hydrogen content was measured via high-resolution NMR as opposed to low-resolution one. Aromatic hydrocarbon content (vol. %) was calculated via HPLC (Shimadzu LC-10 CE) according to D6379. The experimental investigations were conducted at a well-established Fuel Laboratory of Renewable Energy at Purdue University.

5.3 Results and Discussion

5.3.1 Composition of Neat Blending Components

Figure 5.2 shows the chromatograms of all HEFA samples. Due to the fact that the scales of all chromatograms are the same, the distillation range of the samples can be visually compared on x-axis. Hydrocarbon compositions of Jet A and all HEFA samples obtained from GC×GC-FID are shown in Table 5.3. Each HEFA was primarily composed of isoparaffins (~90 wt.%), *n*-paraffins (~10 wt.%), monocycloparaffins (up to 2 wt.%). The content of alkylbenzenes did not exceed 0.1 wt.%. Dicycloparaffin, tricycloparaffin, and cycloaromatic content was zero. CAME contained the highest amount of cycloparaffins, MFAT contained the highest amount of *n*-paraffins, and TALL contained the highest amount of isoparaffins. These data are in a good agreement with literature (Edwards et al., 2012; Jennerwein, Eschner, Gröger, Wilharm, & Zimmermann, 2014; Webster, Rawson, Kulsing, Evans, & Marriott, 2017). Additionally, CAME, TALL, and MFAT contained ca. 480, 350, and 450 compounds (peaks) detected, respectively. Jet A contained ca. 965 compounds detected.

When comparing compositional results from two column configuration used, slight differences were noticed within a few hydrocarbon classes, especially for Jet A sample. For example, the total content of isoparaffins was 30.58 and 26.65 wt. % when DB and Rxi columns were used, respectively. For this reason, the GC×GC method was validated by comparing the results with three federal research labs (NAVAIR, NRL, and AFRL). The results from DB columns were in better agreement with the round robin tests executed by the aforementioned facilities; therefore, results obtained with the DB column were utilized.

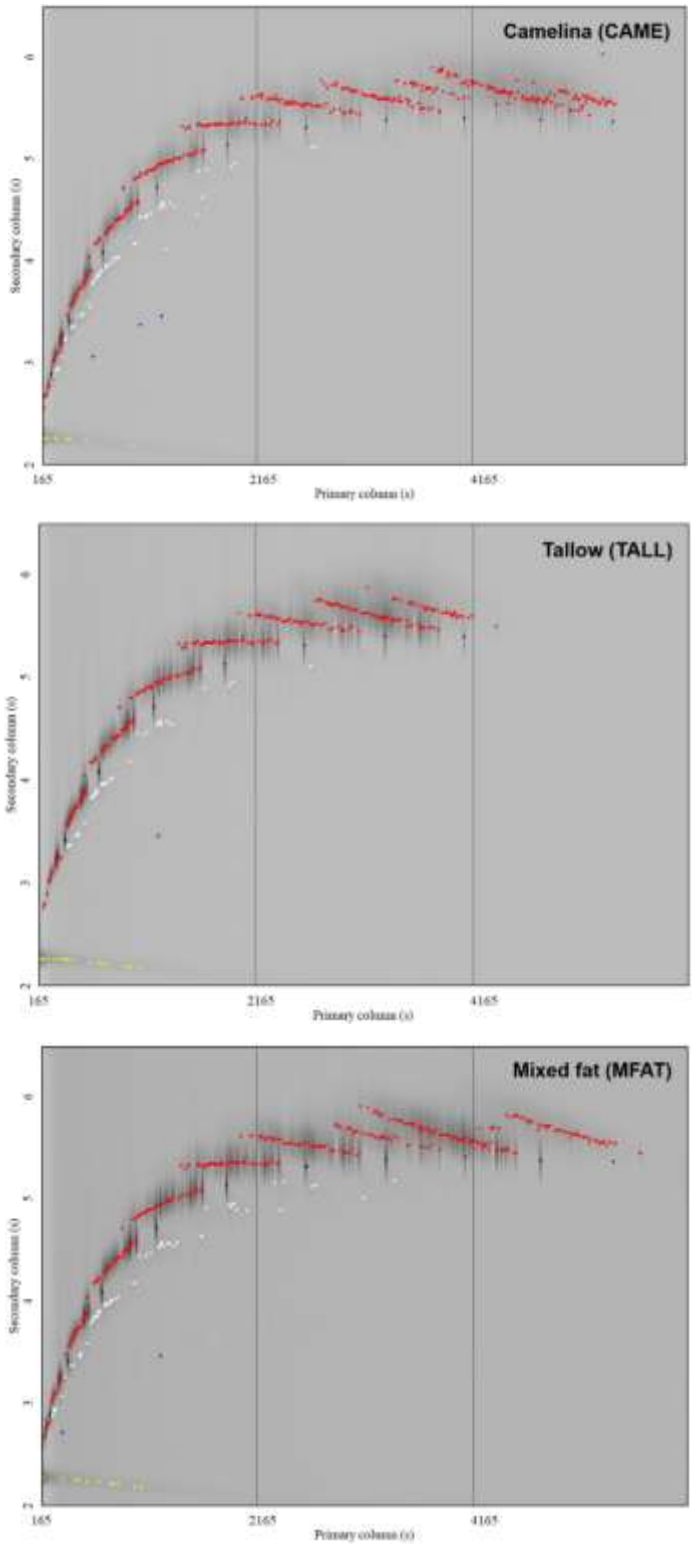

Figure 5.2 Comparison of GC×GC Chromatograms of HEFA Samples
Red denotes isoparaffins, black *n*-paraffins, white cycloparaffins, blue alkylbenzenes, and yellow shows solvent bleed

Table 5.3 Hydrocarbon Type Composition (wt.%) of Jet A and CAME, TALL, and MFAT

Hydrocarbon class	Jet A	CAME	TALL	MFAT
n-paraffins				
C8	0.83	1.56	0.12	0.73
C9	5.05	2.15	1.98	1.13
C10	4.96	1.38	1.73	1.50
C11	3.36	0.96	1.56	1.55
C12	2.37	0.83	1.42	1.46
C13	1.90	0.65	1.04	1.14
C14	1.27	0.25	0.69	1.75
C15	0.76	0.51	0.32	0.14
C16	0.36	0.13	0.00	0.71
C17	0.10	0.10	0.00	0.02
C18	0.02	0.00	0.00	0.00
total *n*-paraffins	20.97	8.53	8.87	10.12
isoparaffins				
C8	0.28	1.48	0.06	2.05
C9	4.97	11.18	6.05	3.68
C10	6.94	11.35	12.11	6.85
C11	5.36	9.87	12.78	10.54
C12	3.69	8.47	13.44	12.35
C13	3.51	8.17	12.36	11.55
C14	2.63	6.29	9.05	13.40
C15	1.97	5.59	21.94	3.93
C16	0.94	2.35	2.74	20.58
C17	0.23	21.26	0.00	0.26
C18	0.06	3.66	0.00	3.25
total isoparaffins	30.58	89.68	90.53	88.46

Table 5.3 continued

Monocycloparaffins				
C7	0.22	0.00	0.00	0.00
C8	3.74	0.81	0.19	0.40
C9	4.47	0.51	0.26	0.43
C10	4.10	0.29	0.10	0.29
C11	2.85	0.08	0.04	0.16
C12	2.25	0.03	0.00	0.05
C13	1.67	0.00	0.00	0.06
C14	0.69	0.00	0.00	0.00
C15	0.12	0.00	0.00	0.00
total monocycloparaffins	20.12	1.73	0.58	1.39
di- and tricycloparaffins				
C8	0.23	0.00	0.00	0.00
C9	0.78	0.00	0.00	0.00
C10	1.01	0.00	0.00	0.00
C11	1.07	0.00	0.00	0.00
C12	0.80	0.00	0.00	0.00
C13	0.27	0.00	0.00	0.00
C14	0.14	0.00	0.00	0.00
total di- and tricycloparaffins	4.30	0.00	0.00	0.00
total cycloparaffins	24.41	1.73	0.58	1.39
Alkylbenzenes				
C8	0.07	0.00	0.00	0.02
C9	1.79	0.01	0.00	0.00
C10	4.86	0.02	0.01	0.00
C11	3.27	0.00	0.00	0.00
C12	2.15	0.00	0.00	0.00
C13	1.72	0.00	0.00	0.00

Table 5.3 continued

C14	1.04	0.00	0.00	0.00
C15	0.35	0.00	0.00	0.00
C16	0.19	0.00	0.00	0.00
C17	0.02	0.00	0.00	0.00
total alkylbenzenes	15.46	0.03	0.01	0.02
cycloaromatics				
C9	0.14	0.00	0.00	0.00
C10	0.78	0.00	0.00	0.00
C11	1.73	0.00	0.00	0.00
C12	2.24	0.00	0.00	0.00
C13	1.26	0.00	0.00	0.00
C14	0.73	0.00	0.00	0.00
C15	0.01	0.00	0.00	0.00
total cycloaromatics	6.89	0.00	0.00	0.00
alkylnaphthalenes				
C10	0.11	0.00	0.00	0.00
C11	0.41	0.00	0.00	0.00
C12	0.64	0.00	0.00	0.00
C13	0.43	0.00	0.00	0.00
C14	0.09	0.00	0.00	0.00
C15	0.01	0.00	0.00	0.00
total alkylnaphthalenes	1.69	0.00	0.00	0.00
total aromatics	24.05	0.03	0.01	0.02

5.3.2 Composition of Fuel Blends

A simplified composition of each mixture (Table 5.4Table 5.6) was calculated utilizing the constituent component weight fractions (vol.% were converted to wt.% using density) and

pertinent individual composition values from Table 5.3. The data displayed in Table 5.4Table 5.6 were validated by measuring representative samples and comparing the results obtained to those calculated. The discrepancy between the measured and the calculated data were below the repeatability error; hence, deemed insignificant.

Table 5.4 Hydrocarbon Type Composition (wt.%) of CAME with Jet A Mixtures

Hydrocarbon class	C-10	C-20	C-30	C-40	C-50	C-60
n-paraffins	19.8	18.6	17.4	16.2	14.9	13.7
isoparaffins	36.2	41.8	47.6	53.4	59.3	65.2
monocycloparaffins	18.4	16.6	14.8	13.0	11.2	9.4
di- and tricycloparaffins	3.9	3.5	3.1	2.6	2.2	1.8
alkylbenzenes	14.0	12.5	11.0	9.5	8.0	6.4
cycloaromatics	6.2	5.6	4.9	4.2	3.5	2.9
alkylnaphthalenes	1.5	1.4	1.2	1.0	0.9	0.7

Table 5.5 Hydrocarbon Type Composition (wt.%) of TALL with Jet A Mixtures

Hydrocarbon class	T-10	T-20	T-30	T-40	T-50	T-60
n-paraffins	19.8	18.7	17.5	16.3	15.1	13.9
isoparaffins	36.2	42.0	47.8	53.7	59.6	65.7
monocycloparaffins	18.3	16.4	14.5	12.6	10.7	8.7
di- and tricycloparaffins	3.9	3.5	3.1	2.6	2.2	1.8
alkylbenzenes	14.0	12.5	11.0	9.5	8.0	6.4
cycloaromatics	6.2	5.6	4.9	4.2	3.6	2.9
alkylnaphthalenes	1.5	1.4	1.2	1.0	0.9	0.7

Table 5.6 Hydrocarbon Type Composition (wt.%) of MFAT with Jet A Mixtures

Hydrocarbon class	M-10	M-20	M-30	M-40	M-50	M-60
n-paraffins	19.9	18.9	17.8	16.8	15.7	14.6
isoparaffins	36.1	41.6	47.3	52.9	58.7	64.5
monocycloparaffins	18.3	16.5	14.7	12.9	11.0	9.1
di- and tricycloparaffins	3.9	3.5	3.1	2.6	2.2	1.8
alkylbenzenes	14.0	12.5	11.0	9.5	8.0	6.4
cycloaromatics	6.2	5.6	4.9	4.2	3.5	2.8
alkylnaphthalenes	1.5	1.4	1.2	1.0	0.9	0.7

5.3.3 Physical Property Analyses

All the property values for the samples were within the limits defined by ASTM D1655 except for density that met the requirements of ASTM D7566 for HEFA. It should be mentioned here that mixing trends were not the main purpose of this study; the purpose of this study was to describe the property changes through the sample composition.

5.3.4 Distillation Profile

Distillation step, which precedes the formation on the final HEFA product, has the main impact on the final fuel properties. In this study, CAME demonstrated the widest distillation range between 5 and 95 vol.% recovered and TALL the narrowest. The distillation profile of MFAT displayed higher boiling points while still having the lowest initial boiling point (IBP). The narrowest distillation profile and the lowest final boiling point (FBP) of TALL can be also derived from their chromatograms as shown in Figure 5.2. Results from SIM DIST are shown in Figure 5.3-Figure 5.6. SIM DIST results were obtained from GC-FID as there are currently no GC×GC SIM DIST methods approved by ASTM. Braun et al. (2016) claimed that the normal boiling point is independent of the molecular structure and does increase only with increasing carbon number. This statement does not always have to be accurate. As displayed in Figure 5.1, isoparaffins for the same carbon number elute before of the n paraffin, whereas cycloparaffins elute after. It should be noted here that the column configuration used in this study was reversed phase; therefore, the separation was based primarily on the polarity. Still, the elution order was

observed to depend on the volatility of the compounds (boiling point) as the compound eluted in the similar order that would be expected from a normal phase column configuration. This phenomenon was also observed by other researchers (UOP990-11, 2011; Gieleciak et al., 2013). Hence, it is expected for isoparaffins to have a lower boiling point than that of n paraffin and cycloparaffins for the same carbon number. For example, *n*-octane boiling point is 125 °C while isooctane boiling point is 99 °C.

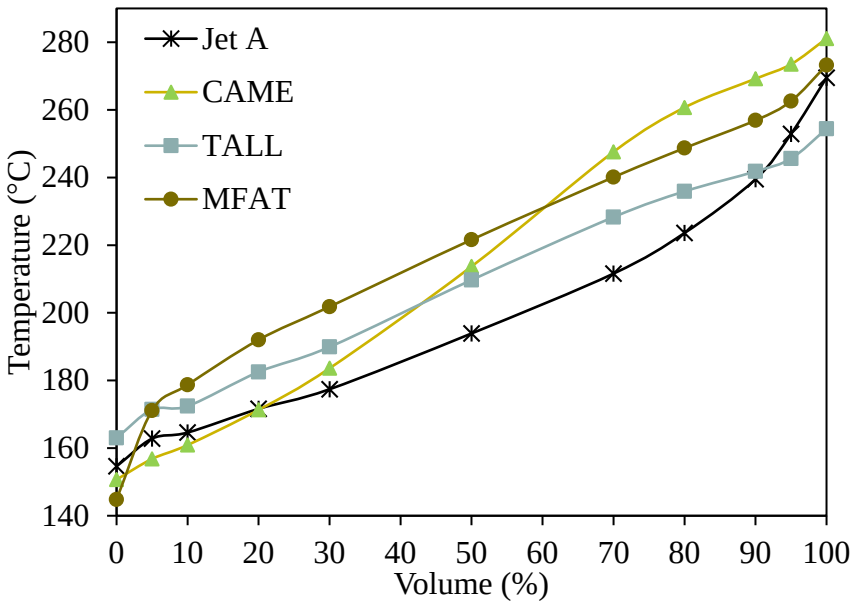

Figure 5.3 Distillation Profile of Jet A, CAME, TALL, and MFAT

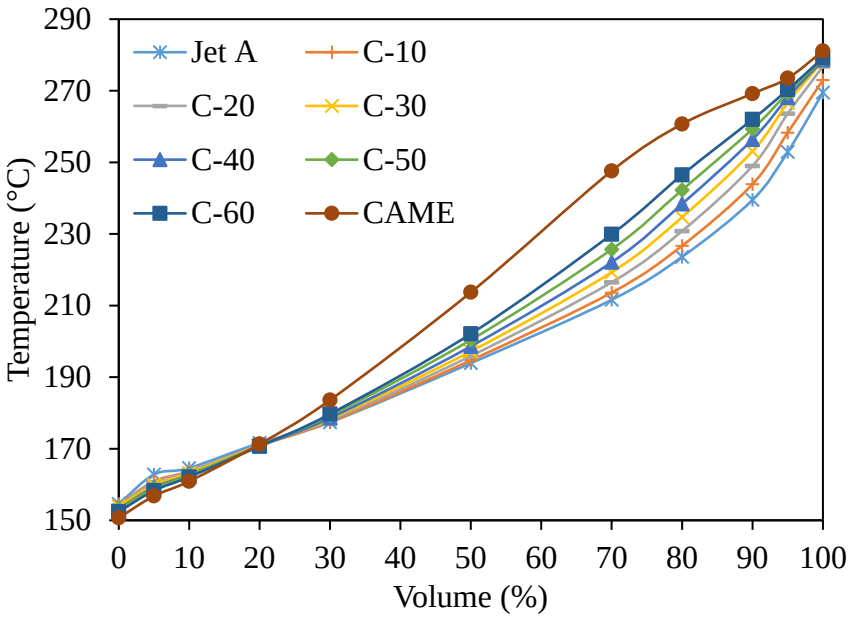

Figure 5.4 Distillation Profile of Jet A, CAME, and Their Mixtures

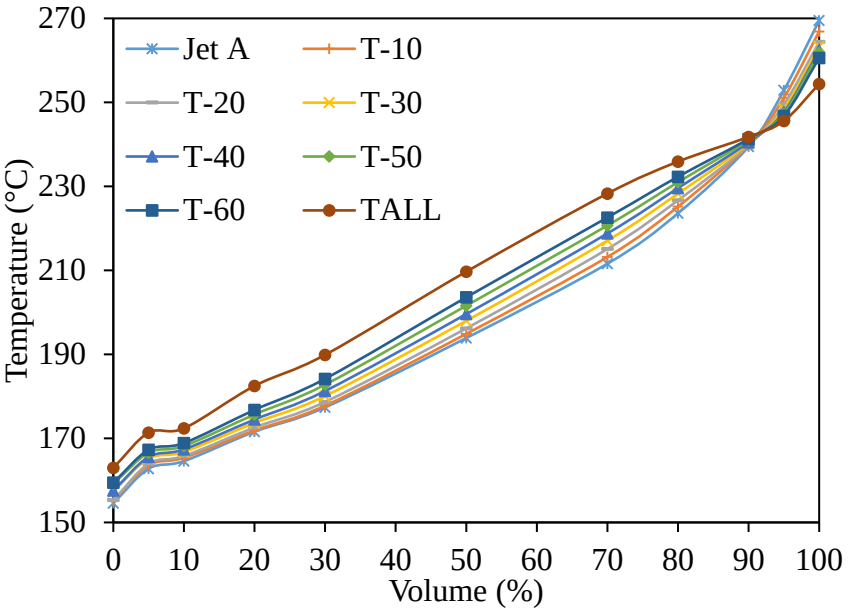

Figure 5.5 Distillation Profile of Jet A, TALL, and Their Mixtures

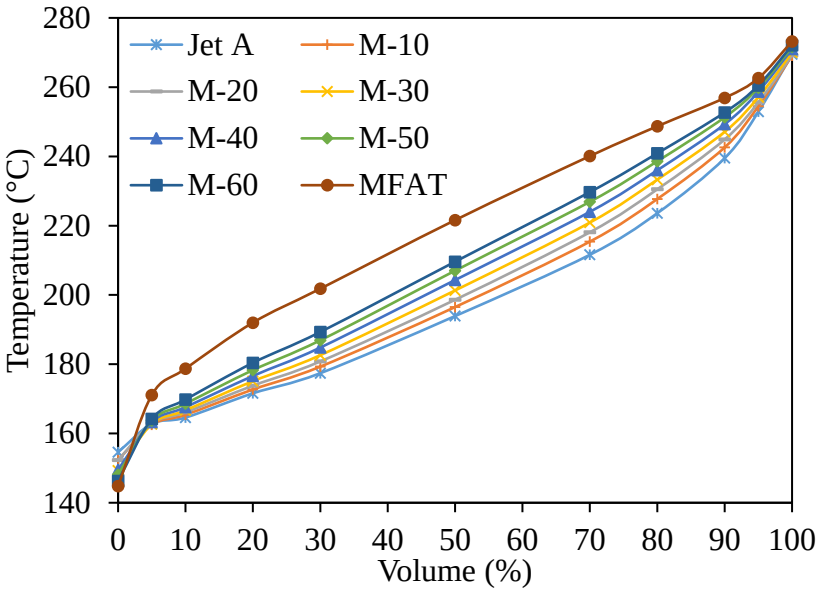

Figure 5.6 Distillation Profile of Jet A, MFAT, and Their Mixtures

5.3.5 Density

Density values of all neat HEFA samples were lower than the minimum limit defined by ASTM D1655 (0.775-0.840 g/cm^3), which was caused by the lack of aromatic components. Therefore, the addition of HEFA to Jet A lowered the density of the final mixtures. Density increases in the order of paraffins < cycloparaffins < aromatics. Density of isoparaffins is in most cases slightly higher than that of *n*-paraffins for the same carbon number. Similarly, alkylnaphthalenes have higher density values than those for alkylbenzenes when the same carbon number is considered (Shi et al., 2017; Braun-Unkhoff et al., 2016). When comparing the neat HEFA samples (Table 5.7), density increased in this order: TALL < CAME < MFAT. This can be simply attributed to the composition. The approach of utilizing weighted average method and average density for each hydrocarbon class and carbon number was utilized to further study the correlation between the density and the chemical composition. A detailed description of this approach can be found elsewhere (Shi et al., 2017; Vozka et al., 2019). Detailed density contribution can be found in Appendix B, Table 8.5. Density group contribution can be calculated as the sum of density contribution for every carbon number from the group. As can be seen in Appendix B, Table 8.6, total *n*-paraffins contribution to the density was calculated as the sum of density values of each *n*-paraffin multiply by the wt. % of pertinent *n*-paraffin. For all

neat HEFA samples, the contribution to the density by each group followed the same order of the total amounts for each hydrocarbon class. For example, density contribution of *n*-paraffins was 0.0630, 0.0659, and 0.0763 g/cm^3 for CAME, TALL, and MFAT, respectively. The total content of *n*-paraffins was 8.53, 8.87, and 10.12 wt.% for CAME, TALL, and MFAT, respectively. All three HEFA samples studied had very similar composition; hence, it was expected to have similar density values for the samples. On the other hand, for samples with a different distribution of each group constituents the trend of density values does not always follow this finding.

The density values of HEFA/Jet A blends increased in the same order with density of neat HEFA fuels: TALL < CAME < MFAT, when equal volumetric mixtures were compared. The relationship between density and the blending component concentration was linear for the mixtures prepared in this study. Moreover, there was no volume change upon mixing. Therefore, it was safe to assume that all the mixtures were ideal and their density values were additive. Consequently, density of each mixture was simply calculated utilizing the constituent density values according to Equation $\rho_m = \sum_i w_i \rho_i$ (5.1).

$$\rho_m = \sum_i w_i \rho_i \quad (5.1)$$

where ρ_m is density of the mixture, w_i is the weight fraction of the neat blend component, and ρ_i is the density of neat blend component. Table 7 shows the measured and calculated results of all samples utilized in this study.

Table 5.7 Density at 15 °C (g/cm3) for Jet A, CAME, TALL, MFAT, and Their Mixtures

	Jet A	C-10	C-20	C-30	C-40	C-50	C-60	CAME
Measured	0.8057	0.8012	0.7966	0.7922	0.7874	0.7828	0.7783	0.7598
Eq. (5.1)	-	0.8013	0.7969	0.7925	0.7880	0.7834	0.7788	-
	Jet A	T-10	T-20	T-30	T-40	T-50	T-60	TALL
Measured	0.8057	0.8009	0.7961	0.7904	0.7861	0.7814	0.7769	0.7573
Eq. (5.1)	-	0.8011	0.7965	0.7918	0.7870	0.7822	0.7774	-
	Jet A	M-10	M-20	M-30	M-40	M-50	M-60	MFAT
Measured	0.8057	0.8007	0.7966	0.7924	0.7877	0.7834	0.7790	0.7612
Eq. (5.1)	-	0.8014	0.7972	0.7928	0.7885	0.7840	0.7796	-

5.3.6 Viscosity

Viscosity is one of the most complex properties that is challenging researchers in this field. Therefore, there is a current knowledge gap on the relationship between fuel composition and viscosity. In this work, viscosity values increased in the order of TALL < CAME < MFAT, following the same trend of density.

Viscosity values at -20 °C of all neat HEFA samples were lower than the maximum limit defined by ASTM D1655 (8.0 mm^2/s); however, all were significantly higher than Jet A viscosity value. Therefore, the addition of HEFA to Jet A did not exceed the limit for viscosity for the final mixtures, but increased the original Jet A viscosity value. Results in this study showed that there is a second-degree (quadratic) polynomial relationship between viscosity value and the blending component concentration. Figure 5.7 displays the viscosity values of the mixtures. Even though, both density and viscosity are fuel properties that greatly depend on the chemical composition, viscosity can be additive at macroscopic quantity, but cannot be easily calculated when the system is divided to every single compound. This was supported by the fact that viscosity was predicted successfully from the chemical composition via the use of non-linear artificial neural network (Cai, Liu, Zhang, Zhao, & Xu, 2018). Despite the non-linear relationship, the viscosity values of binary mixtures can be calculated using the constituent viscosity values. One conclusion that could be drawn was, since CAME viscosity was higher than TALL viscosity, all CAME mixtures in Jet A yielded higher viscosity when compared to the same vol.% mixtures of TALL. Similarly, this was true for MFAT viscosities.

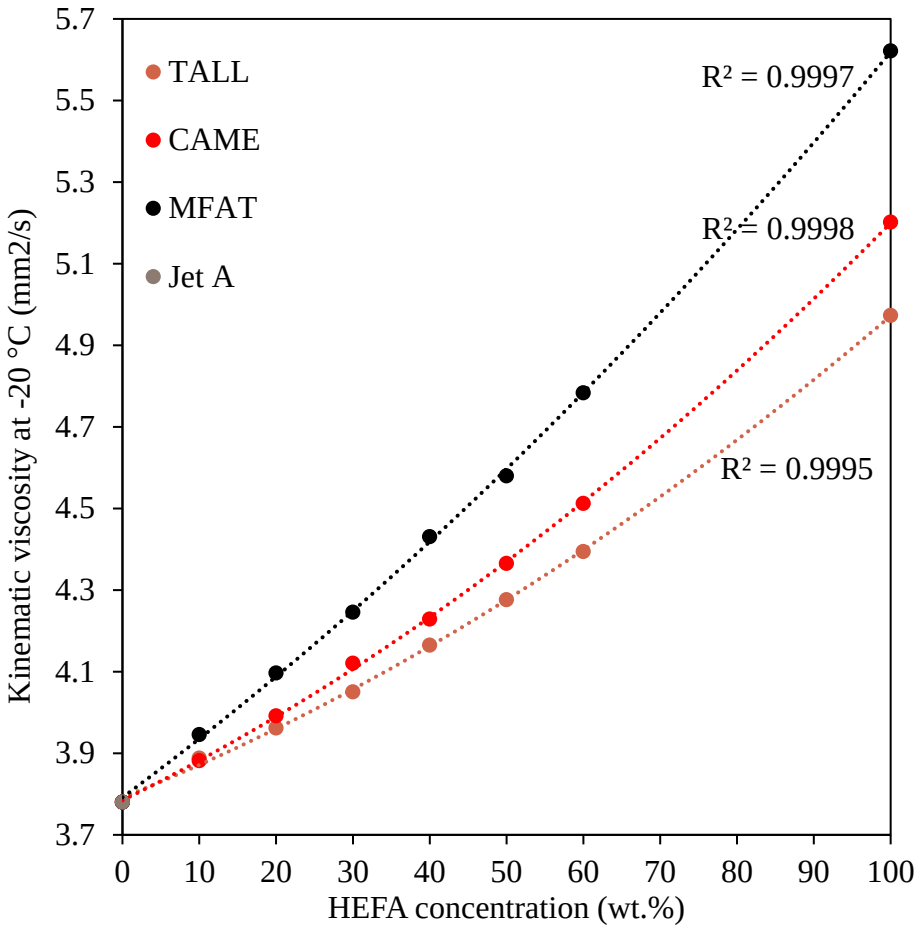

Figure 5.7 Comparison of Kinematic Viscosity at -20 °C for All Prepared Samples

5.3.7 Freezing Point

The freezing point is the most prominent example of how the fuel chemical composition can fundamentally affect its properties. The freezing point of pure hydrocarbons increases with increasing carbon number. The freezing point is strongly dependent on the molecular structure. Due to the fact that HEFA does not contain aromatics, the freezing point of HEFA is directly influenced by the *n*-paraffin content. *n*-Paraffins have the highest freezing points among all the hydrocarbon groups in the fuel (Braun-Unkhoff, 2016). Several researchers have shown how to calculate the freezing point of a mixture from its chemical composition. One of Cookson equations calculated the freezing point only from the total amount of *n*-paraffins (Cookson et al., 1987). An additional equation utilized the total amount of the three heaviest *n*-paraffins (C_{12}-C_{14}) (Cookson et al., 1987), a third one used amount of *n*-paraffins, branched plus cyclic paraffins,

and aromatics (Cookson et al., 1987, 1992). The most recent equation of Cookson included also the boiling point values (Cookson et al., 1995). Authors indicated that every equation had the same three main limitations: (a) the tested property being out of the range studied; (b) the fuel composition being out of the range tested; and (c) the fuel having originated from a different source. The freezing point values focused in Cookson equations were in the range of -50 to -32 °C. Due to the limitation (a) and (c), none of the four Cookson equations could accurately predict the freezing point of the mixtures studied in this work. Table 8.7 in Appendix B displays the comparison between measured and calculated results from all four Cookson equations. Equation based on the total amount of *n*-paraffins provided very similar results to those measured for CAME and MFAT mixtures. The difference was within 2 °C (except for MFAT and M-60). However, this equation did not produce good results for TALL mixtures. This can be contributed to the difference between freezing point of Jet A and HEFA sample. TALL exhibited the highest difference (8 °C), while CAME and MFAT difference from Jet A was 4 and 2.5 °C only. To conclude, none of displayed equations produced accurate results for TALL/Jet A blends.

The total amount of *n*-paraffins would explain the highest freezing point value for MFAT, but would not explain the different freezing points for CAME and TALL. CAME and TALL had similar contents of *n*-paraffins, yet their freezing points were different (TALL freezing point was lower than CAME). This observation can be contributed to the content of the heaviest *n*-paraffins. CAME contained *n*-C_{16} and *n*-C_{17} as opposed to TALL. Therefore, the freezing point of CAME was higher than that of TALL. This finding is in good agreement with Solash[39] and Cookson[22], who stated that the freezing point is more dependent on the three heaviest *n*-paraffins as opposed to the sum of all *n*-paraffins. All freezing point values of the mixtures fell between the freezing points of theirs blending components as shown in

Table 5.8. The maximum values for the freezing point of jet fuels regulated by ASTM are -40 and -47 °C for Jet A and Jet A-1, respectively. Therefore, the addition of HEFA to the Jet A/A-1 does not exceed this value; however, the final freezing point can be increased or decreased in the dependence of freezing point of particulate HEFA used for blending.

Table 5.8 Freezing Point of Jet A, CAME, TALL, MFAT, and Their Mixtures (°C)

	Jet A	C-10	C-20	C-30	C-40	C-50	C-60	CAME
Measured	-51.0	-51.0	-51.5	-52.0	-52.0	-53.0	-53.5	-55.0
	Jet A	T-10	T-20	T-30	T-40	T-50	T-60	TALL
Measured	-51.0	-54.0	-54.0	-54.0	-56.0	-57.0	-58.0	-59.0
	Jet A	M-10	M-20	M-30	M-40	M-50	M-60	MFAT
Measured	-51.0	-51.0	-51.0	-51.0	-50.5	-50.5	-50.5	-48.5

5.3.8 Flash Point

Flash point is defined as the lowest temperature the fuel vapors ignite upon exposure to a source of ignition. Flash point is referred to as one of fuel safety property. The flash point depends on the molecular structure (Shi et al., 2017). Flash point values of pure hydrocarbons increase with increasing carbon number (Braun-Unkhoff, 2016), similar to freezing point. Flash point also increases with increasing boiling point (higher vapor pressure). In other words, isoparaffins of the same carbon number have the lowest flash point amongst all the other hydrocarbon classes (e.g., *n*-paraffins). HEFA samples were composed primarily of *n*-paraffins and isoparaffins. Therefore, in this study, the most influential factor was the isoparaffins content of compound with low carbon number. None of neat HEFA samples contained C_7 isoparaffins; therefore, the C_8 isoparaffins content impacted the HEFA flash point the most. The C_8 isoparaffins content was decreased in following order: MFAT (2.05 wt.%) > CAME (1.48 wt.%) > TALL (0.06 wt.%). Hence, flash point of HEFA samples increased in following order: MFAT < CAME < TALL. This observation additionally was supported by the IBP values of these samples.

In general, for standard kerosene-type jet fuels the flash point value has to be minimum 38 °C; however, a minimum value can be higher upon agreement between purchaser and supplier[5]. All HEFA samples had flash point values higher than 38 °C. The flash point value of Jet A utilized in this study was 43 °C. CAME and MFAT had flash point values lower than Jet A; therefore, all CAME and MFAT mixtures with Jet A had flash point values lower than neat Jet A. On the contrary, TALL had flash point value higher than Jet A, yielding higher flash point

values for each mixture. The repeatability of ASTM D56 method is 1.2 °C, which could be the reason several mixtures had the same flash point value.

Flash point can be predicted or calculated either from the detailed chemical composition[26] or from other fuel properties. ASTM method D7215 displays the steps to calculate flash point equivalent to methods ASTM D93 and D56 from simulated distillation data. The equation for D56 test method is displayed in Equation $CFP_{D56} = -55.5 + 0.164 * T_{IBP} + 0.095 * T_{5\,\%} + 0.453 * T_{10\,\%}$ (5.2).

$$CFP_{D56} = -55.5 + 0.164 * T_{IBP} + 0.095 * T_{5\,\%} + 0.453 * T_{10\,\%} \quad (5.2)$$

Where CFP is calculated flash point, T_{IBP} is the initial boiling point temperature, $T_{5\,\%}$ and $T_{10\,\%}$ are temperatures at which the 5 and 10 vol.% of the sample were recovered, respectively. This method was developed using petroleum-derived diesel and jet fuel samples via partial least squares (PLS) regression. ASTM D7215 can produce reliable results for petroleum-derived samples (Jet A/A-1); however, this equation was not designed nor verified for mixtures of Jet A/A-1 with alternative blending components such as HEFA. Therefore, the original ASTM formula was applied and a new equation was developed in this study to optimize the calculations for such blends. The new formula for calculation of the flash point was created utilizing PLS and the same values (T_{IBP}, $T_{5\,\%}$, and $T_{10\,\%}$) from simulated distillation analysis. The equation developed for ASTM D56 test method is displayed in Equation $CFP_{D56} = -55.5 + 0.164 * T_{IBP} + 0.095 * T_{5\,\%} + 0.453 * T_{10\,\%}$ (5.2).

$$CFP_{D56} = -39.244 + 0.246 * T_{IBP} - 0.058 * T_{5\,\%} + 0.428 * T_{10\,\%} \quad (5.3)$$

The model was cross-validated by choosing different sets of samples that were used for calibration and validation. The mean average percent error was 0.75 °C and the coefficient of determination R^2 was 0.974. Flash point results obtained from direct measurement according to ASTM D56, results calculated using ASTM D7215, and results calculated using Equation $CFP_{D56} = -39.244 + 0.246 * T_{IBP} - 0.058 * T_{5\,\%} + 0.428 * T_{10\,\%}$ (5.3) are displayed in Figure 5.8.

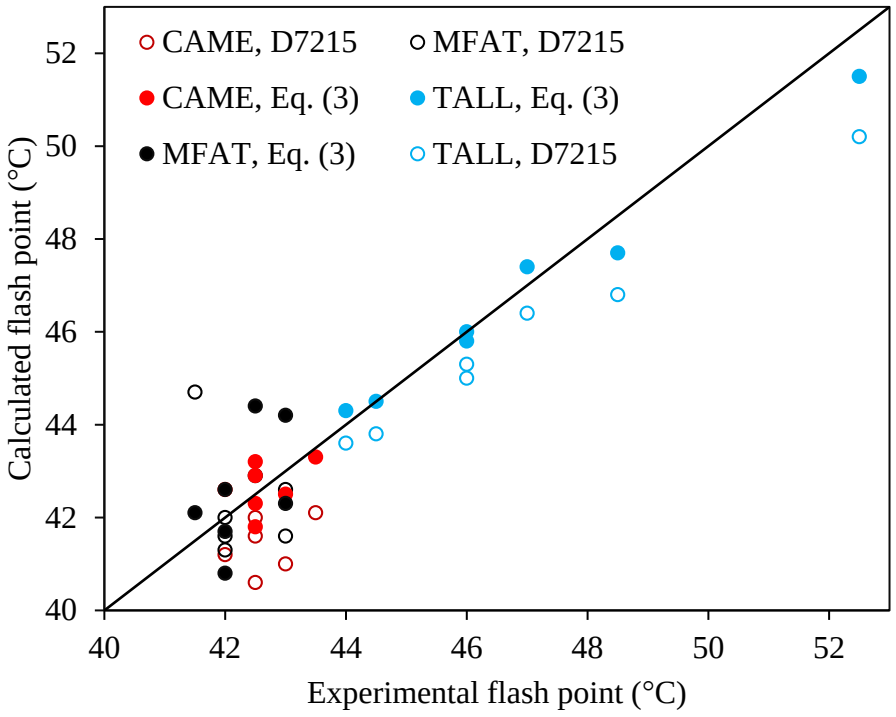

Figure 5.8 Flash Point (°C) Results Obtained from D56, Calculated from D2887, and Eq. (5.3)

5.3.9 Net Heat of Combustion

Net heat of combustion (NHC) values of all neat HEFA samples were higher than the minimum limit defined by ASTM D1655 (42.8 MJ/kg). NHC decreases in the order of paraffins > cycloparaffins > aromatics. NHC of isoparaffins is in most cases slightly lower than that of *n*-paraffins for the same carbon number (Shi et al., 2017; Braun-Unkhoff et al., 2016). Jet A NHC was 43.11 MJ/kg. When comparing the neat HEFA samples (Table 13), NHC increased in the following order: MFAT < CAME < TALL. The same approach that was utilized for density was used for NHC in order to discover how the NHC was affected by the chemical composition. This approach allowed to compare the contribution to the total NHC for each carbon number and each hydrocarbon class. Detailed NHC contribution can be found in Appendix B, Table 8.7. Net heat of combustion calculation from detailed chemical composition was shown in a previous work (Shi et al., 2017).

Although NHC of all HEFA samples was almost the same, the NHC values of HEFA samples slightly increased in the following order: MFAT < CAME < TALL. The relationship

between NHC and the blending component concentration was found to be linear. Consequently, NHC of each mixture can be simply calculated from the Jet A and HEFA NHC values, as displayed in Equation $NHC_m = \sum_i w_i NHC_i$ (5.4).

$$NHC_m = \sum_i w_i NHC_i \quad (5.4)$$

Where NHC_m is net heat of combustion of the mixture, w_i *is* the weight fraction of the neat blend component, and NHC_i is the net heat of combustion of the neat blend component. NHC can be also calculated either from the detailed chemical composition (Shi et al., 2017; Fodor & Kohl, 1993) or from other fuel properties. ASTM methods D1405 and D4529 provide the information on how to calculate NHC from aniline point and density. Another method that can be used for NHC calculations utilizes distillation data, aromatic content (vol.%), and density is the ASTM method D3338. As this calculation method is officially permitted method listed in many world-wide jet fuel specifications, it was applied on all analyzed samples. The results were compared to those obtained empirically via the method ASTM D4809. Even though the net heat of combustion of all samples was in the range of 40.19 and 44.73 MJ/kg as required by ASTM D3338, this method was not originally designed for HEFA samples and/or their blends. However, the difference between both methods did not exceed reproducibility even repeatability values of the method ASTM D4809. Therefore, further improvement of calculation method (ASTM D3338) was not necessary. Comparison of all results obtained from ASTM D4809, D3338, and Eq. (5.4) are shown in Table 5.9.

Table 5.9 Net Heat of Combustion (MJ/kg) of Neat HEFA Samples and Their Mixtures with Jet A Determined Using ASTM D4809 and Calculated from Eq. (5.4) and ASTM D3338

	Jet A	C-10	C-20	C-30	C-40	C-50	C-60	CAME
D4809	43.11	43.16	43.27	43.35	43.45	43.55	43.64	44.15
Eq. (4)	-	43.21	43.31	43.41	43.51	43.61	43.72	-
D3338	43.13	43.24	43.34	43.43	43.53	43.63	43.73	44.13
	Jet A	T-10	T-20	T-30	T-40	T-50	T-60	TALL
D4809	43.11	43.16	43.27	43.35	43.45	43.55	43.64	44.17
Eq. (4)	-	43.21	43.31	43.41	43.52	43.62	43.73	-
D3338	43.13	43.24	43.33	43.44	43.53	43.63	43.72	44.14

Table 5.9 continued

	Jet A	M-10	M-20	M-30	M-40	M-50	M-60	MFAT
D4809	43.11	43.18	43.23	43.35	43.45	43.54	43.64	44.11
Eq. (4)	-	43.21	43.30	43.40	43.50	43.60	43.70	-
D3338	43.13	43.25	43.29	43.44	43.54	43.63	43.73	44.13

5.4 Summary and Conclusion

In this study, detailed compositions of Jet A, HEFA from camelina, tallow, and mixed fat were determined using comprehensive two-dimensional gas chromatography with electron ionization high resolution time-of-flight and mass spectrometry and flame ionization detectors. Approximately one thousand compounds were detected in Jet A fuel, while almost half the number were also found in HEFA samples. HEFA samples were composed of *n*-paraffins, isoparaffins, monocycloparaffins, and minute amount of alkylbenzenes (0.01-0.03 wt.%). Mixtures of Jet A and each HEFA were prepared in volumetric concentrations in the range of 10-60 %. Selected physiochemical properties of all blending components and all mixtures were determined. It was discovered that the distillation profile had the highest impact on the final HEFA composition and properties, especially on flash point. Density of the mixtures was additive and was simply calculated from densities of Jet A and HEFA. Viscosity was not additive; however, the relationship between viscosity and increasing concentration of HEFA in Jet A followed a second-degree polynomial trend. Freezing point of HEFA sourced from mixed fat was higher than that of Jet A; therefore, this particular HEFA negatively influenced the final freezing point. This was caused by the different *n*-paraffin content in each HEFA sample. Freezing point of all mixtures fell between freezing points of individual blend components (Jet A and HEFA), no inconsistencies were observed. Flash point of HEFA from camelina and mixed fat was slightly lower than that of Jet A. Addition of HEFA samples to Jet A thus decreased the final flash point in those cases. A new equation for flash point calculation was introduced in order to improve the D7215 method, which is not accurate for alternative blending components and their mixtures with Jet A. Net heat of combustion of each HEFA sample was higher than that of Jet A; therefore, the blending did not negatively influence the final value. ASTM D3338 method for the calculation of net calorific value from physicochemical properties was validated

and it was shown that this method produced very similar results to those experimentally obtained from ASTM D4309 (bomb calorimeter) method.

CHAPTER 6. CONCLUSION

The goal of this study was to develop correlations between fuel chemical composition and fuel properties. First, the predecessor of this goal was to developed a method for ***detailed chemical characterization*** of aviation fuels. For this purpose, a comprehensive two-dimensional gas chromatography (GC×GC) equipped with time-of-flight mass spectrometry (TOF/MS) and a flame ionization detector (FID) was used. We developed an analytical method that was described in Chapter 3 and 4. Our analytical method was optimized to provide the most thorough fuel analysis via a ***GC×GC-FID***. This method is relatively cheap, fast, and precise. Additionally, our results were compared to those obtained at NAVAIR and NRL to better understand the reproducibility of the test method. One of the most important factors that can affect the quantitative results obtained from GC×GC-FID data is the process of classification. ***Classification*** is a process that has to be completed by the operator and refers to a procedure of assigning to "unknown" peaks their carbon number and hydrocarbon class. The precise and thoroughly detailed step-by-step procedure on the classification process was filed as a patent (Kilaz & Vozka, 2018) and published in *Fuel* (Vozka & Kilaz, 2019). Our collaborators utilized this method for all the related work on fuel sample analysis (Luning Prak, Fries, Gober, Vozka, Kilaz, Johnson, Graft, Trulove, & Cowart, 2019; Romanczyk, Velasco, Xu, Vozka, Dissanayake, Wehde, Roe, Keating, Kilaz, Trice, Luning Prak, & Kenttämaa, 2019).

The next step was to use the data from GC×GC-FID and develop correlations between the Tier 1 fuel properties. In CHAPTER 3, the chemical composition was utilized for predicting hydrogen and carbon content as well as the average molecular weight. Later, this approach served as a core for CHAPTER 4CHAPTER 5. In CHAPTER 4, the method of predicting density at 15 °C from fuel chemical composition was introduced. CHAPTER 5 focuses on three HEFA samples with very similar chemical compositions. This chapter aims to describe the differences in fuel properties upon blending with Jet A. Relationships of these blends were discussed from the perspective of main fuel physio-chemical properties, such as density, viscosity, flash point, freezing point, and net heat of combustion. Additionally, using a similar approach that was described in Chapter 4, correlations were developed for viscosity, net heat of combustion, freezing point, and flash point. All of these predictions were based on a statistical approach as well as methods of partial least squares regression, support vector machine, neural

networks, etc. Due to the high number (96) of correlation coefficients in each equation, the correlations were implemented to an application using Matlab. Thanks to this step, the output from GC×GC-FID can be simply uploaded into the application and the property results are automatically calculated and displayed.

To conclude, our data and publications can serve as a baseline for implementing GC×GC methodology into an ASTM standard. This would enable to evaluate fuel quality based on the chemical composition and not only based on the fuel properties. We believe that our approach bridges the gaps between fuel chemical composition and fuel properties.

6.1 Limitations

The proposed methods in CHAPTER 3, 4, andCHAPTER 5 have several limitations. Although, these limitations were discussed in each chapter separately, below is a summary of the main limitations.

6.1.1 Middle distillates hydrogen content via GC×GC-FID

The only limitation of this paper is the classification process. Classification is a process that has to be accomplished by the operator on GC×GC-FID and refers to a procedure of assigning to "unknown" peaks their carbon number and hydrocarbon class. The hydrogen and carbon content is always the same for all compounds with the same carbon number from the same hydrocarbon class. Therefore, the calculations of the hydrogen content are very dependent on the results from GC×GC-FID. If the classification is developed properly and every compound is assigned with the accurate carbon number and hydrocarbon class, the resulting hydrogen content will be 100% accurate. However, this is a very challenging process; especially because the fuel can contain ca. 2000 compounds. For this reason, we patented a step-by-step procedure on how to develop a very accurate classification. Additionally, our paper focusing on this "problem" is currently under review.

6.1.2 Jet fuel density via GC×GC-FID

There are several limitations to this paper. One limitation is the classification process itself as discussed above. Another limitation stems from the density values selected for each group. It helps to note here that "group" refers to all compounds with the same carbon number from the same hydrocarbon class. Density values of each compound in the same group are not the same (unlike the hydrogen content); however, they are in close proximity (± 0.0050 g/cm^3). Therefore, the representative compound density can influence the final results. Fuels are complex mixtures of many hydrocarbons. The representative compound was selected as the compound with the highest concentration in the fuel. For this reason, the density value should be more reliable than the average density value, which was used previously by other researchers. Still, fuel blending components mixtures that contain only a few compounds (SIP, ATJ, etc.) can result with higher differences between the predicted and measured density values.

6.1.3 Impact of HEFA feedstock on fuel composition and properties in blends with Jet A

In addition to the limitations introduced by the use of GC×GC-FID, there are several other limitations that should be discussed. In Chapter 5, a new equation for predicted flash point was introduced. The precision of this equation is limited by the fuel samples utilized for the development of the equation. Three HEFA samples were used in this study. Currently, these three HEFAs are the only commercially available. However, in the future, there can be additional HEFA samples from different feedstocks than those that have been tested. This should be taken into consideration when this equation is used for predicting of the flash point.

6.2 Future Work

Future work can be divided into two parts: (i) chemical composition and (ii) correlations between fuel chemistry and fuel properties. In terms of chemical composition, several aspects should be addressed in the future. One is the response factors of the hydrocarbon compounds and especially the compounds with higher carbon number. It was assumed that the FID detector has the same response factor for all hydrocarbon compounds. However, these studies were conducted for single GC-FID and not for GC×GC. The additional separation parameter (the secondary column) may have introduced some variance in response factors. This should be evaluated in the

future. One significant limitation of GC×GC is the overlapping of cycloparaffins and olefins. Overlapping refers to the elution space being shared for these types of compounds. In general, petroleum-based jet fuels do not contain any significant amount of olefins; however, the alternative blends, especially those produced via hydroprocessing, can contain olefins in higher amounts. Last but not least, the heteroatoms (S, N, O) overlap with aromatics. Being able to distinguish these groups from one another would be a significant advantage for obtaining a very detailed and accurate chemical composition and in future correlations as these groups may have a significant impact on some physio-chemical properties.

In this study, about 70% of fuel properties from Tier 1 testing were successfully predicted from fuel chemical composition. The future work should be focused on: (i) correlating the rest of these properties such as existent gum content, thermal stability, corrosion, and smoke point to fuel chemical composition, (ii) improving these correlations by expanding the fuel database, and (iii) focusing on correlating the fuel chemistry to Tier 2 and 3 testing.

6.3 Summary

This chapter summarized the main conclusions of our analytical methods for obtaining jet fuel chemical composition as well as the method developed on how to correlate the composition to hydrogen content, carbon content, average molecular weight, and density at 15 °C. In addition, the limitations of all these methods were discussed in Chapters 6.1. The proposed future work was discussed in Chapter 6.2.

APPENDIX A. DENSITY PAPER

Table A.1 Studied Compounds and Their Density Values Measured at Temperatures Different from 15 °C

compound	T_1 °C	density at T_1 (g/cm^3)	T_2 °C	density at T_2 (g/cm^3)
n-tridecane	20	0.7565	25	0.7529
n-tetradecane	20	0.7631	25	0.7593
n-hexadecane	20	0.7734	25	0.7699
n-heptadecane	20	0.7780	25	0.7745
n-octadecane	20	0.7819	30	0.7752
n-nonadecane	20	0.7855	25	0.7821
3,3-dimethylpentane	20	0.6932	25	0.6892
4-ethyl-2-methylhexane	20	0.7230	25	0.7190
2-methylnonane	20	0.7264	25	0.7281
2-methyldecane	20	0.7369	40	0.7216
2,2,4,6,6-pentamethylheptane	20	0.7463	25	0.7418
3-methyldodecane	20	0.7582	40	0.7440
3-methyltridecane	20	0.7649	40	0.7505
2,6,10-trimethyldodecane	20	0.7746	25	0.7682
2,2,4,4,6,8,8-heptamethylnonane	20	0.7850	25	0.7812
4-methylhexadecane	20	0.7790	40	0.7655
2-methylheptadecane	20	0.7803	40	0.7666
2,6,10,14-tetramethylpentadecane	20	0.7828	25	0.7791
ethylcyclopentane	20	0.7665	25	0.7622
ethylcyclohexane	20	0.7882	25	0.7842
1-ethyl-1-methylcyclohexane	20	0.8052	25	0.8050
pentylcyclohexane	20	0.8044	25	0.8002
hexylcyclohexane	20	0.8082	25	0.8045
heptylcyclohexane	20	0.8109	25	0.8074

Table A.1 continued

octylcyclohexane	20	0.8138	25	0.8104
decylcyclohexane	20	0.8186	25	0.8152
undecylcyclohexane	20	0.8206	25	0.8172
dodecylcyclohexane	20	0.8223	25	0.8190
octahydropentalene	20	0.8670	25	0.8638
octahydro-1H-Indene, cis-	20	0.8821	25	0.8803
decahydronaphthalene	20	0.8698	25	0.8659
2-syn-methyl-cis-decalin	20	0.8760	37.8	0.8536
2-ethyldecahydronaphthalene	20	0.8803	37.8	0.8663
2-methyl-1,1'-bicyclohexyl, cis-	20	0.8845	37.8	0.8715
1-(cyclohexylmethyl)-2-methylcyclohexane, trans-	20	0.8850	37.8	0.8746
1,1'-(1-methyl-1,3-propanediyl)bis-cyclohexane	20	0.8800	25	0.8767
1,2,3-trimethylbenzene	20	0.8944	25	0.8904
1,2,3,4-tetramethylbenzene	20	0.9046	25	0.9015
1-sec-butyl-4-methylbenzene	20	0.8660	25	0.8620
hexylbenzene	20	0.8577	30	0.8501
heptylbenzene	20	0.8567	25	0.8530
octylbenzene	20	0.8738	25	0.8699
indane	20	0.9640	25	0.9600
1,2,3,4-tetrahydronaphthalene	20	0.9689	25	0.9650
2,3-dihydro-1,6-dimethyl-1H-indene	20	0.9301	25	0.9289
1,2,3,4-tetrahydro-5,7-dimethylnaphthalene	20	0.9583	25	0.9537
1,2,3,4-tetrahydro-1,1,6-trimethylnaphthalene	20	0.9341	25	0.9320
6-(1-ethylpropyl)-1,2,3,4-tetrahydronaphthalene	20	0.9285	25	0.9249
naphthalene	85	1.0070	95	1.0056
1-methylnaphthalene	18.6	1.0213	20	1.0202
1,7-dimethylnaphthalene	20	1.0030	25	1.0000
1-propylnaphthalene	20	0.9899	25	0.9882
pentylnaphthalene	20	0.9669	25	0.9622

Table A.2 Correlation Coefficients for PLS and SVM Obtained Using 74 Predictors

Coefficients	hydrocarbon class[a]	carbon number	PLS *product*	PLS *composition*	SVM *product*	SVM *composition*
β_0; intercept	-	-	0.8162328	0.8226520	0.0073569	0.0049712
β_1	A	7	0	0	0	0
β_2	A	8	-0.0006900	-0.0006478	0.0122018	0.0100144
β_3	A	9	-0.0004991	-0.0004297	0.0042829	0.0019480
β_4	A	10	-0.0014297	-0.0011731	0.0103105	0.0079045
β_5	A	11	-0.0016791	-0.0013649	0.0069827	0.0054069
β_6	A	12	-0.0010863	-0.0008769	0.0071666	0.0043332
β_7	A	13	-0.0004706	-0.0004031	0.0130461	0.0106900
β_8	A	14	-0.0002416	-0.0002484	0.0070618	0.0050548
β_9	A	15	-0.0000880	-0.0001154	0.0102781	0.0086973
β_{10}	A	16	0.0002640	0.0001804	0.0151150	0.0131163
β_{11}	A	17	0.0001679	0.0001191	0.0091247	0.0081069
β_{12}	A	18	0.0000628	0.0000493	0.0036718	0.0035642
β_{13}	A	19	0.0000218	0.0000170	0.0014881	0.0013963
β_{14}	A	20	0.0000082	0.0000051	0.0004725	0.0003705
β_{15}	B	7	0	0	0	0
β_{16}	B	8	-0.0003096	-0.0002993	0.0049478	0.0025300
β_{17}	B	9	-0.0004500	-0.0003927	0.0136448	0.0108486
β_{18}	B	10	-0.0005642	-0.0004497	0.0058687	0.0031354
β_{19}	B	11	-0.0011664	-0.0009348	0.0121202	0.0092712
β_{20}	B	12	-0.0007390	-0.0006170	0.0101479	0.0077448
β_{21}	B	13	-0.0009758	-0.0008024	0.0100930	0.0078069
β_{22}	B	14	-0.0006874	-0.0006156	0.0114826	0.0097479
β_{23}	B	15	-0.0005770	-0.0005141	0.0097847	0.0076618
β_{24}	B	16	-0.0007725	-0.0006910	0.0087920	0.0062729
β_{25}	B	17	-0.0008090	-0.0006976	0.0091309	0.0066714
β_{26}	B	18	-0.0000808	-0.0000754	0.0109285	0.0098507

Table A.2 continued

β_{27}	B	19	0.0000979	0.0000757	0.0069297	0.0069049
β_{28}	B	20	0.0000332	0.0000203	0.0022453	0.0016735
β_{29}	C	7	0.0000998	0.0000636	0.0141883	0.0121880
β_{30}	C	8	-0.0003776	-0.0003449	0.0187739	0.0155027
β_{31}	C	9	0.0000211	0.0000033	0.0112134	0.0095396
β_{32}	C	10	0.0003274	0.0002658	0.0049682	0.0032336
β_{33}	C	11	0.0007860	0.0006180	0.0115686	0.0101774
β_{34}	C	12	0.0013064	0.0010084	0.0114646	0.0079196
β_{35}	C	13	0.0010254	0.0007446	0.0111348	0.0089085
β_{36}	C	14	0.0008875	0.0006401	0.0102013	0.0082583
β_{37}	C	15	0.0004569	0.0003293	0.0153369	0.0127944
β_{38}	C	16	0.0001621	0.0001199	0.0110505	0.0102152
β_{39}	C	17	0.0000136	0.0000098	0.0028824	0.0028039
β_{40}	C	18	0	0	0	0
β_{41}	C	19	0	0	0	0
β_{42}	C	20	0	0	0	0
β_{43}	D	7	0	-0.0000644	0	0.0008829
β_{44}	D	8	-0.0000360	-0.0000320	0.0039938	0.0036874
β_{45}	D	9	0.0000051	-0.0000018	0.0070061	0.0058943
β_{46}	D	10	0.0004700	0.0003356	0.0043038	0.0032122
β_{47}	D	11	0.0006961	0.0004997	0.0144055	0.0127789
β_{48}	D	12	0.0007573	0.0005412	0.0106231	0.0097217
β_{49}	D	13	0.0002402	0.0001646	0.0066657	0.0060353
β_{50}	D	14	0.0001460	0.0001037	0.0017991	0.0026967
β_{51}	D	15	0.0000332	0.0000231	0.0021438	0.0020748
β_{52}	D	16	0.0000013	0.0000008	0.0008054	0.0007173
β_{53}	D	17	0	0.0000001	0	0.0000764
β_{54}	D	18	0	0	0	0
β_{55}	D	19	0	0	0	0

Table A.2 continued

β_{56}	D	20	0	0	0	0
β_{57}	E	7	0.0000746	0.0000512	0.0010111	0.0003705
β_{58}	E	8	0.0004198	0.0003093	0.0062482	0.0045036
β_{59}	E	9	0.0007797	0.0006098	0.0124155	0.0117340
β_{60}	E	10	0.0007227	0.0005919	0.0180967	0.0175836
β_{61}	E	11	0.0003802	0.0003376	0.0055162	0.0046108
β_{62}	E	12	0.0006786	0.0005374	0.0090743	0.0072675
β_{63}	E	13	0.0006096	0.0004672	0.0144280	0.0125920
β_{64}	E	14	0.0002763	0.0001982	0.0068693	0.0053117
β_{65}	E	15	0.0001550	0.0001119	0.0028323	0.0017046
β_{66}	E	16	0	0.0000500	0	0.0023461
β_{67}	E	17	0	0.0000053	0	0.0005071
β_{68}	E	18	0	0	0	0
β_{69}	E	19	0	0	0	0
β_{70}	E	20	0	0	0	0
β_{71}	F	7	0	0	0	0
β_{72}	F	8	0	0	0	0
β_{73}	F	9	0.0000773	0.0000545	0.0016952	0.0011502
β_{74}	F	10	0.0004175	0.0002959	0.0056549	0.0045579
β_{75}	F	11	0.0008839	0.0006466	0.0112675	0.0099832
β_{76}	F	12	0.0010540	0.0007294	0.0062105	0.0075895
β_{77}	F	13	0.0006168	0.0004207	0.0127688	0.0125338
β_{78}	F	14	0.0003994	0.0002633	0.0042449	0.0039247
β_{79}	F	15	0.0001548	0.0001010	0.0096324	0.0081710
β_{80}	F	16	0	0.0000034	0	0.0002894
β_{81}	F	17	0	0	0	0
β_{82}	F	18	0	0	0	0
β_{83}	F	19	0	0	0	0
β_{84}	F	20	0	0	0	0

Table A.2 continued

β_{85}	G	7	0	0	0	0
β_{86}	G	8	0	0	0	0
β_{87}	G	9	0	0	0	0
β_{88}	G	10	-0.0000242	-0.0000145	0.0036599	0.0030000
β_{89}	G	11	0.0000142	0.0000053	0.0081537	0.0069164
β_{90}	G	12	-0.0000127	-0.0000233	0.0051068	0.0053463
β_{91}	G	13	0.0001048	0.0000587	0.0087572	0.0074968
β_{92}	G	14	0.0000815	0.0000522	0.0061802	0.0050093
β_{93}	G	15	0.0000266	0.0000171	0.0020001	0.0016443
β_{94}	G	16	0	0	0	0
β_{95}	G	17	0	0	0	0
β_{96}	G	18	0	0	0	0
β_{97}	G	19	0	0	0	0
β_{98}	G	20	0	0	0	0

[a]A – *n*-paraffins, B – isoparaffins, C – monocycloparaffins, D – di- and tricycloparaffins, E – alkylbenzenes, F – cycloaromatic compounds, and G – alkylnaphthalenes.

APPENDIX B. HEFA PAPER

Table B.1 Chromatographic Conditions for GC×GC-FID Using Rxi-17 Sil MS and Rxi-1ms Columns

Parameters	Description
Column	Primary: Rxi-17Sil MS Restek (60 m × 0.25 mm × 0.25 μm) Secondary: Rxi-1ms Restek (1.1 m × 0.25 mm × 0.25 μm)
Carrier gas	UHP helium, 1.25 mL/min
Oven temperature	isothermal 40 °C for 0.6 min, followed by a linear gradient of 1 °C/min to a temperature of 180 °C being held isothermally for 5 min
Modulation period	8.0 s with 1.3 s hot pulse time
Offsets	Secondary oven: 35 °C Modulator: 15 °C

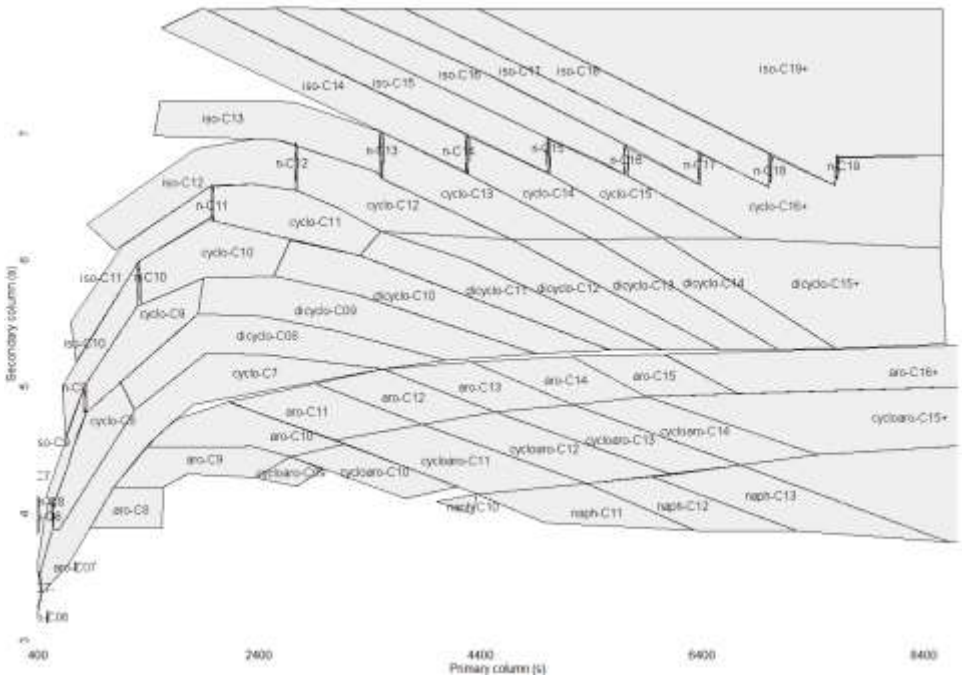

Figure B.1 GC×GC-FID Classification for Jet Fuels Pertinent Hydrocarbon Classes Explanation: isoparaffins (iso-), *n*-paraffins (n-), monocycloparaffins (cyclo-), di- + tricycloparaffins (dicyclo-), alkylbenzenes (aro-), cycloaromatics (cycloaro-), and alkylnaphthalenes (naph-)

Table B.2 Hydrocarbon Type Composition (wt.%) of Jet A, CAME, TALL, and MFAT Utilizing Rxi Columns

Fuel Type	Jet A	CAME	TALL	MFAT
n-paraffins				
C7	0.00	0.00	0.00	0.00
C8	0.67	0.83	0.10	0.54
C9	4.42	1.92	1.84	1.00
C10	4.73	1.40	1.69	1.42
C11	3.44	0.84	1.33	1.36
C12	2.49	0.59	1.12	1.44
C13	1.93	0.49	0.86	0.87
C14	1.31	0.23	0.56	1.67
C15	0.79	0.46	0.32	0.18
C16	0.38	0.20	0.00	0.70
C17	0.09	0.12	0.00	0.01
C18	0.02	0.00	0.00	0.00
total *n*-paraffins	20.26	7.07	7.81	9.20
isoparaffins				
C7	0.01	0.00	0.00	0.01
C8	0.31	1.51	0.06	1.77
C9	4.12	11.09	6.13	3.65
C10	6.63	11.10	12.14	6.69
C11	5.02	9.62	12.60	10.33

Table B.2 continued

C12	3.21	8.27	13.52	12.37
C13	2.95	8.33	12.69	11.54
C14	2.39	6.39	8.75	13.98
C15	1.66	5.42	21.74	4.29
C16	0.87	2.14	4.13	20.73
C17	0.19	21.58	0.00	0.29
C18	0.08	4.71	0.00	3.44
C19	0.00	0.00	0.00	0.00
total isoparaffins	27.46	90.15	91.75	89.11

monocycloparaffins				
C7	0.19	0.10	0.00	0.07
C8	5.81	1.94	0.22	0.76
C9	5.26	0.52	0.18	0.41
C10	4.58	0.15	0.02	0.27
C11	2.82	0.04	0.01	0.14
C12	2.50	0.00	0.00	0.02
C13	1.53	0.00	0.00	0.01
C14	0.65	0.00	0.00	0.00
C15	0.02	0.00	0.00	0.00
C16	0.00	0.00	0.00	0.00
total monocycloparaffins	23.39	2.74	0.44	1.67

Table B.2 continued

di- and tricycloparaffins				
C8	0.86	0.00	0.00	0.00
C9	1.21	0.01	0.00	0.00
C10	1.05	0.00	0.00	0.00
C11	0.80	0.00	0.00	0.00
C12	0.27	0.00	0.00	0.00
C13	0.09	0.00	0.00	0.00
C14	0.00	0.00	0.00	0.00
C15	0.00	0.00	0.00	0.00
total di- and tricycloparaffins	4.27	0.01	0.00	0.00
total cycloparaffins	27.66	2.75	0.44	1.67
alkylbenzenes				
C7	0.07	0.00	0.00	0.01
C8	1.79	0.01	0.00	0.00
C9	4.54	0.02	0.00	0.01
C10	3.27	0.00	0.00	0.00
C11	2.73	0.00	0.00	0.00
C12	1.76	0.00	0.00	0.00
C13	0.98	0.00	0.00	0.00
C14	0.47	0.00	0.00	0.00
C15	0.15	0.00	0.00	0.00

Table B.2 continued

C16	0.00	0.00	0.00	0.00
C17	0.00	0.00	0.00	0.00
total alkylbenzenes	15.76	0.03	0.00	0.02
cycloaromatics				
C9	0.14	0.00	0.00	0.00
C10	0.45	0.00	0.00	0.00
C11	2.43	0.00	0.00	0.00
C12	2.21	0.00	0.00	0.00
C13	1.46	0.00	0.00	0.00
C14	0.42	0.00	0.00	0.00
C15	0.00	0.00	0.00	0.00
C16	0.00	0.00	0.00	0.00
total cycloaromatics	7.13	0.00	0.00	0.00
alkylnaphthalenes				
C10	0.11	0.00	0.00	0.00
C11	0.44	0.00	0.00	0.00
C12	0.63	0.00	0.00	0.00
C13	0.51	0.00	0.00	0.00
C14	0.04	0.00	0.00	0.00
C15	0.00	0.00	0.00	0.00

Table B.2 continued

total alkylnaphthalenes	1.73	0.00	0.00	0.00
total aromatics	24.62	0.03	0.00	0.02
total	100.00	100.00	100.00	100.00

Using this column setup, CAME and MFAT contained ca. 490 compounds (peaks) while TALL had ca. 345 compounds. Jet A contained ca. 1050 compounds.

Table B.3 Density Contribution (g/cm^3) for Every Carbon Number from Each Hydrocarbon Class

Fuel Type	CAME	TALL	MFAT
n-paraffins			
C7	0.0000	0.0000	0.0000
C8	0.0111	0.0009	0.0052
C9	0.0156	0.0143	0.0081
C10	0.0101	0.0127	0.0110
C11	0.0072	0.0116	0.0115
C12	0.0062	0.0107	0.0110
C13	0.0049	0.0079	0.0087
C14	0.0019	0.0053	0.0134
C15	0.0039	0.0025	0.0011
C16	0.0011	0.0000	0.0061
C17	0.0009	0.0000	0.0002
C18	0.0000	0.0000	0.0000
total *n*-paraffins	0.0630	0.0659	0.0763
isoparaffins			
C7	0.0000	0.0000	0.0000
C8	0.0105	0.0004	0.0145
C9	0.0813	0.0440	0.0268

Table B.3 continued

C10	0.0822	0.0878	0.0497
C11	0.0731	0.0947	0.0781
C12	0.0636	0.1009	0.0927
C13	0.0622	0.0942	0.0880
C14	0.0483	0.0696	0.1030
C15	0.0437	0.1713	0.0307
C16	0.0185	0.0216	0.1622
C17	0.1663	0.0000	0.0020
C18	0.0287	0.0000	0.0255
C19	0.0000	0.0000	0.0000
total isoparaffins	0.6785	0.6844	0.6732

monocycloparaffins			
C7	0.0000	0.0000	0.0000
C8	0.0064	0.0015	0.0032
C9	0.0041	0.0021	0.0035
C10	0.0024	0.0008	0.0024
C11	0.0007	0.0003	0.0013
C12	0.0002	0.0000	0.0004
C13	0.0000	0.0000	0.0005
C14	0.0000	0.0000	0.0000
C15	0.0000	0.0000	0.0000
C16	0.0000	0.0000	0.0000
total monocycloparaffins	0.0139	0.0047	0.0112

di- and tricycloparaffins			
C8	0.0000	0.0000	0.0000
C9	0.0000	0.0000	0.0000
C10	0.0000	0.0000	0.0000
C11	0.0000	0.0000	0.0000

Table B.3 continued

C12	0.0000	0.0000	0.0000
C13	0.0000	0.0000	0.0000
C14	0.0000	0.0000	0.0000
C15	0.0000	0.0000	0.0000
total di- and tricycloparaffins	0.0000	0.0000	0.0000
alkylbenzenes			
C7	0.0000	0.0000	0.0000
C8	0.0000	0.0000	0.0001
C9	0.0001	0.0000	0.0000
C10	0.0002	0.0001	0.0001
C11	0.0000	0.0000	0.0000
C12	0.0000	0.0000	0.0000
C13	0.0000	0.0000	0.0000
C14	0.0000	0.0000	0.0000
C15	0.0000	0.0000	0.0000
C16	0.0000	0.0000	0.0000
C17	0.0000	0.0000	0.0000
total alkylbenzenes	0.0003	0.0001	0.0002
TOTAL	0.7556	0.7551	0.7609
	MIDDLE	LOWEST	HIGHEST

Here should be noted that the measured density values were slightly different: 0.7598, 0.7573, and 0.7612 g/cm^3 for CAME, TALL, and MFAT, respectively. However, the prediction error followed the same trend.

Table B.4 Freezing Point of Jet A, CAME, TALL, MFAT, and Their Mixtures (°C) Calculated from Cookson Equations

	Jet A	C-10	C-20	C-30	C-40	C-50	C-60	CAME
Measured	-51.0	-51.0	-51.5	-52.0	-52.0	-53.0	-53.5	-55.0
Cookson eq.[a]	-49.3	-50.0	-50.7	-51.4	-52.2	-52.9	-53.7	-56.8
Cookson eq.[b]	-55.7	-56.0	-56.3	-56.6	-56.9	-57.3	-57.6	-58.9
Cookson eq.[c]	-48.7	-49.6	-50.5	-51.5	-52.4	-53.4	-54.4	-58.4
Cookson eq.[d]	-49.2	-50.0	-50.3	-51.1	-52.2	-53.6	-55.4	-63.7
	Jet A	T-10	T-20	T-30	T-40	T-50	T-60	TALL
Measured	-51.0	-54.0	-54.0	-54.0	-56.0	-57.0	-58.0	-59.0
Cookson eq.[a]	-49.3	-49.3	-50.6	-52.0	-53.4	-54.8	-56.2	-56.6
Cookson eq.[b]	-55.7	-55.9	-56.1	-56.3	-56.5	-56.7	-56.9	-57.7
Cookson eq.[c]	-48.7	-48.9	-50.5	-52.1	-53.7	-55.3	-57.0	-58.2
Cookson eq.[d]	-49.2	-50.2	-53.2	-56.0	-59.0	-61.9	-64.9	-70.0
	Jet A	M-10	M-20	M-30	M-40	M-50	M-60	MFAT
Measured	-51.0	-51.0	-51.0	-51.0	-50.5	-50.5	-50.5	-48.5
Cookson eq.[a]	-49.3	-49.9	-50.5	-51.2	-51.8	-52.5	-53.1	-55.9
Cookson eq.[b]	-55.7	-55.8	-55.9	-56.0	-56.1	-56.2	-56.3	-56.7
Cookson eq.[c]	-48.7	-49.5	-50.4	-51.2	-52.1	-52.9	-53.8	-57.4
Cookson eq.[d]	-49.2	-50.0	-51.0	-52.2	-53.4	-54.7	-56.2	-61.8

[a]$FP = 60.7[n] - 62.0$; [b]$FP = 85.5[C_{12}\text{-}C_{14}] - 60.3$; [c]$FP = = -0.8[n] - 63.8[BC] - 55.9[Ar]$; [d]$FP = 81.1[n] + 53.6[Ar] + 0.255T_{10} + 0.338T_{90} - 206.2$; where [n], [BC], and [Ar] are total amounts of *n*-paraffins, branched + cyclic paraffins, and aromatics, respectively; $[C_{12}\text{-}C_{14}]$ is total amount of C_{12} to C_{14} *n*-paraffins, T_{10} and T_{90} are temperatures at which 10 and 90 vol.% of the fuel sample are collected, respectively.

Table B.5 Net Heat of Combustion Contribution (MJ/kg) for Every Carbon Number from Each Hydrocarbon Class

Fuel Type	CAME	TALL	MFAT
n-paraffins			
C7	0.0000	0.0000	0.0000
C8	0.6955	0.0543	0.3266
C9	0.9554	0.8780	0.5000
C10	0.6110	0.7662	0.6629
C11	0.4259	0.6893	0.6845
C12	0.3642	0.6282	0.6451
C13	0.2854	0.4598	0.5034
C14	0.1120	0.3048	0.7698
C15	0.2246	0.1430	0.0608
C16	0.0563	0.0000	0.3103
C17	0.0458	0.0000	0.0079
C18	0.0000	0.0000	0.0000
total *n*-paraffins	3.7762	3.9237	4.4712
isoparaffins			
C7	0.0000	0.0000	0.0000
C8	0.6594	0.0265	0.9120

Table B.5 continued

C9	4.9522	2.6820	1.6324
C10	5.0179	5.3562	3.0307
C11	4.3575	5.6426	4.6529
C12	3.7371	5.9255	5.4457
C13	3.5989	5.4449	5.0893
C14	2.7675	3.9836	5.8962
C15	2.4577	9.6466	1.7295
C16	1.0325	1.2029	9.0420
C17	9.3317	0.0000	0.1122
C18	1.6070	0.0000	1.4283
C19	0.0000	0.0000	0.0000
total isoparaffins	39.5193	39.9109	38.9712

monocycloparaffins			
C7	0.0012	0.0000	0.0000
C8	0.3542	0.0840	0.1735
C9	0.2225	0.1108	0.1887
C10	0.1275	0.0430	0.1272
C11	0.0362	0.0154	0.0687
C12	0.0125	0.0008	0.0229
C13	0.0000	0.0000	0.0245
C14	0.0000	0.0000	0.0000

Table B.5 continued

C15	0.0000	0.0000	0.0000
C16	0.0000	0.0000	0.0000
total monocycloparaffins	0.7540	0.2540	0.6054
total di- and tricycloparaffins	0.0000	0.0000	0.0000
alkylbenzenes			
C7	0.0000	0.0000	0.0070
C8	0.0036	0.0000	0.0000
C9	0.0081	0.0035	0.0031
C10	0.0000	0.0000	0.0000
C11	0.0000	0.0000	0.0000
C12	0.0000	0.0000	0.0000
C13	0.0000	0.0000	0.0000
C14	0.0000	0.0000	0.0000
C15	0.0000	0.0000	0.0000
C16	0.0000	0.0000	0.0070
C17	0.0036	0.0000	0.0000
total alkylbenzenes	0.0118	0.0035	0.0101
TOTAL	44.0614	44.0921	44.0579
	MIDDLE	HIGHEST	LOWEST

Here should be noted that the measured net heat of combustion values were slightly different: 44.15, 44.17, and 44.11 MJ/kg for CAME, TALL, and MFAT, respectively. However, the prediction error followed the same trend.

LIST OF REFERENCES

Ali, I., & Basit, M. A. (1993). Significance of hydrogen content in fuel combustion. *International journal of hydrogen energy*, 18(12), 1009-1011.

ASTM International. (2011). ASTM D3242-11 Standard test method for acidity in aviation turbine fuel. doi: 10.1520/D3242-11

ASTM International. (2016). ASTM D3343-16 Standard test method for estimation of hydrogen content of aviation fuels. doi: 10.1520/D3343-16

ASTM International. (2016). ASTM D4054-16 Standard practice for qualification and approval of new aviation turbine fuels and fuel additives. doi: 10.1520/D4054-16

ASTM International. (2016). ASTM D5291-16 Standard test methods for instrumental determination of carbon, hydrogen, and nitrogen in petroleum products and lubricants. doi: 10.1520/D5291-16

ASTM International. (2016). ASTM D7171-16 Standard test method for hydrogen content of middle distillate petroleum products by low-resolution pulsed nuclear magnetic resonance spectroscopy. doi: 10.1520/D7171-16

ASTM International. (2016). ASTM D7566-16b Standard specification for aviation turbine fuel containing synthesized hydrocarbons. doi: 10.1520/D7566-16B

ASTM International. (2017). ASTM D1655-17 Standard specification for aviation turbine fuels. doi: 10.1520/D1655-17

Blažek, J., & Rábl, V. (2006). *Základy zpracování a využití ropy*. Praha, Czech Republic: Vydavatelství VŠCHT.

Bottou, L. (2010). Large-scale machine learning with stochastic gradient descent. In *Proceedings of COMPSTAT'2010* (pp. 177-186). Physica-Verlag HD.

Braun-Unkhoff, M., Kathrotia, T., Rauch, B., & Riedel, U. (2016). About the interaction between composition and performance of alternative jet fuels. *CEAS Aeronautical Journal*, 7(1), 83-94.

Cai, G., Liu, Z., Zhang, L., Zhao, S., & Xu, C. (2018). Quantitative Structure–Property Relationship Model for Hydrocarbon Liquid Viscosity Prediction. *Energy & Fuels*, 32(3), 3290-3298.

Colket, M., Heyne, J., Rumizen, M., Gupta, M., Edwards, T., Roquemore, W. M., ... & Condevaux, J. (2017). Overview of the national jet fuels combustion program. *AiAA Journal*, 1-18. http://dx.doi.org/10.2514/1.J055361

Cookson, D. J., & Smith, B. E. (1990). Calculation of jet and diesel fuel properties using 13C NMR spectroscopy. *Energy & Fuels*, 4(2), 152-156.

Cookson, D. J., & Smith, B. E. (1992). Observed and predicted properties of jet and diesel fuels formulated from coal liquefaction and Fisher-Tropsch feedstocks. *Energy & Fuels*, 6(5), 581-585.

Cookson, D. J., Iliopoulos, P., & Smith, B. E. (1995). Composition-property relations for jet and diesel fuels of variable boiling range. *Fuel*, 74(1), 70-78.

Cookson, D. J., Latten, J. L., Shaw, I. M., & Smith, B. E. (1985). Property-composition relationships for diesel and kerosene fuels. *Fue*l, 64(4), 509-519.

Cookson, D. J., Lloyd, C. P., & Smith, B. E. (1987). Investigation of the chemical basis of kerosene (jet fuel) specification properties. *Energy & Fuels*, 1(5), 438-447.

Coordinating Research Council, Inc. (1983). *Handbook of aviation fuel properties* (Report No. 530). Atlanta, GA.

Coordinating Research Council. (2017). *Adequacy of existing test methods for aviation jet fuel and additive property evaluation* (Report No. AV-23-15). Retrieved from https://crcao.org/reports/recentstudies2017/AV-23-15/CRC%20AV-23-15%20-%20Final%20Report%20rev%207.pdf

Cramer, J. A., Hammond, M. H., Myers, K. M., Loegel, T. N., & Morris, R. E. (2014). Novel data abstraction strategy utilizing gas chromatography–mass spectrometry data for fuel property modeling. *Energy & Fuels*, 28(3), 1781-1791.

Csonka, S. (2016, September). *Sustainable alternative jet fuel – scene setting discussion*. Paper presented at U.S. Department of Energy Bioenergy Technologies Office's Alternative Aviation Fuel Workshop, Macon, GA.

Dallüge, J., Beens, J., & Udo, A. (2003). Comprehensive two-dimensional gas chromatography: a powerful and versatile analytical tool. *Journal of Chromatography A*, 1000(1-2), 69-108.

Dancuart, L. (2000, March). Processing of Fischer-Tropsch syncrude and benefits of integrating its products with conventional fuels. In *NPRA Annual Meeting*, AM-00-51.

De Klerk, A. (2014). U.S. Patent Application No. 13/999,021.

Diniz, A. P. M., Sargeant, R., & Millar, G. J. (2018). Stochastic techno-economic analysis of the production of aviation biofuel from oilseeds. *Biotechnology for biofuels*, 11(1), 161.

Edwards, J. T., Shafer, L. M., & Klein, J. K. (2012). *US Air Force hydroprocessed renewable jet (HRJ) fuel research* (Report No. AFRL-RQ-WP-TR-2013-0108). Retrieved from http://www.dtic.mil/dtic/tr/fulltext/u2/a579552.pdf

Edwards, T. (2003). Liquid fuels and propellants for aerospace propulsion: 1903-2003. *Journal of propulsion and power*, 19(6), 1089-1107.

Freye, C. E., Fitz, B. D., Billingsley, M. C., & Synovec, R. E. (2016). Partial least squares analysis of rocket propulsion fuel data using diaphragm valve-based comprehensive two-dimensional gas chromatography coupled with flame ionization detection. *Talanta*, 153, 203-210.

Gawron, B., & Białecki, T. (2018). Impact of a Jet A-1/HEFA blend on the performance and emission characteristics of a miniature turbojet engine. *International Journal of Environmental Science and Technology*, 15(7), 1501-1508.

Gieleciak, R., & Fairbridge, C. (2013). *Detailed hydrocarbon analysis of FACE diesel fuels using comprehensive two-dimensional gas chromatography* (Report No. CDEV-2013-2065-RT). Natural Resources Canada, Division Report.

Gieleciak, R., & Oro N. (2013). A Study of FID Response factor of GC× GC systems for hydrocarbon compound classes existing in diesel fractions (Report No. CDEV-2013-1979). Natural Resources Canada, Division Report.

Gupta, K. K., Rehman, A., & Sarviya, R. M. (2010). Bio-fuels for the gas turbine: A review. *Renewable and Sustainable Energy Reviews*, 14(9), 2946-2955.

Haenlein, M., & Kaplan, A. M. (2004). A beginner's guide to partial least squares analysis. *Understanding statistics*, 3(4), 283-297.

Hemighaus, G., & Rumizen, M. (2016). Discussion on uses of the specification for turbine fuels using synthesized hydrocarbons (ASTM D7566). ASTM International.

Ho, C. H., & Lin, C. J. (2012). Large-scale linear support vector regression. *Journal of Machine Learning Research*, 13(Nov), 3323-3348.

Hsieh, C. J., Chang, K. W., Lin, C. J., Keerthi, S. S., & Sundararajan, S. (2008, July). A dual coordinate descent method for large-scale linear SVM. In *Proceedings of the 25th international conference on Machine learning* (pp. 408-415). ACM.

ICAO. (2011). Alcohol to jet (ATJ) emerging through ASTM. In *ICAO aviation and sustainable alternative fuels workshop*, BYOGY Renewables: Montreal, Canada.

International Renewable Energy Agency. (2018). *Biofuels for aviation. Technology brief*. 2018. Retrieved from http://www.irena.org/documentdownloads/publications/irena_biofuels_for_aviation_2017.pdf

Jennerwein, M. K., Eschner, M., Gröger, T., Wilharm, T., & Zimmermann, R. (2014). Complete group-type quantification of petroleum middle distillates based on comprehensive two-dimensional gas chromatography time-of-flight mass spectrometry (GC× GC-TOFMS) and visual basic scripting. *Energy & Fuels*, 28(9), 5670-5681.

Kehimkar, B., Hoggard, J. C., Marney, L. C., Billingsley, M. C., Fraga, C. G., Bruno, T. J., & Synovec, R. E. (2014). Correlation of rocket propulsion fuel properties with chemical composition using comprehensive two-dimensional gas chromatography with time-of-flight mass spectrometry followed by partial least squares regression analysis. *Journal of Chromatography A*, 1327, 132-140.

Khadim, M. A., Wolny, R. A., Al-Dhuwaihi, A. S., Al-Hajri, E. A., & Al-Ghamdi, M. A. (2003). Determination of hydrogen and carbon contents in crude oil and petroleum fractions by NMR spectroscopy. *Arabian Journal for Science and Engineering. Section B: Engineering*, 28(2A), 147-162.

Kilaz, G., & Vozka, P. (2018). Set of standards for GC×GC-FID classification developing. *U.S. Patent Application No. 62751331*, filed October 2018. Patent Pending.

Kochetkova, D., Blažek, J., Šimáček, P., Staš, M., & Beňo, Z. (2016). Influence of rapeseed oil hydrotreating on hydrogenation activity of CoMo catalyst. *Fuel Processing Technology*, 142, 319-325.

Liu, G., Wang, L., Qu, H., Shen, H., Zhang, X., Zhang, S., & Mi, Z. (2007). Artificial neural network approaches on composition–property relationships of jet fuels based on GC–MS. *Fuel*, 86(16), 2551-2559.

Liu, Z., & Phillips, J. B. (1991). Comprehensive two-dimensional gas chromatography using an on-column thermal modulator interface. *Journal of Chromatographic Science*, 29(6), 227-231.

Luning Prak, D. J., Brown, E. K., & Trulove, P. C. (2013). Density, viscosity, speed of sound, and bulk modulus of methyl alkanes, dimethyl alkanes, and hydrotreated renewable fuels. *Journal of Chemical & Engineering Data*, 58(7), 2065-2075.

Luning Prak, D., Fries, J., Gober, R., Vozka, P., Kilaz, G., Johnson, T., Graft, S., Trulove, P., & Cowart, J. (2019). Densities, Viscosities, Speeds of Sound, Bulk Moduli, Surface Tensions, and Flash Points of Quaternary Mixtures of n-Dodecane (1), n-Butylcyclohexane (2), n-Butylbenzene (3), and 2,2,4,4,6,8,8-Heptamethylnonane (4) at 0.1 MPa as Potential Surrogate Mixtures for Military Jet Fuel, JP-5, J. *Chem. Eng. Data*, 64 (4), 1725-1745.

Luning Prak, D. J., Romanczyk, M., Wehde, K. E., Ye, S., McLaughlin, M., Luning Prak, P. J., Foley, M.P, Kenttämaa, H.I, Trulove, P.C., Kilaz, G. Xu, L., & Cowart, J.S. (2017). Analysis of catalytic hydrothermal conversion jet fuel and surrogate mixture formulation: components, properties, and combustion. *Energy & Fuels*, 31(12), 13802-13814.

Martens, H., Tøndel, K., Tafintseva, V., Kohler, A., Plahte, E., Vik, J. O., ... & Omholt, S. W. (2013). PLS-based multivariate metamodeling of dynamic systems. In *New Perspectives in Partial Least Squares and Related Methods* (pp. 3-30). Springer, New York, NY.

Ministry of Defense. (2015). Defense Standard 91-91, Issue 7.

Mo, H., & Raftery, D. (2008). Solvent signal as an NMR concentration reference. *Analytical chemistry,* 80(24), 9835-9839.

Mo, H., Balko, K. M., & Colby, D. A. (2010). A practical deuterium-free NMR method for the rapid determination of 1-octanol/water partition coefficients of pharmaceutical agents. *Bioorganic & medicinal chemistry letters*, 20(22), 6712-6715.

Mondal, S., Kumar, R., Bansal, V., & Patel, M. B. (2015). A ^{1}H NMR method for the estimation of hydrogen content for all petroleum products. *Journal of Analytical Science and Technology*, 6(1), 24.

Morris, R. E., Hammond, M. H., Cramer, J. A., Johnson, K. J., Giordano, B. C., Kramer, K. E., & Rose-Pehrsson, S. L. (2009). Rapid fuel quality surveillance through chemometric modeling of near-infrared spectra. *Energy & Fuels*, 23(3), 1610-1618.

Pires, A. P., Han, Y., Kramlich, J., & Garcia-Perez, M. (2018). Chemical Composition and Fuel Properties of Alternative Jet Fuels. *BioResources*, 13(2), 2632-2657.

Radich, T. (2015). *The flight paths for biojet fuel*. Washington, DC: U.S. Energy Information Administration.

Rand, S. & Verstuyft, A., (Eds.). (2016). *MNL69-EB fuels specifications: what they are, why we have them, and how they are used*. Retrieved from https://doi-org.ezproxy.lib.purdue.edu/10.1520/MNL69-EB

Romanczyk, M., Velasco, J.R.V., Xu, L., Vozka, P., Dissanayake, P., Wehde, K.E., Roe, N., Keating, E., Kilaz, G., Trice, R.W., Luning Prak, D.J., & Kenttämaa, H. (2019). The capability of organic compounds to swell acrylonitrile butadiene o-rings and their effects on o-ring mechanical properties. *Fuel*, 238, 483-492.

Rumizen, M. (2016, October). *Certification-Qualification Breakout*. Paper presented at the Commercial Aviation Alternative Fuels Initiative, Washington, DC.

Schoenmakers, P. J., Oomen, J. L., Blomberg, J., Genuit, W., & van Velzen, G. (2000). Comparison of comprehensive two-dimensional gas chromatography and gas chromatography–mass spectrometry for the characterization of complex hydrocarbon mixtures. *Journal of Chromatography A*, 892(1-2), 29-46.

Shi, X., Li, H., Song, Z., Zhang, X., & Liu, G. (2017). Quantitative composition-property relationship of aviation hydrocarbon fuel based on comprehensive two-dimensional gas chromatography with mass spectrometry and flame ionization detector. *Fue*l, 200, 395-406.

Šimáček, P., Kubička, D., Pospíšil, M., Rubáš, V., Hora, L., & Šebor, G. (2013). Fischer–Tropsch product as a co-feed for refinery hydrocracking unit. *Fuel*, 105, 432-439.

Solash, J., Hazlett, R. N., Hall, J. M., & Nowack, C. J. (1978). Relation between fuel properties and chemical composition. 1. Jet fuels from coal, oil shale and tar sands. *Fuel*, 57(9), 521-528.

Starck, L., Pidol, L., Jeuland, N., Chapus, T., Bogers, P., & Bauldreay, J. (2016). Production of hydroprocessed esters and fatty acids (HEFA)–optimisation of process yield. *Oil & Gas Science and Technology–Revue d'IFP Energies nouvelles*, 71(1), 10.

Striebich, R. C., Shafer, L. M., Adams, R. K., West, Z. J., DeWitt, M. J., & Zabarnick, S. (2014). Hydrocarbon group-type analysis of petroleum-derived and synthetic fuels using two-dimensional gas chromatography. *Energy & Fuels*, 28(9), 5696-5706.

Suykens, J. A., Van Gestel, T., & De Brabanter, J. (2002). *Least squares support vector machines*. World Scientific.

U.S. Department of Defense. (2008). *Turbine fuel, aviation, kerosene type, JP-8 (NATO F-34), NATO F-35, and JP-8+ 100 (NATO F-37)* (Report No. MIL-DTL-83133G). Retrieved from https://www.alcorpetrolab.com/images/stories/Specifications/MIL-DTL-83133G.PDF

U.S. Department of Energy, Office of Energy Efficiency and Renewable Energy (EERE). (2017). *Alternative aviation fuels: overview of challenges, opportunities, and next steps* (Report No. DOE/EE-1515). Washington, DC.

UOP LLC. (2011). ASTM UOP 990-11 Organic analysis of distillate by comprehensive two-dimensional gas chromatography with flame ionization detection. Retrieved from https://www-astm-org.ezproxy.lib.purdue.edu/cgi-bin/resolver.cgi?3PC+UOP+UOP990-11+en-US

Vozka, P., Kilaz, G. (2019). How to obtain a detailed chemical composition for middle distillates via GC×GC-FID without the need of GC×GC-TOF/MS, *Fuel*, 247, 368-377.

Vozka, P., Mo, H., Šimáček, P., & Kilaz, G. (2018). Middle distillates hydrogen content via GC× GC-FID. *Talanta*, 186, 140-146.

Vozka, P., Modereger, B. A., Park, A. C., Zhang, W. T. J., Trice, R. W., Kenttämaa, H. I., & Kilaz, G. (2019). Jet fuel density via GC× GC-FID. *Fuel*, 235, 1052-1060.

Vozka, P., Šimáček, P., Kilaz, G. (2018). Impact of HEFA Feedstocks on Fuel Composition and Properties in Blends with Jet A, *Energy & Fuels*, 32 (11), 11595-11606.

Vozka, P., Vrtiška, D., Šimáček, P., Kilaz, G. (2019). Impact of Alternative Fuel Blending Components on Fuel Composition and Properties in Blends with Jet A, *Energy & Fuels*, 33 (4), 3275-3289.

Wang, H., Henseler, J., Vinzi, V. E., & Chin, W. W. (2010). *Handbook of Partial Least Squares: Concepts*, Methods and Applications.

Wang, W. C., & Tao, L. (2016). Bio-jet fuel conversion technologies. *Renewable and Sustainable Energy Reviews*, 53, 801-822.

Webster, R. L., Rawson, P. M., Kulsing, C., Evans, D. J., & Marriott, P. J. (2017). Investigation of the thermal oxidation of conventional and alternate aviation fuels with comprehensive two-dimensional gas chromatography accurate mass quadrupole time-of-flight mass spectrometry. *Energy & Fuels*, 31(5), 4886-4894.

Wilson III, G. R., Edwards, T., Corporan, E., & Freerks, R. L. (2013). Certification of alternative aviation fuels and blend components. *Energy & Fuels*, 27(2), 962-966.

Wilson III, G. R., Edwards, T., Corporan, E., & Freerks, R. L. (2013). Certification of alternative aviation fuels and blend components. *Energy & Fuels*, 27(2), 962-966.

Yildirim, U., & Abanteriba, S. (2012). Manufacture, qualification and approval of new aviation turbine fuels and additives. *Procedia Engineering*, 49, 310-315.

Zschocke, A., Scheuermann, S., & Ortner, J. (2017). *High biofuel blends in aviation (HBBA)* (Report No. ENR/C2/2012/420-1). Retrieved from https://ec.europa.eu/energy/sites/ener/files/documents/final_report_for_publication.pdf

PUBLICATIONS

JOURNALS

Vozka, P., Vrtiška, D., Šimáček, P., Kilaz, G. (2019). Impact of Alternative Fuel Blending Components on Fuel Composition and Properties in Blends with Jet A, *Energy & Fuels*, 33 (4), 3275-3289.

Vozka, P., Kilaz, G. (2019). How to obtain a detailed chemical composition for middle distillates via GC×GC-FID without the need of GC×GC-TOF/MS, *Fuel*, 247, p. 368-377.

Luning Prak, D., Fries, J., Gober, R., Vozka, P., Kilaz, G., Johnson, T., Graft, S., Trulove, P., Cowart, J. (2019). Densities, Viscosities, Speeds of Sound, Bulk Moduli, Surface Tensions, and Flash Points of Quaternary Mixtures of n-Dodecane (1), n-Butylcyclohexane (2), n-Butylbenzene (3), and 2,2,4,4,6,8,8-Heptamethylnonane (4) at 0.1 MPa as Potential Surrogate Mixtures for Military Jet Fuel, JP-5, *J. Chem. Eng. Data*, 64(4), p.1725-1745.

Romanczyk, M., Velasco, J.R.V., Xu, L., Vozka, P., Dissanayake, P., Wehde, K.E., Roe, N., Keating, E., Kilaz, G., Trice, R.W., Luning Prak, D.J., Kenttämaa, H. (2019). The capability of organic compounds to swell acrylonitrile butadiene o-rings and their effects on o-ring mechanical properties, *Fuel*, 238, p. 483-492.

Vrtiška, D., Vozka, P., Váchová, V., Šimáček, P., Kilaz, G. (2019). Prediction of HEFA content in jet fuel using FTIR and chemometric methods, *Fuel*, 236, p. 1458-1464.

Vozka, P., Modereger B., Park, A., Zhang, J., Trice, R., Kenttämaa, H., Kilaz, G. (2019). Jet fuel density via GC×GC-FID, *Fuel*, 235, p. 1052-1060.

Vozka, P., Šimáček, P., Kilaz, G. (2018). Impact of HEFA Feedstock on Fuel Composition and Properties in Blends with Jet A, *Energy & Fuels*, 32(11), p. 11595-11606.

Vozka, P., Mo, H., Šimáček, P., Kilaz, G. (2018). Middle distillates hydrogen content via GC×GC-FID, *Talanta*, 186C, p. 140-146.

Zhao, X., Zhang, Y., Cooper, B.C., Vozka, P., Kilaz, G. (2018). Optimization of comprehensive two-dimensional gas chromatography with time-of-flight mass spectrometry (GC×GC/TOF-MS) for conventional and alternative jet fuels analysis, *Advanced Materials and Technologies Environmental Sciences*, 2(1), p. 138-148.

Vozka, P., Orazgaliyeva, D., Šimáček, P., Blažek, J., Kilaz, G. (2017). Activity comparison of Ni-Mo/Al_2O_3 and Ni-Mo/TiO_2 catalysts in hydroprocessing of middle petroleum distillates and their blend with rapeseed oil. *Fuel Processing Technology*, 167, p. 684-694.

Vozka P., Váchová V., Blažek J.: Katalyzátory pro hydrogenaci kapalných produktů zpracování biomasy [Catalysts for hydrotreating of liquid products from processing of biomass]. *Paliva*, 2015, 7(3), p. 59–65.

Váchová V., Vozka P.: Hydrogenace rostlinných olejů na paliva pro vznětové motory [Processing of vegetable oils to diesel fuel]. *Paliva*, 2015, 7(3), p. 66-73.

Vozka, P., Straka, P., Maxa, D.: Effect of asphaltenes on structure of paraffin particles in crude oil. *Paliva*, 2015, 7(2), p. 42 – 47.

CONFERENCE PROCEEDINGS

Wehde, K., Romanczyk, M., Vozka, P., Ramírez, J.H., Trice, R., Kilaz, G., Kenttämaa, H. (2017, June). *Composition Analysis of Aviation Fuels and Fuel Additives for Rational Development of Renewable Aviation Fuels*. Paper presented at The 65th American Society for Mass Spectrometry (ASMS) Conference, Indianapolis, IN.

PATENTS

Kilaz, G., Vozka, P. 2018. Set of standards for GC×GC-FID classification developing. U.S. Patent Application, filed October 2018. Patent Pending.

POSTERS

Vozka, P., Romanczyk, M., Velasco, J. R., Trice, R., Kenttämaa, H., & Kilaz, G. (2018, October*). Relationship between fuel chemical composition and fuel properties*. Poster presented at the Annual ONR NEPTUNE Program Review, UC Davis, CA.

Manheim, J., Wehde, K., Zhang, J., Romanczyk, M., Vozka, P., Kilaz, G., & Kenttämaa, H. (June, 2017). *Identification and Quantitation of Linear Saturated Hydrocarbons in Lubricant Base Oils by Using (APCI)LQIT MS and GC×GC/(EI)TOF MS*. Poster presented at American Society for Mass Spectrometry (ASMS) Conference, San Diego, CA.

Romanczyk, M., Velasco, J. R., Vozka, P., Xu, L., Wehde, K., Modereger, B., Trice, R., Kilaz, G., & Kenttämaa, H. (2017, November). *Design of Next Generation Renewable Fuels*. Poster presented at the ONR Neptune Program Review, Annapolis, MD.

Romanczyk, M., Velasco, J. R., Wehde, K., Vozka, P., Modereger, B., Xu, L., Roe, N., Keating, E., Healy, J., Gordon, A., Trice, R., Kilaz, G., & Kenttämaa, H. (2017, May). *Composition/Property/Performance Correlations for Rational Development of Renewable Aviation Fuels*. Poster presented at the MIT Energy Initiative, Boston, MA.

Vozka, P., Romanczyk, M., Wehde, K., Velasco, J. R., Trice, R., Kenttämaa, H., & Kilaz, G. (2017, May). *Alternative Aviation Fuel Chemistry-Performance Correlations Towards a Sustainable Future*. Poster presented at the Purdue Spring Reception 2017, West Lafayette, IN.

Romanczyk, M., Wehde, K., Vozka, P., Kong, J., Velasco, J. R., Yerabolu, R., Kenttämaa, H., Kilaz, G., & Trice, R. (2016, November*). Fundamental Studies on Composition/ Performance Correlations for Aviation Fuels*. Poster presented on the Naval Enterprise Partnership Teaming with Universities for National Excellence, UC Davis, CA.